

WINGLET DESIGN AND OPTIMIZATION FOR UAVS

By

JACOB R. WEIERMAN

Bachelor of Science in Applied Physics
Oklahoma State University
Stillwater, OK, USA
2003

Submitted to the Faculty of the
Graduate College of
Oklahoma State University
in partial fulfillment of
the requirements for
the Degree of
MASTER OF SCIENCE
July, 2010

WINGLET DESIGN AND OPTIMIZATION FOR UAVS

Thesis Approved:

Dr. Jamey Jacob

Thesis Advisor

Dr. Andrew Arena

Dr. David G. Lilley

Dr. A. Gordon Emslie

Dean of the Graduate College

ACKNOWLEDGMENTS

I would like to thank Dr. Jamey D. Jacob for his mentorship which was invaluable during the course of my research. I would like to thank Dr. Jay Kudva and NextGen Aeronautics for the opportunity they gave me to validate test results at the Kirsten wind tunnel at the University of Washington in Seattle, WA. I would like to thank Fred Keating, Ben Loh, Alan Larson and Johnny Chandler for their help and support in building physical models. I would like to thank the committee members for their time and contributions. I would like to thank Oklahoma State University for the outstanding support and facilities they provide to their students. I would also like to thank Ray Schatzer and the OSU New Product Development Center for their contributions in rapid prototyping models. Finally I would like to thank my wife, Amy, and my children for their love and support.

TABLE OF CONTENTS

Chapter	Page
1 Introduction	1
1.1 Motivation	1
1.2 Goals	3
1.2.1 Develop Winglet Designs Applicable for Generic Small UAVs	3
1.2.2 Determine Performance Improvements When Implementing Winglet Designs On UAVs	8
1.3 Objectives	10
1.3.1 Develop a Design Methodology Based on VLM for Winglet Design	10
1.3.2 Design Winglets	12
1.3.3 Test Winglet Models	12
1.3.4 Evaluate Selected Platforms and Determine Benefits of Winglet Designs	12
1.4 Thesis Outline	13
2 Methodology	15
2.1 Winglet Design	15
2.2 Vortex Lattice Method	17
2.2.1 Vortex Lattice Theory	17
2.2.2 Tornado	20
2.2.3 Pecos	21
2.2.4 Pecos: Getting Started	22
2.2.5 Pecos: Step 1 - Geometry	23

2.2.6	Pecos: Winglets	29
2.2.7	Pecos: Step 2 - State	35
2.2.8	Pecos: Step 3 - Processing	38
2.2.9	Pecos: Step 4 - Post Processing	42
2.3	Wind Tunnel Testing	45
2.3.1	Small Scale Testing	45
2.3.2	University of Washington Aero Lab Wind Tunnel	48
3	Results	52
3.1	VLM	52
3.2	UAV Performance Evaluation	54
3.2.1	Wing Configuration Study	56
3.3	Wind Tunnel Testing	61
3.3.1	Vortex Dynamics Study	61
4	Impact on UAV Design and Performance	76
4.1	Winglet Design for RQ7 Shadow	76
4.2	Winglet Performance for RQ7 Shadow	77
4.3	Winglet Design for Predator A	80
4.4	Winglet Performance for Predator A	82
5	Conclusions	87
5.1	Design	87
5.2	Performance	88
5.3	Future Work	88
	BIBLIOGRAPHY	90

LIST OF FIGURES

Figure		Page
1.1	In 1979, NASA attached a winglet to a KC135 to evaluate its performance as part of their early winglet research efforts. [21]	2
1.2	The winglet geometry used by Richard T. Whitcomb in his research at NASA Langley wind tunnel included an upper winglet aligned with the main wing trailing edge, and a lower winglet, aligned to the leading edge of the main wing. [29]	4
1.3	Adding a toe-out angle to the winglet will produce a force opposite the air velocity which acts like a thrust to reduce the drag.	5
1.4	The Learjet Longhorn 55 was the first production turbojet powered aircraft to be certified with winglets. [6]	7
1.5	The Boeing BBJ (based on the Boeing 737) has blended winglets for improved performance and “aesthetic appeal”. [5]	7
1.6	Winglets help improve the aerodynamic efficiency by reducing the size of the wing tip vortex.[30]	8
1.7	The Global Hawk HALE (high altitude long endurance) UAV is built by Northrop Grumman and is used the by US Air Force. It has a wingspan of 130 feet and can carry a payload of 3,000 lbs. It is the largest production UAV currently in service.[27]	9
1.8	The Predator UAV is manufactured by General Atomics. The Predator has a wingspan of 55 feet and can carry both internal and external payloads totaling more than 700 lbs. Nearly 200 Predators are in service.[27]	10

1.9	The ScanEagle UAV developed by Insitu has a wingspan of 10.2 feet. It is launched using a catapult system, so it doesn't need a runway.[13]	10
1.10	The Shadow UAV is manufactured by the AAI Corporation. The Shadow 200 has a wingspan of 20.4 feet, and like the ScanEagle, is launched using a catapult system.[30]	11
2.1	Parameters used to define the winglet geometry include: root chord, tip chord, sweep, height (length), radius, cant and twist.	16
2.2	The Prandtl lifting-line theory uses a horseshoe vortex to calculate the lift produced by the wing.[3]	18
2.3	A vortex filament induces a velocity in the space surrounding it.[3]	19
2.4	The velocity at point P can be determined by Γ and h.[3]	19
2.5	The wing is divided into a grid. For each section of the grid, there is horseshoe vortex filament with strength Γ placed at the 1/4 chord, and a collocation point placed at the 3/4 chord. The flow tangent to the surface at the collocation point must be equal to zero.	20
2.6	The wing geometry for the RQ7 Shadow 200 modeled in Tornado VLM for MATLAB. On the left are the side, front, top and isometric views of the wings with partitions, panels, MAC, and reference point. The figure on the right shows the model with the collocation points associated with each panel.	21
2.7	The PECOS Main window for includes 4 buttons, one for each step: Geometry, State, Processing, and Post Processing.	22
2.8	The PECOS Geo window contains all the necessary controls to input the data for every geometry parameter.	23
2.9	The Mesh Type drop down list includes options for: Linear, Span wise half-cosine, Span wise half-cosine Chord wise cosine, and Span wise cosine Chord wise cosine.	28

2.10	The four different types of panel distributions available in Tornado. The panels are configured slightly differently for each option, as can be seen in these top views of the wings. In each of these configurations there are eight panels span wise and eight panels chord wise for each wing.	29
2.11	The PECOS Winglets window contains the controls for automatic blended winglet geometry generation.	31
2.12	A diagram of the different geometric parameters and how they are defined for the winglet geometry. In this figure are the wing, winglet, dihedral, cant, and blend radius	32
2.13	The arc segment for this winglet is set to 0.5 meters, while the blend radius is set to 0.75 meters. A segment length of 0.5 meters is very coarse and results in large angles between the each segment.	33
2.14	Using the same dimensions for the winglet as in fig. 2.13, but setting the segment length to a shorter 0.15 meters, the blend of the radius is better defined, with smaller angles between each segment of the arc.	33
2.15	The PECOS State window allows the user to input the flight conditions to evaluate the aerodynamic performance of the model. The user can adjust the angle of attack, speed, and altitude.	36
2.16	There are four options for speed type in the Speed Type drop down list: True Airspeed, Equivalent Airspeed, Calibrated Airspeed, and Mach Number.	37
2.17	The unit converter can make conversions for the speed and altitude settings of the state.	38
2.18	Inputs for speed can be kilometers per hour, meters per second, milers per hour, feet per second and knots, While inputs for altitude include kilometers, meters, miles, feet, and inches.	39

2.19	The PECOS Processing window contains options for various type of calculations to be performed using the Tornado Vortex Lattice Method.	40
2.20	The PECOS Processing window contains options for various type of calculations to be performed using the Tornado Vortex Lattice Method.	43
2.21	The definitions of the variables used by Tornado for VLM in relation to the geometry and coordinate axis.	44
2.22	Example of wind tunnel model.	45
2.23	For PIV measurements, a scale model of the wing was placed in 12x12 cross section wind tunnel. A prism was placed downstream of the model. A high speed camera was placed above the prism to capture a cross section of the downstream flow at Stations 1, 2, 3, 4, and 5. . .	47
2.24	For PIV measurements, A scale model of the wing was placed in 12x12 cross section wind tunnel. A prism was placed downstream of the model. A high speed camera was placed above the prism to capture a cross section of the downstream flow at Stations 1, 2, 3, 4, and 5. . .	48
2.25	Three wings were modeled for PIV measurements. Wing 1 has no winglets, wing 2 has straight winglets, wing 3 has a straight lower winglet and a blended upper winglet.	49
2.26	Diagram of the Kirsten wind tunnel at the University of Washington in Seattle. The wind tunnel is a closed-loop double return design.[28]	50
2.27	The Kirsrtten Wind Tunnel features 2 massive propellers measuring 11 ft. 4 in. in diameter, with seven blades.[28]	51
2.28	Winglet models were milled from solid aluminum for wind tunnel testing at the University of Washington Aero Lab. The image on the left is the optimized blended winglet, and the Whitcomb winglet is on the right.	51

3.1	MATLAB plot for configuration BFC03 with blend radius varying from 0.1 to 0.9 meters. Angle of attack varies from -10° to 20° . Left plot indicates C_L/C_D , right plot shows the root bending moment.	54
3.2	MATLAB plot for configuration BFC03 with cant angle varying from 50° to 90° . Angle of attack varying from -10° to 20° . Left plot indicates C_L/C_D , right plot shows the root bending moment.	55
3.3	MATLAB plot for configuration BFC03 with sweep angle varying from 0° to 40° . Angle of attack varying from -10° to 20° . Left plot indicates C_L/C_D , right plot shows the root bending moment.	56
3.4	MATLAB plot for configuration BFC03 with cant angle varying from 60° to 90° and the radius varying from .1 to .9 meters. Left plot indicates C_L/C_D , right plot shows the root bending moment.	57
3.5	MATLAB plot for configuration BFC04 with tip twist angle varying from -15° to 5° . Sweep angle varying from 10° to 60° . Left plot indicates C_L/C_D , right plot shows the root bending moment.	58
3.6	Graph of VLM results for the test model with no winglet, a Whitcomb winglet and the optimized winglet for comparison of C_L/C_D vs. Alpha and root bending moment vs. Alpha.	59
3.7	Geometry plot for wing 1 with panels. Wing 1 does not have any winglets	60
3.8	Geometry plot for wing 2 with panels. Wing 2 has the lower winglets and straight upper winglets.	61
3.9	Geometry plot for wing 3 with panels. Wing 3 has the lower winglets and blended upper winglets.	62
3.10	C_L vs. Alpha plots for 3 wing configurations. Results from wind tunnel testing and results from VLM model. Correlation is strong in lower angles, correlation decreases as the wind tunnel model approaches the stall angle.	65

3.11	C_L/C_D vs. Alpha plots for 3 wing configurations. Results from wind tunnel testing and results from VLM model. VLM does not calculate viscous drag, so the curve for the VLM models is higher. Though the trends for three wings are similar for both the wind tunnel test and VLM model.	66
3.12	C_L/C_D vs. Alpha plots for 3 wing configurations. For the VLM plots, C_{D0VLM} was replaced by C_{D0WT} for C_D in the calculation of C_L/C_D . The curves are much closer when using C_{D0WT}	67
3.13	C_L vs. C_D for 3 wing configurations. Results from wind tunnel testing and results from VLM model. There is strong correlation between the graphs at lower drag values and lower lift values. The relations between the different wings are similar for both methods.	68
3.14	Wing or winglet position relative to MATLAB graphs showing the cross sectional vorticity for wing 1, 2, and 3. Wing tip or upper winglet tip is near the center of the image.	68
3.15	MATLAB graphs showing the cross sectional velocity and vorticity for wing 1, with an angle of attack set to 0° , at stations 1, 2, and 3. . . .	69
3.16	MATLAB graphs showing the cross sectional velocity and vorticity for wing 2, with an angle of attack set to 0° , at stations 1, 2, and 3. . . .	70
3.17	MATLAB graphs showing the cross sectional velocity and vorticity for wing 3, with an angle of attack set to 0° , at stations 1, 2, and 3. . . .	71
3.18	MATLAB graphs showing the cross sectional velocity and vorticity. Results for wing 1 are at the top, wing 2 are in the middle row, wing 3 results are at the bottom. Each plot is taken from station 1. Each wing is positioned at an angle of attack 10°	72
3.19	Γ values for wing 1, wing 2, and wing 3 at station 1. Alpha for each wing was set at 10°	73

3.20	MATLAB graphs showing the cross sectional velocity and vorticity. Results are for wing 1 with an angle of attack at 10° . The plots in the top row are taken from station 1, the middle row shows results from station 2, and the bottom row is from station 3.	74
3.21	Γ values for wing 1 at station 1, 2, and 3. Alpha was set at 10°	75
3.22	Wind tunnel model with a winglet that can be set to variable angles for the cant.	75
4.1	Winglets applied to RQ7 Shadow must fit within the defined constraints: winglets must not extend the overall length of the wing by more than 50% of the chord length, winglets must be no higher than 25% of the semi span of the main wing, and winglets must extend no further than 25% of the chord length beyond the wingtip trailing edge.	78
4.2	Graphs for Shadow, blended winglet (configuration B1), radius and angle of attack are varied from .0 to .25 meter and -5° to 15° respectively. The graph on the left plots C_L/C_D , and the graph on the right plots root bending moment in relation to each parameter.	78
4.3	Graphs for Shadow, blended winglet (configuration B2), tip twist and angle of attack are varied from -5° to 5° and -5° to 15° respectively. The graph on the left plots C_L/C_D , and the graph on the right plots root bending moment in relation to each parameter.	80
4.4	Graphs for Shadow, Whitcomb winglet (configuration W1), the cant is varied from 54° to 90° while the angle of attack was varied from -5° to 15° . The graph on the left plots C_L/C_D , and the graph on the right plots root bending moment in relation to each parameter.	81

4.5	Graphs for Shadow, Whitcomb winglet (configuration W2), the tip twist is varied from -5° to 5° while the angle of attack is varied from -5° to 15° . The graph on the left plots C_L/C_D , and the graph on the right plots root bending moment in relation to each parameter.	82
4.6	Graphs comparing the C_L/C_D and root bending moment versus alpha for 3 configurations for the RQ7 Shadow UAV.	83
4.7	Graph of the results from XFOIL calculations performed for the NACA 4415 airfoil at airspeed of 90 knots and an altitude of 10,000 ft.	84
4.8	L-R: Shadow UAV, VLM model of Shadow UAV, VLM model of Shadow UAV with Whitcomb winglets, VLM model of Shadow UAV with optimized blended winglets.	84
4.9	Plots showing the percent change for configuration PW01 from the base configuration at the same flight conditions. Left plot is the change in C_L/C_D and the right plot is the change in the root bending moment.	85
4.10	Plots showing the percent change for configuration PW04 from the base configuration at the same flight conditions. Left plot is the change in C_L/C_D and the right plot is the change in the root bending moment.	85
4.11	Left to Right: Predator UAV, Predator VLM model, Predator VLM model with optimized blended winglets.	86
4.12	VLM results for the base Predator configuration with no winglets compared to Predator with optimized winglets. Left plot shows the predicted values for C_L/C_D vs. Alpha and the right plot shows the root bending moment vs. Alpha.	86

CHAPTER 1

Introduction

1.1 Motivation

Winglets are small wing like structures at the end of a wing. The purpose of winglets is to improve aerodynamic efficiency of the wings to which they are attached. Research has shown that winglets do in fact improve performance. Research into winglet technology for commercial aviation was pioneered by Richard Whitcomb in the mid 1970's.[29] Whitcomb's research focused on applications for large airplanes like the Boeing 737 at a high subsonic airspeed. Research in full size aircraft revealed that winglets can provide improvements in efficiency of more than 7%. Winglets offer greater lift without a greater wingspan. For large airplanes like the Boeing 747, winglets can increase lift while maintaining a fixed maximum wingspan requisite for many international airports. Unmanned Air Vehicles (UAVs) however, generally operate at much lower Reynolds numbers, and UAVs would seem to have little restriction for wingspan. However winglets might offer some benefits to UAVs. A small improvement in efficiency would allow for greater time in flight, a heavier payload, or increased range for example.

The motivation for this research is to develop an efficient method for winglet design and optimization for UAV platforms. While research in winglets has been dominated by commercial applications, with some research applied to sailplanes, little is documented on the methods for optimizing all the parameters for a successful winglet configuration. Research details the parameters and applications for winglets but there are no tools for creating an optimized geometry that can be tailored to each

individual application. Using a MATLAB based Vortex Lattice Method (VLM) to calculate the aerodynamic properties of the winglet geometry, an array of geometries can be created and evaluated at specific flight conditions to determine the optimum solution. The optimization approach is based on parametric analysis. This research focuses on an open source code with low computational requirements for aerodynamic analysis using the Tornado VLM[20]. Building upon that foundation, a graphical user interface was created along with algorithms for generating winglet geometries for specific air vehicle platforms. Using these tools, parametric analysis of various winglet geometries was possible for winglet optimization. These techniques however, are not necessarily limited to UAVs.



Figure 1.1: In 1979, NASA attached a winglet to a KC135 to evaluate its performance as part of their early winglet research efforts. [21]

1.2 Goals

This research has two goals, including the development of winglet designs applicable for generic small UAVs and determining performance improvements when implementing winglet designs on UAVs. While these goals are linked, realization of the first goal does not automatically lead to implementation of the winglet design on a specific UAV. Each air vehicle must be examined on its own merits to determine if the aerodynamic performance outweighs the additional cost and increased weight from a winglet. Each of these is discussed in turn along with previous work relevant to each goal.

1.2.1 Develop Winglet Designs Applicable for Generic Small UAVs

Richard T. Whitcomb laid the groundwork upon which modern winglets are built. Whitcomb's research detailed a few of the parameters that contribute to a successful wingtip device. Fig. 1.2 depicts the geometry that Whitcomb used for the winglets in his research. The parameters for these winglets include an upper winglet with sweep, cant, taper, and a non-symmetric airfoil with a toe-out angle. Whitcomb suggested that winglets should have a toe-out angle. The toe angle refers to the incidence of the winglet with respect to the X-Z plane. A toe-out angle would slant the incidence of the winglet away from the main body. Fig. 1.3 depicts the toe-out geometry and forces. The toe-out configuration reorients what would be the lifting force for a wing in the horizontal position, it now has a component opposite to the air velocity providing a force similar to thrust, thereby decreasing the overall drag. The upper winglet is aligned with the trailing edge of the wingtip. There is also a lower winglet with sweep, cant, and taper ratio, which is aligned with the leading edge of the wingtip. Though many modern researchers are able to investigate a much broader range of geometries using computational methods, Whitcomb's experiments focused on just a few winglet designs grounded in practical applications. While some

(including this research) mainly look at the increased efficiency in terms of increasing L/D , Whitcomb compared successful winglets against simple wing-tip extensions, which would have a similar impact on the root bending moment of the wing. After all, if the increased lift can only be used to lift the added structural weight necessary to support the winglet in the first place, can it really be an improvement? Whitcomb's winglets did perform better than wing-tip extensions. Whitcomb's research showed that winglets could improve L/D by 9% and reduce lift induced drag by nearly 20% at Reynolds numbers of 5.25×10^6 . A wing tip extension with an equivalent impact on the root bending moment only improved L/D by 4%. Even with these impressive improvements, Whitcomb realized that his winglets were "undoubtedly not optimum" [29] due to the limitations of the methods used in the research. While this research is relevant, the Reynolds numbers used in Whitcomb's research are far greater than most UAVs will ever encounter.

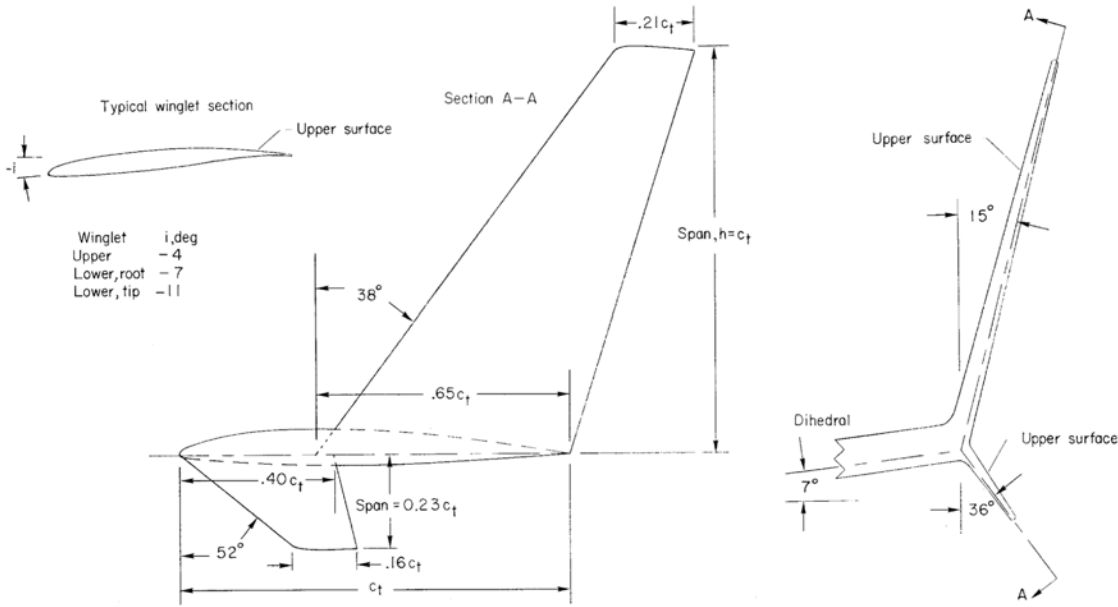


Figure 1.2: The winglet geometry used by Richard T. Whitcomb in his research at NASA Langley wind tunnel included an upper winglet aligned with the main wing trailing edge, and a lower winglet, aligned to the leading edge of the main wing. [29]

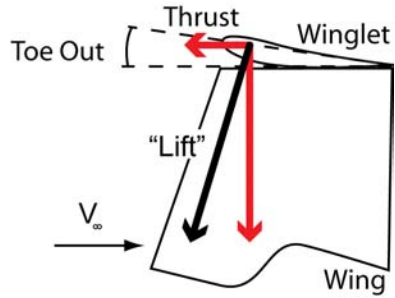


Figure 1.3: Adding a toe-out angle to the winglet will produce a force opposite the air velocity which acts like a thrust to reduce the drag.

N. Conley’s research into the toe-out angle for the winglets on the Gates Longhorn Learjet showed that small variations in the toe-out angle could help to fine-tune the performance, but ultimately, as is the case with so many aspects of airplane design, the “optimum” design would depend on which performance characteristic was most important.[8] Importantly, it showed that “tweaking” the design *could* improve performance. For most designers, a parametric analysis of hundreds or just dozens of designs in a wind tunnel for a chance to find a more optimum design is simply not feasible. UAV designers especially, may be limited by time and budget constraints which require a more robust approach to finding an optimum geometry. The Learjet winglets were based on the work by Whitcomb and were simple, straight wing structures mounted vertically at the wing tip. Conley notes that the winglet should be placed aft of the main wing quarter chord so as to not superimpose the “increased velocities over the inner surface of the winglet... on the high velocities over the forward region of the wing upper surface.”[8]

Takenaka et. al. used computational models to investigate the fluid dynamics and structural stresses associated with winglets and showed that wave drag develops at the wing/winglet junction when the winglet is not blended into the main wing[25]. In the multidisciplinary approach the design parameters applied to a commercial aviation airplane at Mach 0.8, and a Reynolds number of about 1.2×10^6 . Takenaka

et. al. optimized their winglet design for “multiple objectives and a small number of design variables.” [25] Through this approach the winglets could be optimized based on minimizing block fuel and GTOW, which are “indirectly affected by the performance of the winglets.” Importantly, this study shows how interdependent each aspect of aircraft design is, and how winglet optimization can be useful for various aspects of design and development. Takenaka’s optimizations resulted in a blended winglet design with a leading edge aft of the main wing leading edge. In the design phase Takenaka notes that the dominant parameters for drag reduction are the span length and the cant angle of the winglet.

Other research has focused on more radical designs such as the C-wing.[14] However, such optimization is based mainly on reducing drag due to lift and increasing L/D with little regard to the physical structures that would be necessary to support such a design. This previous research lays a foundation for the validity of the winglet concept, but individually do not specifically account for the advantages that might be obtained on smaller platforms like UAVs. The previous research also underscores the many parameters which should be considered when determining what factors influence an “optimum” design. Though the most obvious measurement for winglet performance is the reduced drag due to lift, and increased L/D , the weight of the added structure should be considered as well as the ultimate mission for the aircraft.

Maughmer’s winglets for high-performance sail planes operated at Reynolds numbers from 7.0×10^4 to 1.0×10^6 . [19] This is similar to the operating conditions for small to mid-size UAVs. For sailplanes, Maughmer suggests airfoils that can operate at very low Reynolds numbers. Maughmer describes the “break-even point” as the point “at which halving the Reynolds number causes the profile drag coefficient to double.” [19] The break-even point is used to determine the height of the winglet.

Unmanned Air Vehicles (UAVs) are aircraft that can be piloted from a remote control station by a trained operator or can be programmed to fly autonomously using



Figure 1.4: The Learjet Longhorn 55 was the first production turbojet powered aircraft to be certified with winglets. [6]



Figure 1.5: The Boeing BBJ (based on the Boeing 737) has blended winglets for improved performance and “aesthetic appeal”. [5]

onboard sensors, computers and GPS. Increasingly, the dangerous and monotonous work that was once done by manned aircraft is being turned over to UAVs. UAV design is mainly focused around the intended mission and size is not limited by the constraints of providing a habitat for a human pilot but rather by the size of the intended payload. While there are some UAVs that are very large such as the Predator and the Global Hawk, other UAVs are much more diminutive, such as the Shadow and ScanEagle. Smaller UAVs cost less to purchase and operate, and because there is no human pilot, UAVs can be considered expendable. UAVs seem to have sparked a renaissance in aircraft design. Designers and engineers are using all their ingenuity to design UAVs for every mission imaginable, which has led to an explosion



Figure 1.6: Winglets help improve the aerodynamic efficiency by reducing the size of the wing tip vortex.[30]

in the number of aircraft being designed and built. Because UAV size is only limited by technology and the laws of physics, engineers are free to develop unique aircraft systems for which there is equivalent in current commercial aviation. For each unique design, there are unique challenges, with unique and often unconventional solutions. For the more conventional solutions, the goal is to determine if winglet technology can be applied for improved performance.

1.2.2 Determine Performance Improvements When Implementing Winglet Designs On UAVs

Whitcomb's criteria measured performance as reduced lift induced drag, increased L/D with equal root bending moment[29]. Takenaka measured performance relative to MTOW and fuel block. Takenaka's approach used CFD and FEA with analytic comparisons to determine the best performance[25]. Maughmer used a modified crossover point to describe the performance as a function of weight, lift and drag[19].



Figure 1.7: The Global Hawk HALE (high altitude long endurance) UAV is built by Northrop Grumman and is used the by US Air Force. It has a wingspan of 130 feet and can carry a payload of 3,000 lbs. It is the largest production UAV currently in service.[27]

This helped to constrain the winglet geometries to parameters within performance limits. Maughmer’s cross-over point compares the change in drag, $\Delta D_{profile}$ and $\Delta D_{induced}$, of the wing with winglets to the wing with no winglets where:

$$\Delta D_{profile} + \Delta D_{induced} = 0 \quad (1.1)$$

There is a critical speed above which the cross-over point is exceeded and winglets are no longer beneficial[19]. For UAV design it is important to optimize the design for operational speeds well below the cross-over point. Calculating lift and drag forces as well as lift and drag coefficients help to fill in the equations used for evaluating performance. Range, endurance, and take off distance are just a few examples of the types of performance that can be evaluated, compared, and optimized. For a transcontinental airliner, range would be important. For a spy plane that needs to loiter over a geographic location, endurance would be critical. For a STOL vehicle, takeoff distance is an important performance parameter. When defining performance improvements it is important to specify what type of performance is most important.



Figure 1.8: The Predator UAV is manufactured by General Atomics. The Predator has a wingspan of 55 feet and can carry both internal and external payloads totaling more than 700 lbs. Nearly 200 Predators are in service.[27]



Figure 1.9: The ScanEagle UAV developed by Insitu has a wingspan of 10.2 feet. It is launched using a catapult system, so it doesn't need a runway.[13]

1.3 Objectives

To achieve the goals outlined in § 1.2, we have identified 3 objectives that are detailed below.

1.3.1 Develop a Design Methodology Based on VLM for Winglet Design

The first objective is to develop a design methodology for winglet design using the VLM, which is an extension of the Prandtl Lifting Line theory[3]. Tornado[20] is an



Figure 1.10: The Shadow UAV is manufactured by the AAI Corporation. The Shadow 200 has a wingspan of 20.4 feet, and like the ScanEagle, is launched using a catapult system.[30]

open source code developed to solve the equations of the vortex lattice method. It is the objective of this research to leverage the open source code of Tornado[20] and apply it to solving the equations of the vortex lattice method for winglet geometries. A design methodology based on Tornado and implemented using the GUIDE graphical user interface template in MATLAB is proposed. This methodology is called Pecos (for Pecos Bill the tornado tamer). Pecos will require the computing resources of only a single computer workstation running MATLAB. The Pecos methodology should offer greater flexibility and speed for narrowing the field of possible geometries to an optimum solution. The design methodology will focus on optimizing blended winglet designs. As Tornado defines wing geometry, separate partition definitions are required any time the wing changes dihedral, sweep, taper ratio, or twist. For a blended winglet, many partitions will need to be defined to describe the blended section of the winglet. In actuality, the blended section contains an infinite number dihedral angles, but in the proposed methodology, this will only be approximated using a finite number of dihedral angles. Eventually search algorithms can be used, such as GAs, to optimize a particular winglet design.

1.3.2 Design Winglets

Using the methodology described in the previous section, winglets will be designed for various UAV platforms. Parameters will be set for a starting point of each design, along with optimization goals for each design. Parameters may include maximum length, minimum cant, sweep angle restrictions, or overall height. Optimization goals will include maximizing L/D and minimizing the increase in the root bending moment of the main wing. Using a parametric approach, the winglet parameters will be analyzed using Pecos with the Tornado VLM. The results will then be plotted to determine the optimum design. A set of winglet designs for a notional UAV have been designed for performance comparison.

1.3.3 Test Winglet Models

Once the design for the winglets has been optimized in VLM, and modeled in CAD, physical prototypes will be built for testing and validation of VLM results. A wing with a blended winglet based on VLM optimization will be constructed and compared to the wing without the winglet, and a wing with a Whitcomb winglet. Various scales will be built for different diagnostics, including PIV, wake surveys, and force balance measurements. Test results will be compared to VLM results for comparison of C_L , C_D , and C_L/C_D .

1.3.4 Evaluate Selected Platforms and Determine Benefits of Winglet Designs

The design methodologies developed and tested for a notional UAV will be applied to existing UAV platforms. Pecos will be used to design and optimize winglets for the RQ7 Shadow UAV. Constraints will consist mainly of hypothetical geometric size restrictions. The optimization goal will be to increase L/D by as much as possible. Next, Pecos will be used to design and optimize winglets for the Predator UAV. Design

constraints will consist mainly of the additional overall length. The optimization goal will be to maximize C_L/C_D while restricting the increase in root bending moment of the main wing to a predetermined amount. Results from VLM models with optimized winglets will be compared to results from VLM models without winglets to determine the overall impact on estimated range and endurance.

1.4 Thesis Outline

The thesis outline is as follows:

- Methodology
 - Winglet Design
 - Vortex Lattice Method
 - Tornado
 - Pecos
- Wind Tunnel Testing
 - UWAL
 - PIV
- Results
 - VLM
 - UAV Performance Evaluation
 - Wind Tunnel Testing
 - * Vortex Dynamics Study
 - * Wing Configuration Study
- Continuing Work

- Conclusions

CHAPTER 2

Methodology

This chapter describes the approach used for designing winglets. There are several types of winglets that can be applied to an aircraft and each has many parameters which must be considered in the design. With these design parameters in mind, the vortex lattice method (VLM) will be used to evaluate each design. A methodology is built around the Tornado Vortex Lattice Method for the design and evaluation of winglet configurations for UAVs. The interface for the design and optimization is called Pecos and is described in detail. Wind tunnel testing will be used to validate results from the VLM. A 3/8 scale model of a notional UAV will be tested at the Kirsten Wind Tunnel at the University of Washington in Seattle, WA. Smaller scale models will be tested in the wind tunnels at Oklahoma State University in Stillwater, OK.

2.1 Winglet Design

The focus of this research is winglets that operate at much lower Reynolds numbers. As such, generic UAV requirements are used as a baseline based on typical Group 2 and Group 3 UAVs. The specific flight conditions are for velocity of 65 knots at an altitude of 10,000 ft. For the specific application, a swept and tapered wing with a tip chord of 18 inches is used for the base configuration, this results in a Reynolds number below one million. Winglet geometries investigated include straight Whitcomb type winglets as well as blended winglets. Blended winglet designs will be the main focus for optimization because they have been shown to provide up to 60%

improvement over conventional wingtips[11], and are prominent in wing tip design for major commercial aviation designs. Various airfoils are included in the investigation, including NACA 0009, Eppler 396, and Selig S9026. NACA airfoils help to validate and benchmark data, while other airfoils were selected for their performance at the Reynolds numbers being investigated. Winglet parameters that will be considered include: airfoil, root chord, taper ratio, sweep, cant, semi span, twist (toe-out/in), and blend radius. Fig. 2.1 illustrates the many parameters that define the winglet geometry.

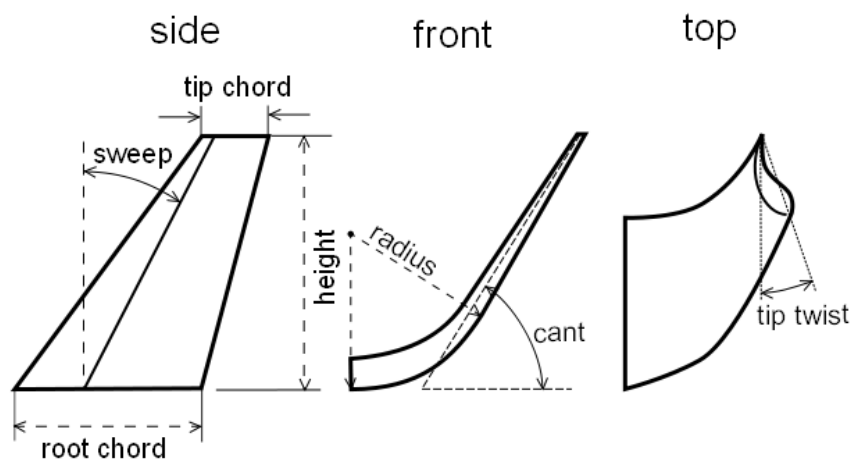


Figure 2.1: Parameters used to define the winglet geometry include: root chord, tip chord, sweep, height (length), radius, cant and twist.

A properly designed winglet will diffuse the vortex that is shed at the tip of the wing. The winglet must produce a side force in order to be effective.[29] The side forces reduce the inflow above the wing at the tip, and the outflow below the wing at the tip. The reduction in the inflow and outflow help to normalize the lift distribution along the entire span of the wing, just as a wing with a higher aspect ratio will have a more even lift distribution. A winglet should produce the same lift distribution as extending the length of the wing by 45% of the height of the winglet.[15] The winglet should cause the downwash over the surface of the wing to remain constant, with no sidewash.[15] By improving the flow of the downwash the lifting efficiency of the wing

is improved, and by diffusing the wingtip vortex the drag is reduced. Winglets can offer a great advantage when the wing span is limited or an existing wing must be modified for extended performance.

2.2 Vortex Lattice Method

The vortex lattice method is the foundation for the optimization methods that were used. Computer algorithms for solving the vortex lattice method were employed to determine the fitness of each design iteration. The underlying math and theory for the vortex lattice method and the algorithms used to solve the vortex lattice method are discussed in this section.

2.2.1 Vortex Lattice Theory

Vortex lattice theory is based on Prandtl's lifting line theory. Prandtl suggested that a fixed vortex filament would be subject to a force from the Kutta Jukowski theorem in eqn. (2.1). To determine the lifting force on a wing, Prandtl replaced the wing with a fixed vortex filament, and since a vortex cannot end in a fluid, Prandtl connected a vortex at each end that extend to infinity. Fig. 2.2 shows how the horseshoe vortex replaces the wing. The combination of vortices is known as a horseshoe vortex[3]. The downwash created by the fixed vortex along the span of the wing could be determined using eqn. (2.2), where the vortex along the wing is located from $-b/2$ to $b/2$. For a more precise calculation of the lift along the span of the wing, more horseshoe vortices can be added, each with a span less than the previous. Extending the number of horseshoe vertices results in the integral form of the induced velocity along the span of the wing eqn. (2.3), then the lift can be calculated as the integral over the span of the wing eqn. (2.4).

$$L' = \rho_{\infty} V_{\infty} \Gamma \tag{2.1}$$

$$w(y) = -\frac{\Gamma}{4\pi} - \frac{b}{(b/2)^2 - y^2} \quad (2.2)$$

$$w(y_0) = -\frac{1}{4\pi} \int_{-b/2}^{b/2} \frac{(d\Gamma/dy)dy}{y_0 - y} \quad (2.3)$$

$$L = \rho_\infty V_\infty \int_{-b/2}^{b/2} \Gamma(y)dy \quad (2.4)$$

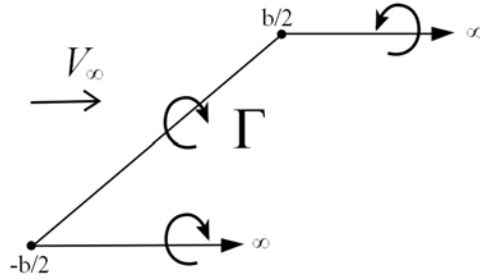


Figure 2.2: The Prandtl lifting-line theory uses a horseshoe vortex to calculate the lift produced by the wing.[3]

$$V = \frac{\Gamma}{4\pi h} \quad (2.5)$$

The vortex lattice theory[3] begins with a basic two dimensional definition of the wing geometry then superimposes a grid on top of the wing. For each square in the grid there is a control point and a horseshoe vortex. The velocity at the control point is deduced by applying the Biot-Savart law, eqn. (2.6), to each segment of the horseshoe vortex that surrounds the control point. The Biot-Savart law eqn. (2.6) describes the strength of each vortex line in the horseshoe. From the strength of each vortex the velocity at the control point can be determined using eqn. (2.7). The boundary condition, eqn. (2.8), stipulates that the flow must be parallel to the surface. These equations are placed in a matrix corresponding to their location in the lattice across the surface of the wing. Computer algorithms are able to solve these

matrices quite efficiently. The code used to solve the equations of the vortex lattice method in this research is Tornado[20].

$$\mathbf{dV} = \frac{\Gamma}{4\pi} \frac{\mathbf{dl} \times \mathbf{r}}{|\mathbf{r}|^3} \quad (2.6)$$

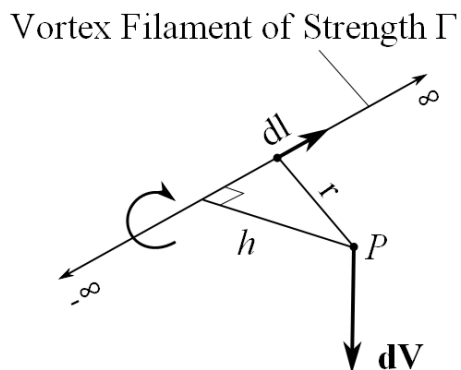


Figure 2.3: A vortex filament induces a velocity in the space surrounding it.[3]

$$V = \frac{\Gamma}{4\pi h} \quad (2.7)$$

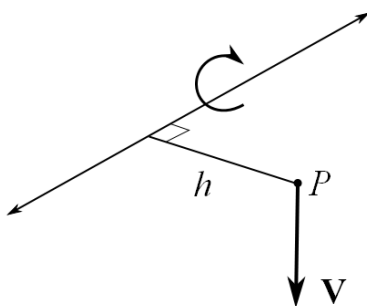


Figure 2.4: The velocity at point P can be determined by Γ and h . [3]

$$\mathbf{b} = v_{\infty} \sin(\alpha) \quad (2.8)$$

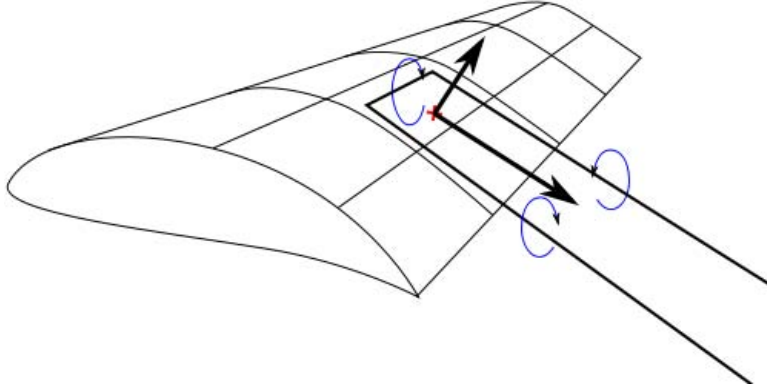


Figure 2.5: The wing is divided into a grid. For each section of the grid, there is horseshoe vortex filament with strength Γ placed at the $1/4$ chord, and a collocation point placed at the $3/4$ chord. The flow tangent to the surface at the collocation point must be equal to zero.

2.2.2 Tornado

Tornado is an open source program written in MATLAB by Thomas Melin[20]. Tornado is a solver for the Vortex Lattice Method. The power of Tornado lies in its robust wing geometry definition. The parameters that can be defined for wings in Tornado include span, root chord, taper ratio, sweep, dihedral, root airfoil, tip airfoil, root twist, tip twist, x, y and z location. Tornado can also include flaps for control surfaces which can be set to different angles. Fig. 2.6 shows how wings can be defined using Tornado. Using multiple partitions for a wing allows variable sweep and taper ratio along a single wing. In this example, a wing has even been defined to represent the fuselage of the plane. Because it is open source, Tornado is easily modified to automate the geometry generation and computations for parametric analysis. Tornado is written in MATLAB, so it works equally well on any computer that supports MATLAB. The power of MATLAB lies in its ability to solve sets of equations in matrix form. In this way it is a perfect platform for dealing with problems like vortex lattice theory, which use a matrix to represent the mathematics of the problem.

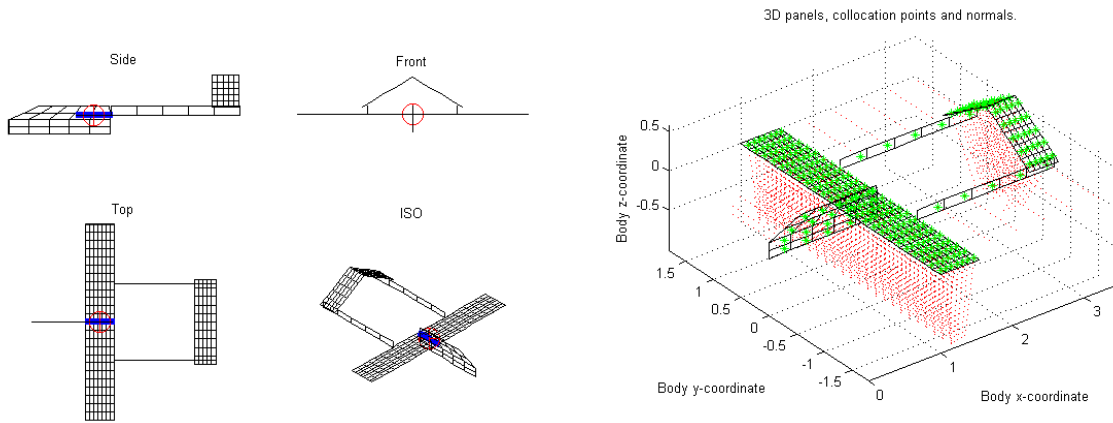


Figure 2.6: The wing geometry for the RQ7 Shadow 200 modeled in Tornado VLM for MATLAB. On the left are the side, front, top and isometric views of the wings with partitions, panels, MAC, and reference point. The figure on the right shows the model with the collocation points associated with each panel.

2.2.3 Pecos

Tornado is very capable at solving the vortex lattice method, however it is not especially user friendly. In an effort to make Tornado more user friendly, the author programmed a graphical user interface using the GUIDE tool in MATLAB. The graphical interface is called Pecos (short for Pecos Bill, the Tornado Wrangler). Pecos was designed to automate some of the basic data inputs required for geometry and state definition as well as provide an immediate feedback to the user for each change made to the geometry. Pecos links the user to all the functions of the Tornado program without the need to navigate various menus and commands. The main window for Pecos holds the root level commands for Tornado. These include: Geometry, State, Processing, and Post Processing. From the main window, the user can see which geometry file is currently open, as well as the current state, and current Job ID. By selecting “Geometry”, a window is opened with the interface for opening, creating, or editing the desired geometry. With the original Tornado program, once the state was defined, the user had no way to go back and see what the current state settings were,

however with Pecos, the user need simply to click on the “State” button and if a state is defined, all the parameters will be displayed. Like Tornado, states can be created, opened, and saved. Unlike Tornado, there is a useful tool for any unit conversions that the user might need to carry out to obtain the standard units used by Tornado. Using the unit converter, lengths and speeds can be converted from multiple SI and English units to meters per second or knots. Likewise, length units can be converted to meters or feet. The converted values can even be copied directly to the “State” setup window.

2.2.4 Pecos: Getting Started

The Main window for Pecos displays four individual steps for completing a vortex lattice calculation. The first step is to define the geometry. The second step is to define the state. The third step is to complete the desired type of processing. Finally, the fourth step is Post Processing, where the data can be graphed and analyzed.

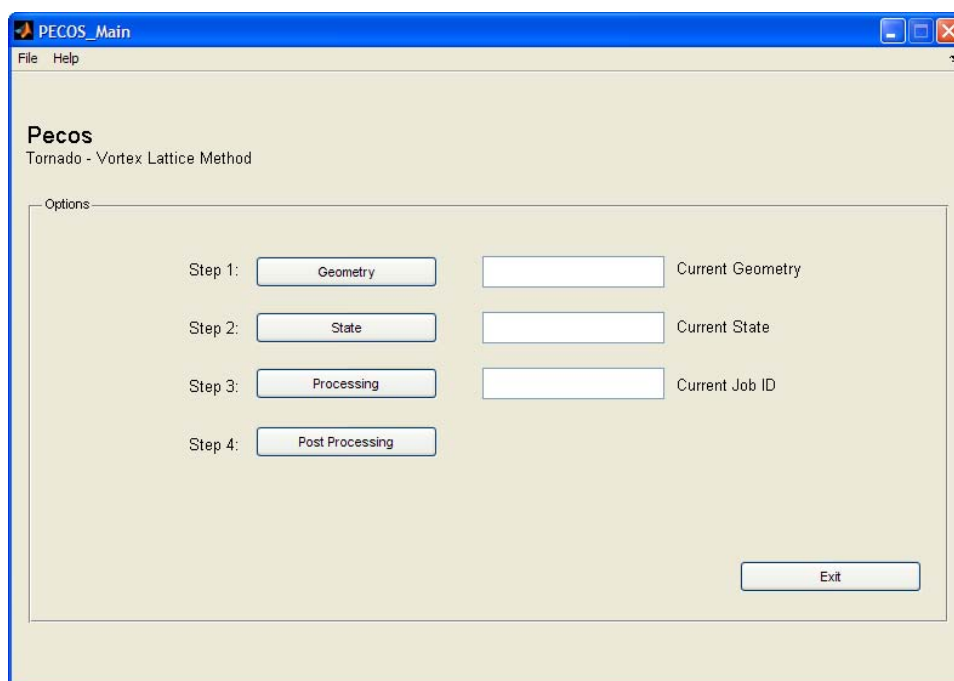


Figure 2.7: The PECOS Main window for includes 4 buttons, one for each step: Geometry, State, Processing, and Post Processing.

2.2.5 Pecos: Step 1 - Geometry

The first step is to define the geometry. The geometry can either be created or an existing geometry can be opened. Once the geometry is defined, the name of the file that contains the geometry definition will appear in the box labeled “Current Geometry”. By clicking the “Geometry” button, a new window is displayed. The “PECOS Geo” window is where all the parameters can be defined, or a geometry file can be opened.

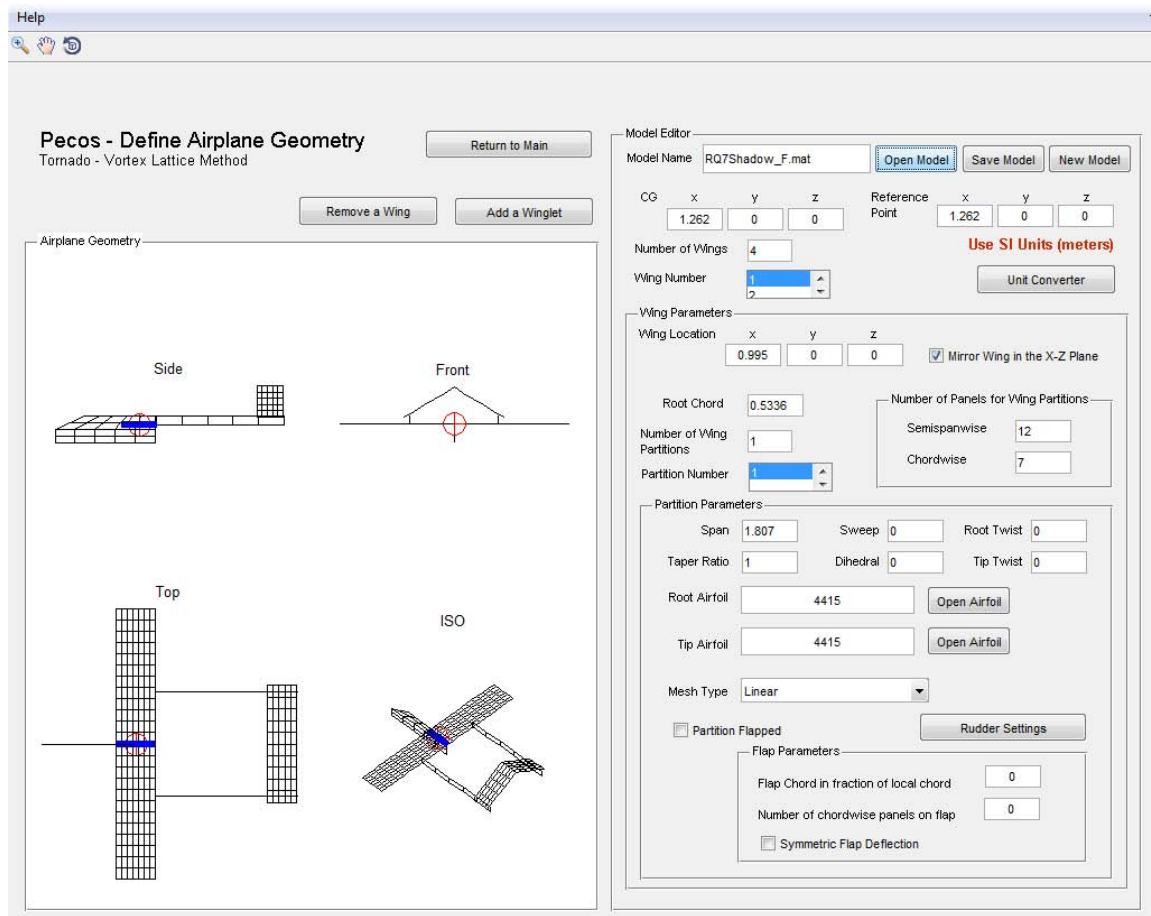


Figure 2.8: The PECOS Geo window contains all the necessary controls to input the data for every geometry parameter.

Most of the parameters are self explanatory, with a few caveats. For example when defining the center of gravity, reference point, and wing location it is important to

remember that Tornado uses a backwards Cartesian coordinate system compared to most standard methodologies. That is to say, (in Tornado) X is positive from forward to aft, and Z is positive in the up direction. This means that Y is still positive in the starboard direction. Also of note, Tornado uses SI units for defining the geometry. All units should be input in meters. If all of your measurements are in units other than meters, do not fear, Pecos includes a handy unit converter application that is easily accessed by clicking the “Unit Converter” button. Units for angles are in degrees. On the left side of the window the current geometry configuration is displayed. Each of the views can be manipulated by selecting the magnifying glass, hand, or rotate icon from the top left corner of the window. Selecting the magnifying glass then clicking and dragging on one of the four views, will zoom in or out, making the image larger or smaller. Selecting the hand allows the user to pan the view of the model, moving the model left, right, up, or down within the preview window. Selecting the rotate icon allows the user to rotate the geometry for viewing from different angles. There are three buttons above the preview window: Return to Main, Remove a Wing , and Add a Winglet . The first button, Return to Main closes the PECOS Geo window and returns the user to the main window of Pecos, where the user can continue to the second step. The Remove a Wing Button will remove the last wing added to the geometry. The Add a Winglet Button opens the window with options for generating blended winglet geometries. See the section: Winglets, for more information.

Loading, Saving, New Geometry

In order to open a geometry file, click the Open Model button. A dialog containing all available geometries will be displayed, from which the desired file can be selected. Tornado relies on a set file hierarchy, so the user cannot change the location from where the geometry is opened or to where the file is saved. Once a file is opened, the file name appears in the Model Name text box. This text can be changed to save to

a different file name. If the user has a file open and wants to start a new geometry, simply click the New Model button. The geometry will return to a single wing.

CG and Reference Point

As mentioned before, when inputting the X, Y, Z coordinates for the center of gravity and the reference point, just remember that X is positive from fore to aft and Z is positive in the up direction. The CG just defines the location of the center of gravity relative to the geometry of plane. The reference point is the point about which Tornado makes all its calculations. Generally placing the reference point at the CG is a good rule of thumb, unless moments are needed about some other point.

Number of Wings

Inputting a number in the text box for Number of Wings then pressing enter, will automatically generate the desired number of wings. To select an individual wing to edit, simply select the desired wing number from the Wing number drop down list, located directly below the Number of Wings text box. This drop down is automatically changed to reflect the current number of wings. Tornado assumes that the first wing, wing number one, is always the main wing, and it is this wing geometry that is used for determining wing span, wing area, etc. when calculating coefficients.

Wing Parameters

For each wing, the specific geometry can be input in the Wing Parameters section. Each time a different wing is selected from the Wing Number drop down list, the Wing Parameters section will be updated to reflect the values of that individual wing.

Wing Location

The Wing Location defines the X,Y,Z coordinate of the leading edge of the root of the wing.

Mirror Wing in the X,Z plane

By default the check box for Mirror Wing in the X,Z Plane is selected. Since most planes have symmetric wings. However, this option can be deselected for defining the geometry of the vertical stabilizer, or for other asymmetric configurations.

Root Chord

The text box for Root Chord defines the chord length at the root of the wing.

Number of Wing Partitions

Tornado can break the wing into multiple partitions if the geometry is not constant along the wingspan. Each section can have a different span, dihedral, sweep, taper ratio, twist, and even different airfoils. This allows for complex wing geometries. Entering a number greater than one will generate the desired number of partitions for the current wing. Each partition can then be individually selected and edited using the Partition Number drop down list.

Panels

For each partition, the number of chord wise and span wise panels must be entered. The panels are the heart of the vortex lattice method. More chord wise panels will capture the camber of the airfoil more accurately, but will require more time for processing. Likewise, more span wise panels will more accurately calculate effects from taper, sweep, dihedral and twist. Though even if the wing is just rectangular there will still need to be a minimum number of partitions for the best results. Tornado can

determine the optimum number of partitions, this feature is found in the Processing section.

Partition Parameters

For each wing partition, the user can enter values for the span, taper ratio, sweep, dihedral, root twist, tip twist, root airfoil and tip airfoil. The chord length is calculated using the value entered for the root chord, which is the length of the root chord of the first partition, and the taper ratio of the previous/current partition. Default values of zero angles are entered for each new partition's sweep, dihedral, root/tip twist angles.

Airfoils

By clicking the Open Airfoil button, the user can select one of many airfoil data files that come with Tornado. New airfoil data can be created using data from a source such as the airfoil coordinates database at UIUC (http://www.ae.illinois.edu/m-selig/ads/coord_database.html). They must be saved in the Aircraft/Airfoil folder as .dat files. The coordinates must also be ordered from the leading edge to trailing edge for upper wing surface first, then again from the leading edge to the trailing edge for the lower wing surface. Separate airfoils can be loaded for the root and tip sections of each partition.

NACA Airfoils

As an alternative to loading coordinates for an airfoil, Tornado recognizes NACA four digit airfoil codes. By simply typing the NACA four digit code for an airfoil, Tornado can calculate the chamber of each airfoil.

Mesh Type

In the Mesh Type drop down list, see fig. 2.9, there are four options for the mesh type. These options control how the mesh is divided along the surface of the wing. The default option is linear. A linear mesh divides the surface into even an even grid as can be seen in fig. 2.10. The second option is span wise half-cosine. This is illustrated in the second wing in fig. 2.10. Span wise half cosine will divide the mesh into even parts chord wise, but will apply an increasing finer grid outward along the span of the wing. The Span wise half cosine, chord wise cosine option will apply a fine grid to the leading edge and trailing edge of the wing with a coarser grid in the center section. The grid will be increasingly finer outward along the wing span, as illustrated in the third wing in fig. 2.10. Span wise cosine, chord wise cosine will apply a finer grid along all the edges of the wing with a coarser grid in the center of the wing, this option is illustrated in the right most wing in fig. 2.10. These options allow for faster processing without sacrificing detail in the more complex regions of the geometry.

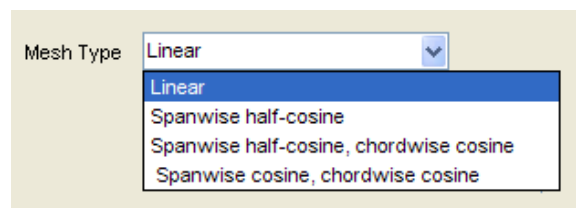


Figure 2.9: The Mesh Type drop down list includes options for: Linear, Span wise half-cosine, Span wise half-cosine Chord wise cosine, and Span wise cosine Chord wise cosine.

Partition Flapped

The final section in the partition parameters is for flapped partitions. This allows for the integration of ailerons, rudders, trim tabs etc. In other words, any part of the

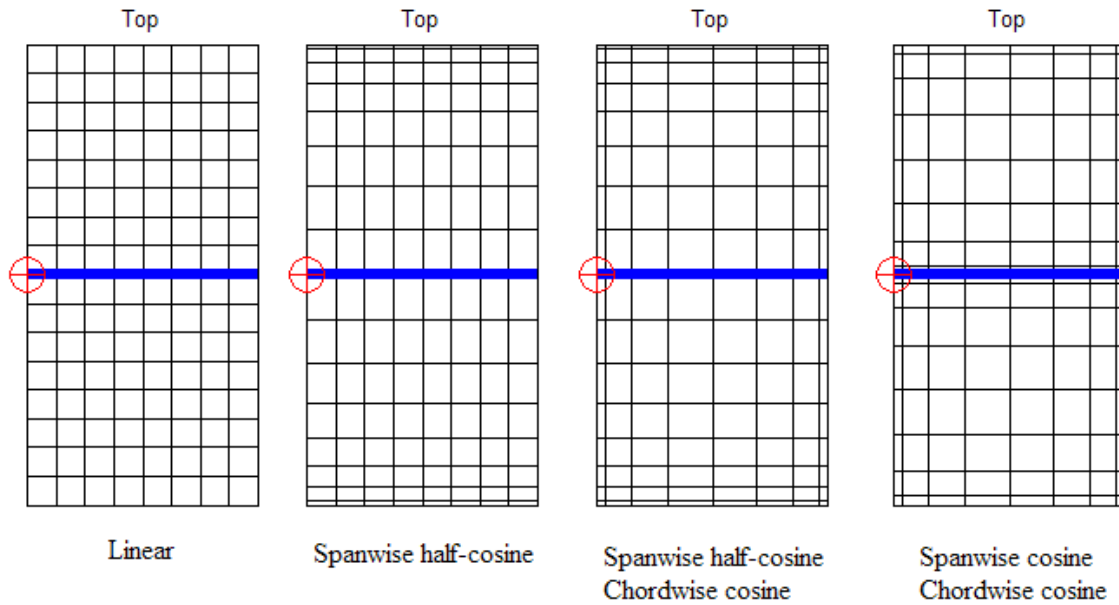


Figure 2.10: The four different types of panel distributions available in Tornado. The panels are configured slightly differently for each option, as can be seen in these top views of the wings. In each of these configurations there are eight panels span wise and eight panels chord wise for each wing.

wing that moves. This is useful for determining the effect of changes in the control surface on the dynamics of plane. The Flap Chord in fraction of local chord lets the user determine how large the flap is in the chord wise direction. The flap will span the entire length of the wing partition, so multiple wing partitions will be required if flap does not span the entire wing. The number of chord wise panels determines the grid detail for each flap. Finally, Tornado can apply symmetric or asymmetric flap deflection. If the wing is mirrored in the XZ plane, there will be a flap on each wing, but they do not need to move symmetrically.

2.2.6 Pecos: Winglets

The most unique feature of Pecos is the winglet feature. The winglet generator generates blended winglets. To generate blended winglets a wing is defined with

many partitions, each partition has a slightly different dihedral angle. In Tornado this would be a tedious and painstaking task to enter the geometry for each specific segment. With Pecos, the geometry for each partition is generated automatically from just a few parameters. To access the winglet generator, from the PECOS Geo window, the user can click the button: Add a Winglet , and the PECOS Winglets window will appear. This window has a preview of the geometry on the left side, the same as the PECOS Geo window. Instead of options for wing geometry, there are options for blended winglets. At the top of the Winglet Editor is the name of the file for the current geometry. Next to this text box there is a button to save the geometry. An existing wing can be selected from the Winglet Wing Number list, or a new wing can be added for the winglet geometry. By clicking the Add a Wing for the Winglet button a wing will be added to the geometry and the new wing number will be highlighted in the Winglet Wing Number list. The location for the new wing is automatically placed at the tip of the main wing (wing number one). The root chord of the winglet is automatically set to the length of the tip chord of the main wing. Other parameters are left in their default state.

Winglet Location

Winglet location can be edited using the X,Y, and Z text boxes under Wing Location in the Winglet Parameters section. Though these values are not reflected in real time, they can be easily updated by clicking the Generate Winglet button at the bottom of the Wing Parameters section.

Total Length

The length of the winglet, is the length of the winglet from the root span wise along the radius to the tip. Should the Total Length be greater than the arc length of the blend radius, a straight section of winglet will be placed beyond the arc. In fig. 2.12

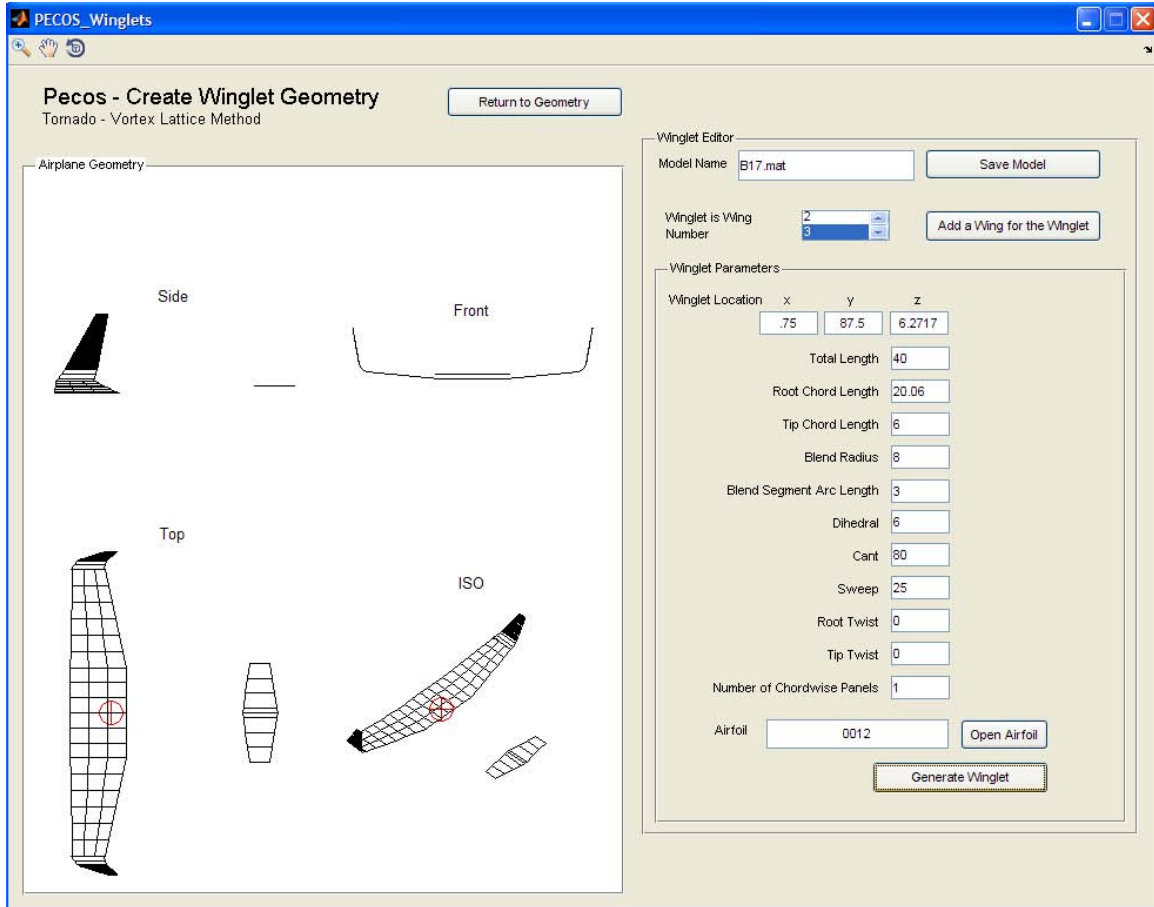


Figure 2.11: The PECOS Winglets window contains the controls for automatic blended winglet geometry generation..

The total length would be the blend radius times 69 degrees plus the length of the winglet beyond that.

Winglet Chord Length

In the winglet generator, the root chord length of the winglet is entered the same way as in the wing parameters. The tip chord length, however, is entered manually, as opposed to entering a taper ratio. If a new wing is added in the winglet generator, the root chord length of the winglet will automatically be set to the length of the wing tip chord.

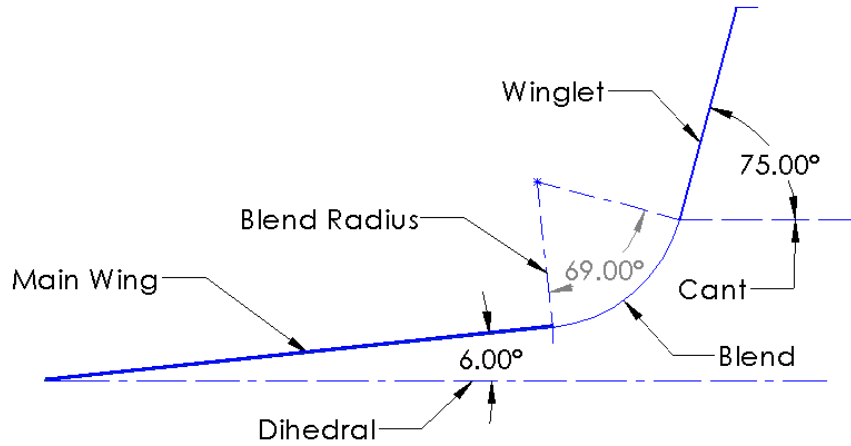


Figure 2.12: A diagram of the different geometric parameters and how they are defined for the winglet geometry. In this figure are the wing, winglet, dihedral, cant, and blend radius

Blend Radius and Segment Arc Length

The root of the winglet has the same dihedral as the tip of the wing, then gradually increases along the specified radius. By increasing the radius of the blend, the winglet will have a more gradual change in dihedral. Entering a radius of zero will result in an straight winglet at the end of the wing, similar to the winglets Whitcomb[29] experimented with. The segment arc length determines the length of each partition along the radius of the blended section of the winglet. The number of partitions along the blend radius will be equal to the arc length of the blend radius divided by the segment arc length. Shorter segments, means more partitions for more accurate results such as in fig. 2.14, but longer computational time. To calculate the dihedral angle for each segment, the total angle of the blend, θ_b , is calculated using eqn. (2.9), θ_b is the difference between the cant angle, θ_{cant} and the dihedral angle at the root of the winglet, $\theta_{dihedral}$. The number of panels used to define the blended section of the winglet is determined by eqn. (2.10). The number of panels, N_{panels} is equal to the blend radius, r_b , multiplied by the blend angle, θ_b , and divided by the length for

each partition segment, $b_{segment}$. Then the dihedral for partition i is calculated using eqn. (2.11).

$$\theta_b = \theta_{cant} - \theta_{dihedral} \quad (2.9)$$

$$N_{panels} = \frac{r_b * \theta_b}{b_{segment}} \quad (2.10)$$

$$\theta_{panel_i} = \frac{\theta_b}{N_{panels}} * i \quad (2.11)$$

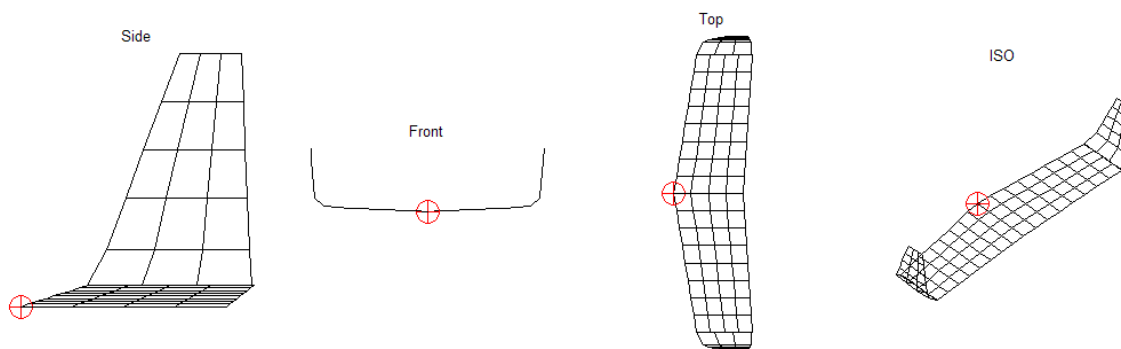


Figure 2.13: The arc segment for this winglet is set to 0.5 meters, while the blend radius is set to 0.75 meters. A segment length of 0.5 meters is very coarse and results in large angles between the each segment.

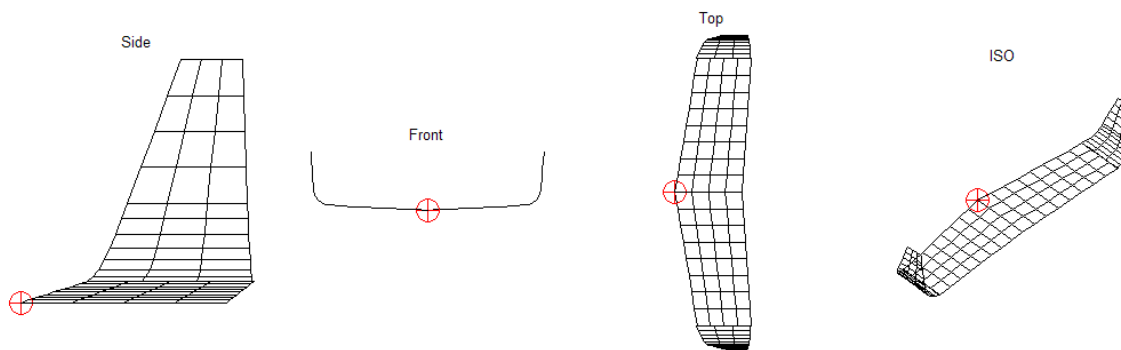


Figure 2.14: Using the same dimensions for the winglet as in fig. 2.13, but setting the segment length to a shorter 0.15 meters, the blend of the radius is better defined, with smaller angles between each segment of the arc.

Winglet Dihedral and Cant

The dihedral measures the dihedral angle of the root of the winglet. If a new wing is added in the winglet generator, this value is automatically set to the dihedral of the main wing tip, but can be changed to user specifications. The cant is the angle of the tip of the winglet, sometimes cant is measured from the vertical position, however, in this application, the angle is defined from the horizontal plane to be consistent with the dihedral angle. This way, the program can define the angle of the blend as eqn. (2.9).

Other Winglet Parameters

In the Pecos winglet generator, the sweep, root twist and tip twist work the same as in the main wing parameters. The twist per unit length θ_t , is calculated using eqn. (2.12), where \mathbf{T}_{tip} is the twist angle at the tip of the winglet, \mathbf{T}_{root} is the twist of the airfoil at the root, and b is the span of the winglet. For a blended winglet, \mathbf{T}_{root} might be set to the tip twist of the main wing to which the winglet is attached. For a Whitcomb winglet, \mathbf{T}_{root} would be the toe-out angle. For each section of the winglet that is generated, the root twist for partition i is $\mathbf{T}_{i,1}$, and is set to the tip twist of the previous partition, $\mathbf{T}_{i-1,2}$, unless $i = 1$, then $\mathbf{T}_{i,1}$ is set to \mathbf{T}_{root} . To set the twist at the tip of each partition in the winglet, $\mathbf{T}_{i,2}$ is calculated using eqn. (2.14). Eqn. (2.14) adds the twist per unit length, θ_b , multiplied by the span of the section, b , to the root twist of the partition i . If a new wing is created in the winglet generator, the root twist will automatically be set to match the twist of the tip of the main wing. Likewise, the number of chord wise panels works the same as before. A separate partition is created for each arc segment of the blended radius of the winglet so it is not possible to assign a separate airfoil to the root and tip of the winglet. For this reason only a single airfoil may be selected for the entire span of the winglet. If it is necessary to enter a different winglet for the tip, each partition

of the winglet can be edited manually after returning to the PECOS Geo window.

$$\theta_t = \frac{\mathbf{T}_{tip} - \mathbf{T}_{root}}{b} \quad (2.12)$$

$$\mathbf{T}_{i,1} = \mathbf{T}_{i-1,2} \quad (2.13)$$

$$\mathbf{T}_{i,2} = \mathbf{T}_{i,1} + \theta_t * b \quad (2.14)$$

Generate Winglet

After entering all the desired parameters for the winglet, simply click the Generate Winglet button. All of the geometry will be calculated and displayed in the preview window on the left side. This button can be clicked at any point during the winglet parameterization process to see the results of each input. Should the results need to be changed, simply edit the desired parameter and click the Generate Winglet button again to see a preview of the resulting geometry. Once the user is satisfied with the results, it is recommended that the model be saved using the Model Name text box and Save Model button. This will save the geometry of the entire model as well as all of the parameters for the winglet. This is important if the user wishes to use the batch process feature to generate and evaluate multiple variations of the winglet geometry.

2.2.7 Pecos: Step 2 - State

The user can open a saved state file, save the current state to a file, or reset the parameters to start a new state.

Angle of Attack

In the section titled Angle of Attack, the value for the pitch angle can be entered in the text box labeled Alpha, in units of degrees. The side sweep angle, or Yaw angle

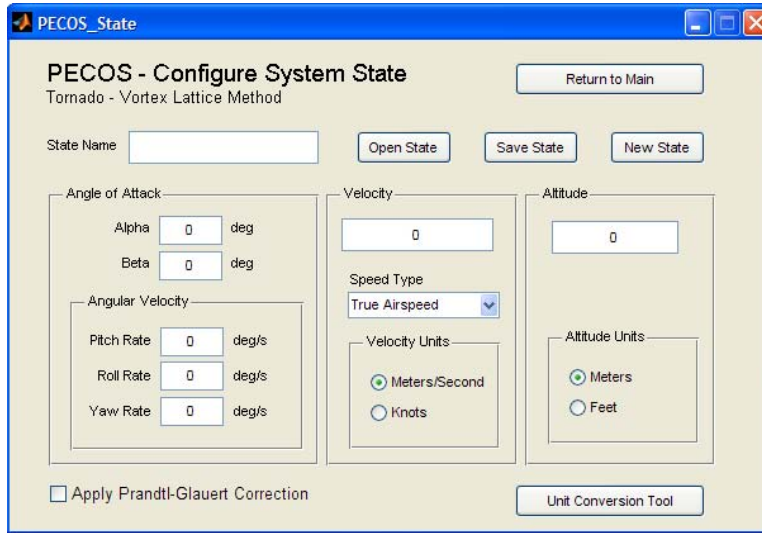


Figure 2.15: The PECOS State window allows the user to input the flight conditions to evaluate the aerodynamic performance of the model. The user can adjust the angle of attack, speed, and altitude.

can be entered in the text box labeled Beta. Angular velocities may also be entered for Pitch, Roll and Yaw rates. These are entered in units of degrees per second.

Velocity and Altitude

To enter a value for velocity, simply type the number in the text box in the velocity section. In the center of the velocity section is the Speed Type drop down list. Fig. 2.16 shows the options available in this list. The speed type can be true airspeed, equivalent airspeed, calibrated airspeed or Mach number. It should be noted that Tornado is a purely subsonic calculator, and will not calculate forces and moments for a Mach number greater than 0.3. At the bottom the velocity section, the user can select whether this value is in knots or meters per second. The section on the right hand side of the State window is for entering the value for the altitude. Tornado accepts inputs in either meters or feet for the altitude.

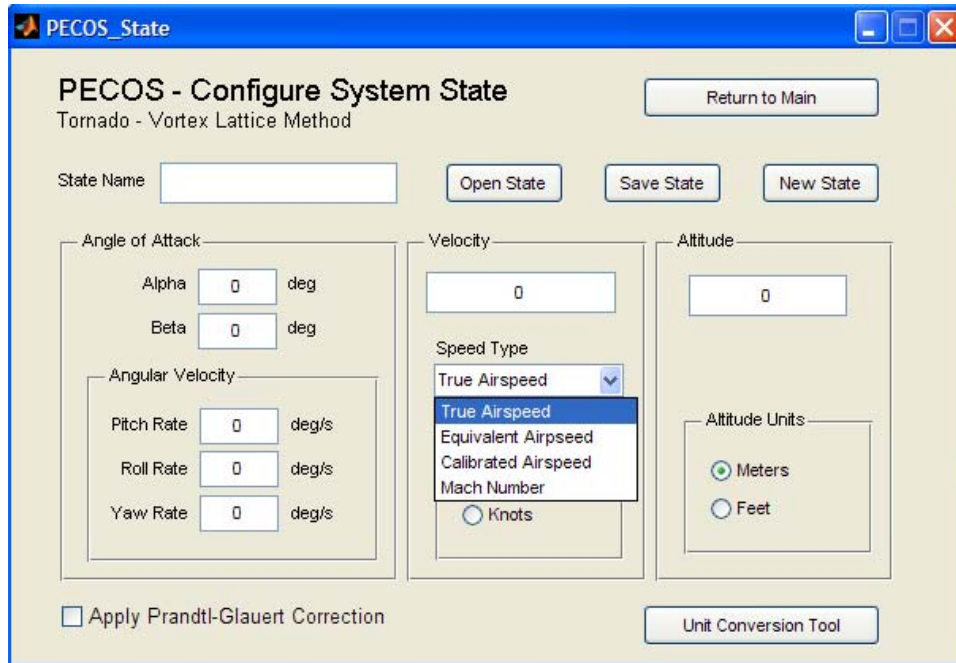


Figure 2.16: There are four options for speed type in the Speed Type drop down list: True Airspeed, Equivalent Airspeed, Calibrated Airspeed, and Mach Number.

Unit Conversion Tool

Should the user have units for velocity and or altitude in something other than what is listed in the PECOS State window, there is a unit conversion tool conveniently located at the bottom of the window. Simply click the Unit Conversion Tool button, and a new window will appear with options for converting units to meters per second or knots for the velocity and to meters or feet for the altitude, see fig. 2.17. On the left side the desired units for the input are selected from a drop down list, see fig. 2.18. Velocity can be input in units of kilometers per hour, meters per second, miles per hour, feet per second or knots. These units are then converted to either meters per second or knots. The units for altitude can be input as either kilometers, metes, miles, feet or inches, see fig. 2.18. Then output to either meters or feet. On the right side of the unit converter window there are options to copy either one or both of the new values to their respective text boxes in the PECOS State window.

Or by clicking the Cancel button, the new values can be disregarded.

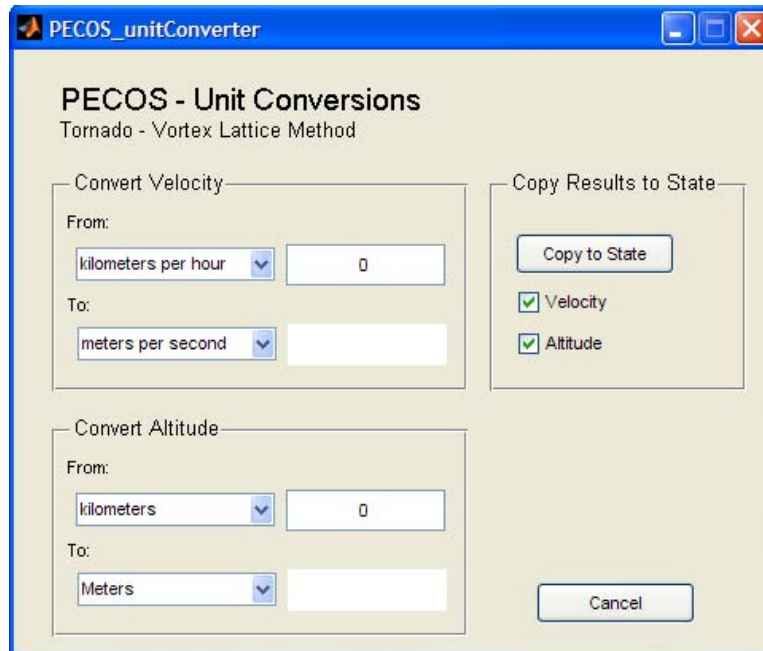


Figure 2.17: The unit converter can make conversions for the speed and altitude settings of the state.

2.2.8 Pecos: Step 3 - Processing

The Pecos processing window, see fig. 2.19, contains all of the standard processing options available with Tornado. These are the options on the left hand side of the window. While Tornado has batch processing capabilities, Pecos has automated the batch process. The Batch processing features are on the right hand side of the PECOS Processing window. Before processing can be started a Job Identity (JID) must be entered in the Job Identity text box at the top of the PECOS Processing window. This is the name that will be given to the file where the results are stored. By clicking the Simple Solution button Tornado will perform a vortex lattice method calculation on the current geometry and state just as they are. This is the backbone for most of the Tornado calculations. Once a simple solution is completed, the results can be viewed in the Post Processing section. The simple solution provides calculations for

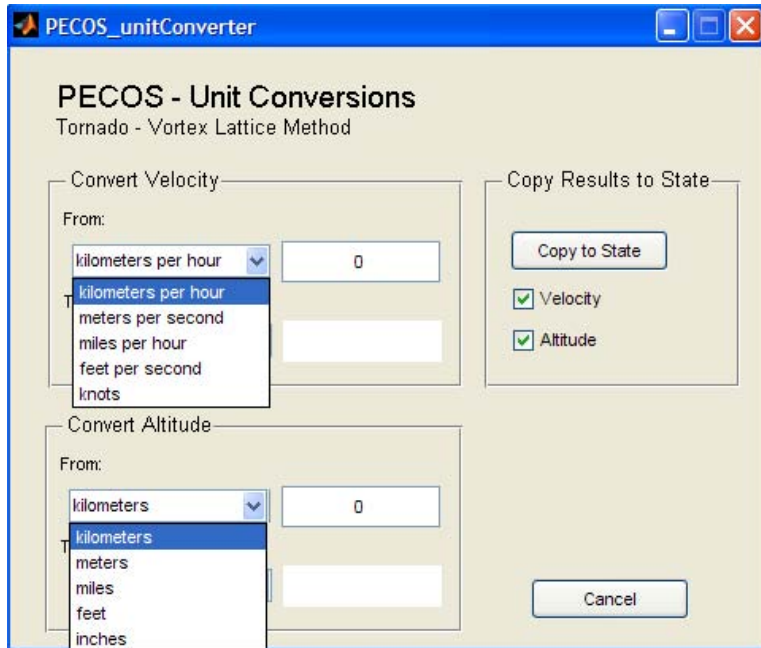


Figure 2.18: Inputs for speed can be kilometers per hour, meters per second, milers per hour, feet per second and knots, While inputs for altitude include kilometers, meters, miles, feet, and inches.

lifting forces, drag forces (induced by lift), moments, and coefficients for every axis (X,Y,Z). While these calculations do not include effects from thickness or viscous effects, they still provide excellent results for designing and optimizing the plan form of an airplane.

Sweep Calculations

The first processing feature is the sweep calculations. Tornado can perform as series of computations varying a single parameter in the angle of attack. Sweeps include: Alpha, Beta, Pitch Rate, Yaw Rate, and Roll Rate. The user selects the desired angle to sweep, then enters a starting angle, or angular rate, then the amount to increment the angle for each iteration, and finally the End Angle. By entering a smaller number in the Angle Increments box, more iterations will be computed.

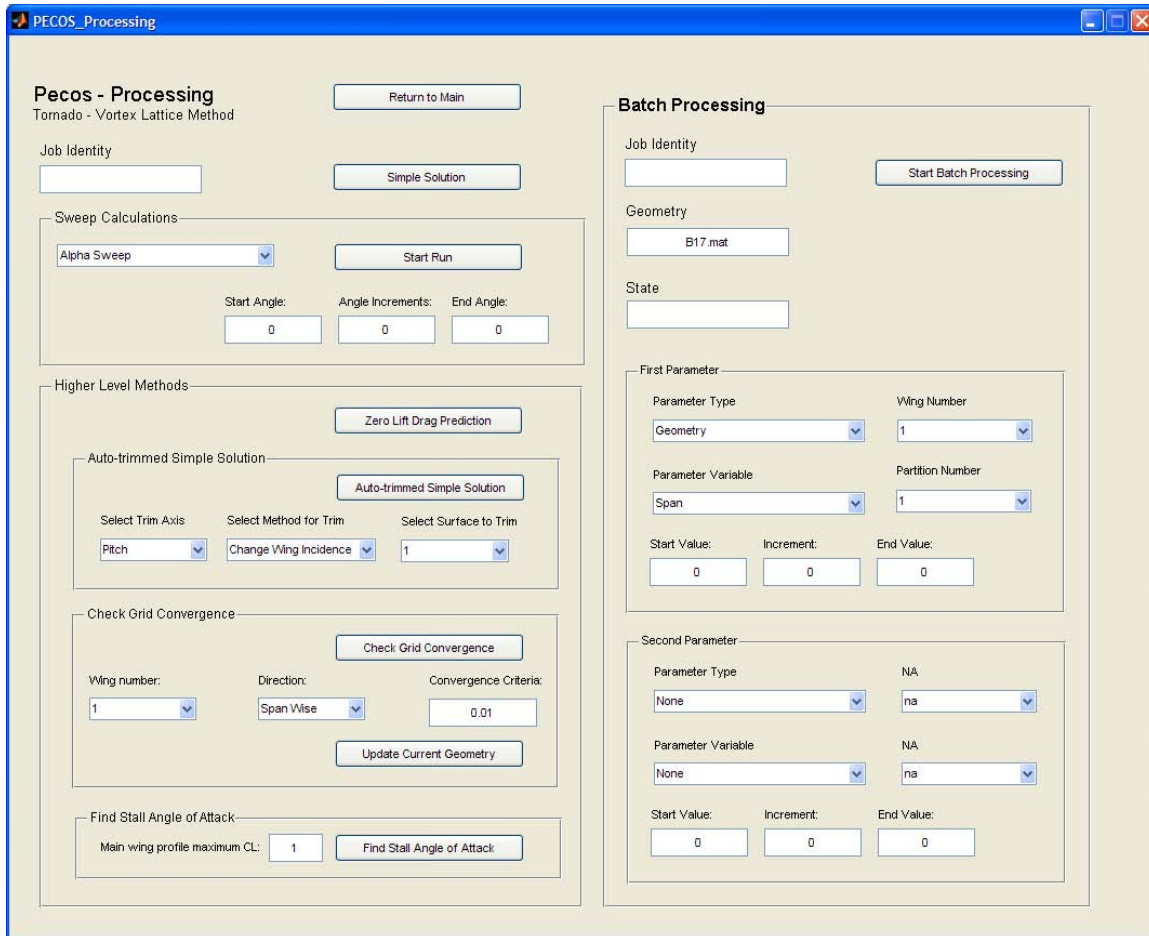


Figure 2.19: The PECOS Processing window contains options for various type of calculations to be performed using the Tornado Vortex Lattice Method.

Higher Level Methods

The first of the higher level methods that is standard to the Tornado, Vortex Lattice Method, is the Zero Lift Drag Prediction. There are no options for this feature, simply click the Zero Lift Drag Prediction button. Tornado uses the velocity and altitude settings from the state to determine the angle for zero lift, then approximates the viscous forces acting on the surfaces of the defined geometry. Remember, this is only an approximation. These results can be coupled with the forces calculated for drag due to lift for better estimates of airplane performance.

Auto Trimmed Simple Solution

Next in the Higher level-methods is the Auto-trimmed simple solution. This is similar to the Simple Solution in that it uses the only the setting from the current state. The difference is that Tornado will adjust the selected trim axis using the selected method. The axis can be pitch, roll, or yaw. The available methods are Changing the Wing Incidence, or Attitude of an Effector (Control Surface or Rudder). Then the specific wing or effector can be selected from the Surface to Trim drop list. This list is automatically populated by the available wing numbers or rudder numbers.

Check Grid Convergence

The Check Grid Convergence routine will adjust the number of panels, either chord wise or span wise for the selected wing. Tornado will compare each iteration with the last until the results deviate by less than the Convergence Criteria. Once convergence is reached, the current geometry can be updated to reflect the optimum number of grid sections.

Batch Processing

On the right hand side of the PECOS Processing window is the Batch Processing section. The user can adjust a single parameter or two parameters at a time. In the First Parameter section, the user first selects the Parameter Type. Types include: Geometry, State, and Winglet. Once the desired type is selected, the Parameter Variable list box is populated with the corresponding set of variables. The batch variables that can be selected for geometry are: Span, Root Chord, Taper Ratio, Sweep, Dihedral, Root Twist, Tip Twist, X Location, Y Location, Z Location, CG X, CG Y and CG Z. Variables for state that can be selected are: Airspeed, Angle of Attack, Sideslip Angle, Roll Rate, Pitch Rate, Yaw Rate, and Altitude. The angles and angular rates here, work the same as the sweep functions in the regular

processing section. However in the batch processing section they can be coupled with other variable. For winglet optimization, the user can adjust the X Location, Y Location, Z Location, Length, Root Chord, Tip Chord, Radius, Segment Arc Length, Dihedral, Cant, Sweep, Root Twist, and Tip Twist. In order to use the Winglet batch processing, a winglet must be defined for the current geometry. When the winglet parameters are entered into the Winglet generator of the geometry section of Pecos, the parameters are saved to a file with the same name as the geometry file. The parameters contained in this file, will be used during the batch processing to define each iteration of the winglet geometry along with the variable defined the batch processing. If the current geometry does not have an associated winglet geometry file, the winglet batch processing will not work.

2.2.9 Pecos: Step 4 - Post Processing

The final step is Post Processing. This is where Tornado and Pecos graph the results from the Processing step. Fig. 2.20 shows the PECOS PostProcessing window. At the top of the post processing window the current geometry and current state files are listed. To see the current geometry, click the Plot Geometry button. This displays the geometry and trailing vortex lines, the collocation points and vectors, the center of gravity and reference point. The Derivative Definitions button will display the the values that are calculated by Tornado as well as the orientation of the axis definition. The standard Tornado Post Processing functions are on the left side of the window. If the current JID (Job Identity) Name is not listed in the JID Name box, the user can click the Open Output File button and a window will appear with a list of available output files.

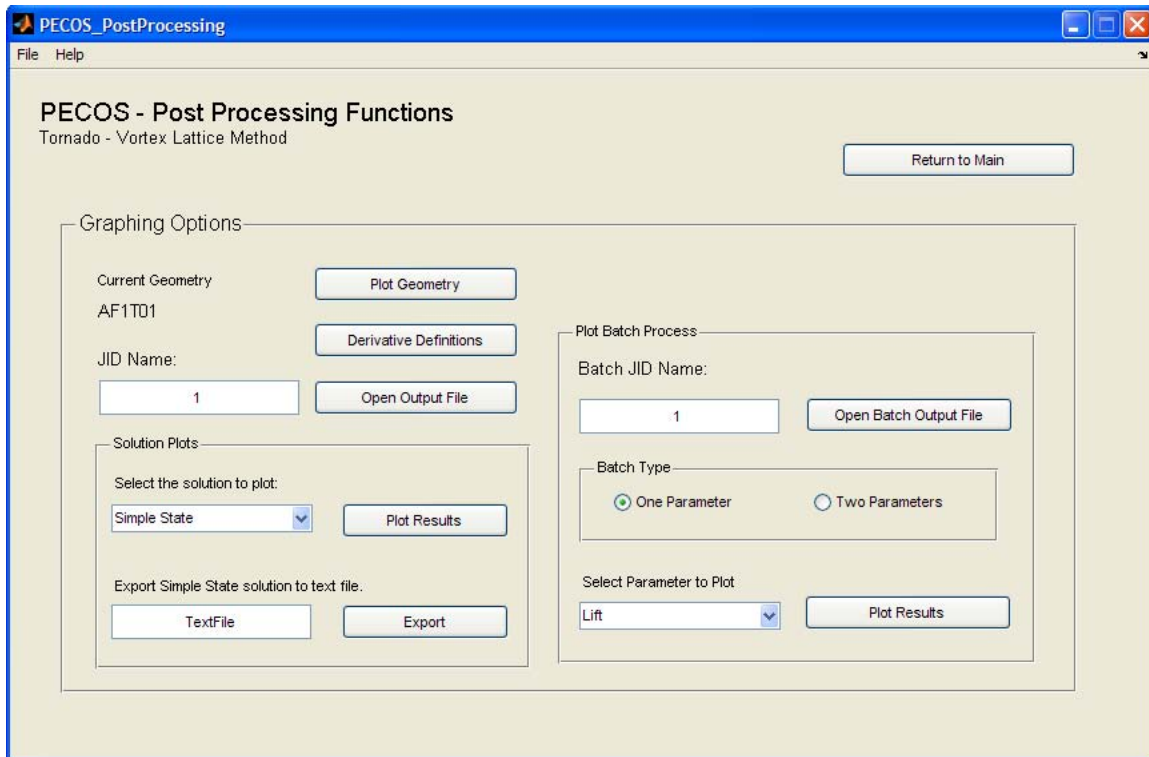


Figure 2.20: The PECOS Processing window contains options for various type of calculations to be performed using the Tornado Vortex Lattice Method.

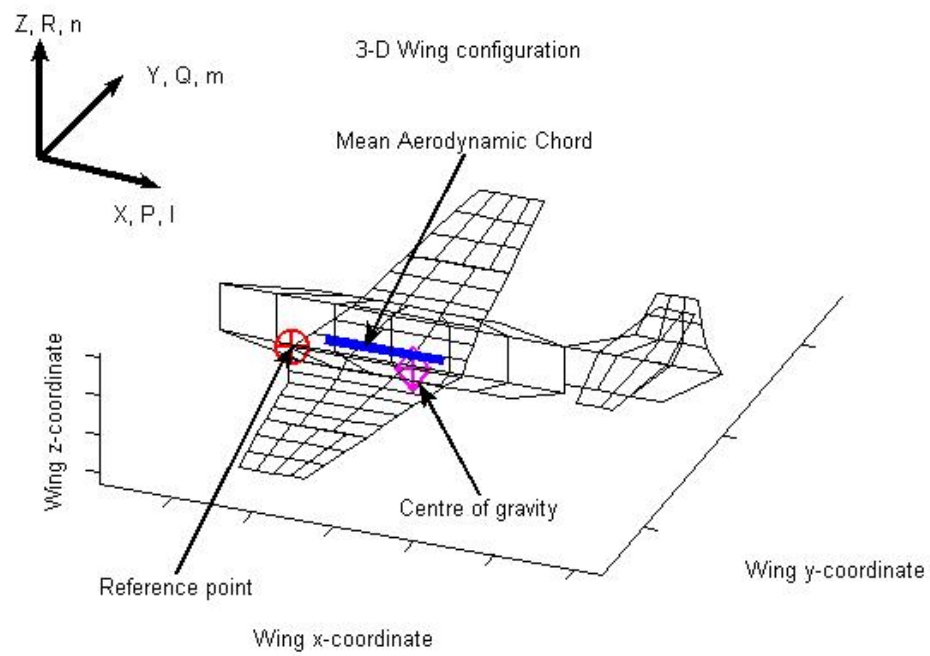


Figure 2.21: The definitions of the variables used by Tornado for VLM in relation to the geometry and coordinate axis.

2.3 Wind Tunnel Testing

In addition to the numerical design tools, winglet performance was evaluated in multiple wind tunnel tests. This included tests of small scale winglets to investigate wake vortex formation, evaluation of lift and drag performance of a wing and winglet combination using different winglet designs, and evaluation of a scale model of a complete UAV design. In the latter case, the vehicle was tested under flight conditions without winglets, with traditional Whitcomb winglets, and with blended winglets. An example of the wing and winglet combination tunnel model is shown in Fig. 2.22.

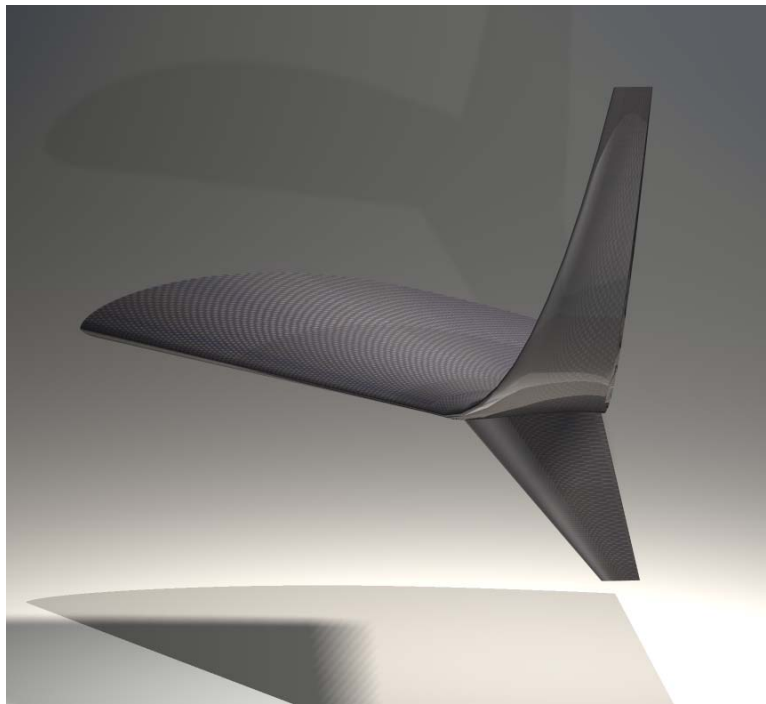


Figure 2.22: Example of wind tunnel model.

2.3.1 Small Scale Testing

PIV stands for Particle Image Velocimetry. It is a means by which a two dimensional map of airflow velocity is recorded and measured. To perform PIV, a particle source,

in this case a fog machine, introduces very small particles that are carried by the velocity of the flow. A laser is focused to create a sheet of light through the flow to illuminate the particles. A high speed camera is focused on the particles illuminated by the laser sheet. The camera is used to capture image pairs in quick succession. A computer algorithm processes the image pairs and isolates individual particles in the image pair. The algorithm measures the distance and direction between the location of the particle from the first image to the second image. The user must calibrate the image to tell the algorithm the time between the image pair, and the distance from one pixel to the next, then the algorithm can compute the velocity of each particle in the flow. Because the algorithm can not isolate every particle in the image, a series of image pairs will be processed, then the velocities will be averaged and interpolated to create a 2-D velocity map of the flow illuminated by the laser sheet.

Three wings were modeled for PIV testing. Each wing had an Eppler 396 airfoil profile for the main wingspan. Wing 1 included the wing only, wing 2 had a Whitcomb style winglet with a Selig S9026 airfoil on both the upper and lower winglets, wing 3 had a blended winglet and a lower winglet. The wing models were approximately 1/12 scale. Fig. 2.25 shows the three wing configurations with wing 1 on the left, wing 2 center, and wing 3 on the right. For the PIV measurements, a mounting plate was constructed to fit in the HAL 12 inch by 12 inch cross section wind tunnel. The mounting plate was constructed to pivot about the quarter chord of the root of the wing. The quarter chord for each wing was mounted at one quarter the length of the wind tunnel. PIV measurements were taken at downstream stations equal to one, two, and three mean aerodynamic chord lengths from the trailing edge of wing one. Fig. 2.24 illustrates the experimental setup with wing 3 in the wind tunnel. A high speed camera was placed at the top of the wind tunnel, and focused on a prism placed inside the wind tunnel downstream of the test wing. Lasers were placed on the side of the wind tunnel and lenses were used to produce a thin sheet of laser light

across the wind tunnel at the desired downstream location. A fog machine at the inlet side of the wind tunnel provided particles in the flow to illuminate and visualize the flow. The laser and camera are synchronized via a signal generator set to pulse at 50 milliseconds. This configuration allowed for the capture of the flow in a cross section downstream of the test model. The wind tunnel was set to 1230 rpms for each test case. For each wing at each downstream station, measurements were taken for angles of attack of zero, five, and 10 degrees . After processing data from the camera, MATLAB was used to graph the data.

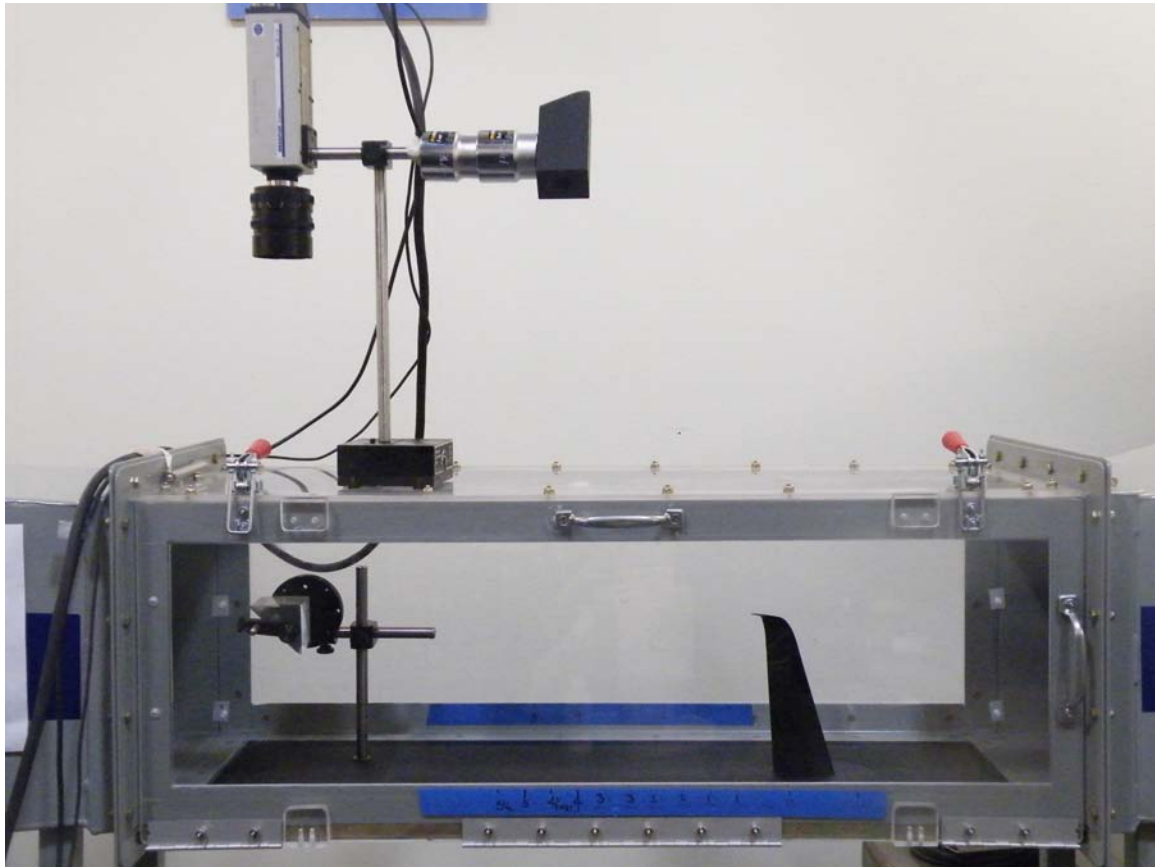


Figure 2.23: For PIV measurements, a scale model of the wing was placed in 12x12 cross section wind tunnel. A prism was placed downstream of the model. A high speed camera was placed above the prism to capture a cross section of the downstream flow at Stations 1, 2, 3, 4, and 5.

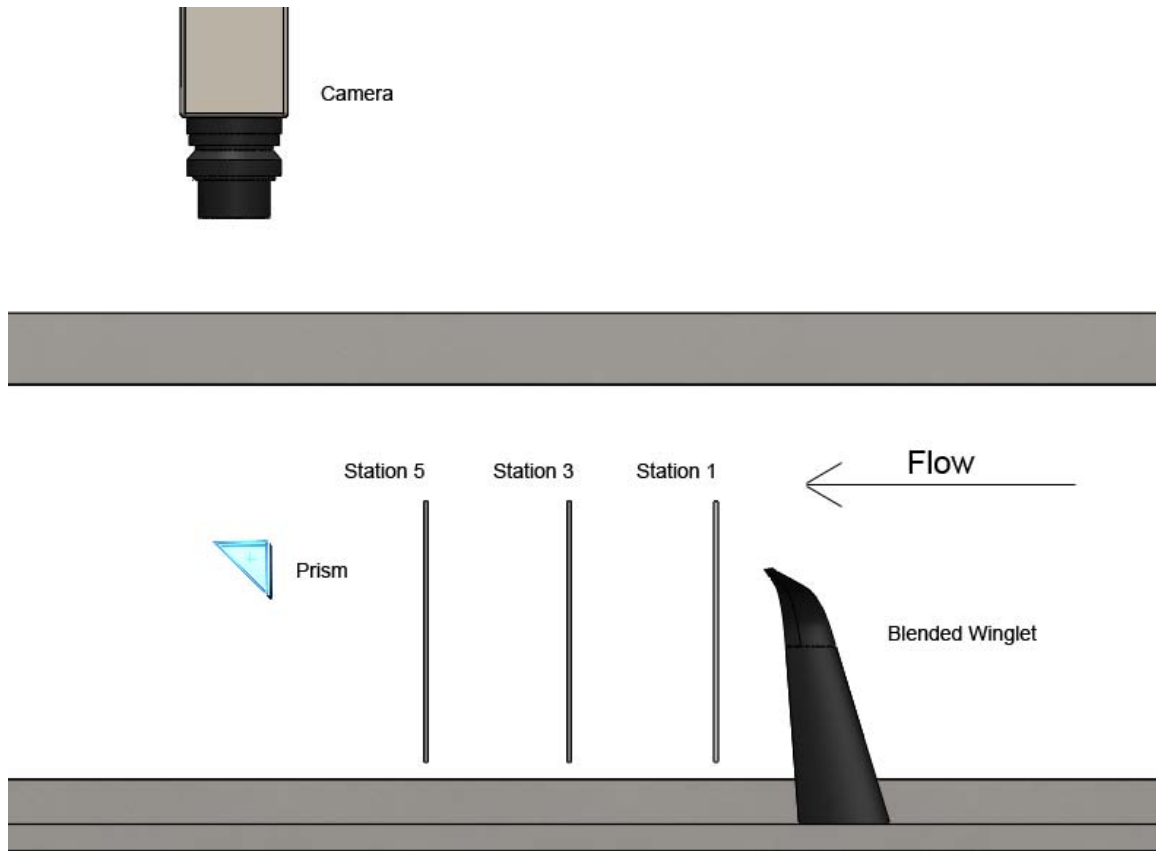


Figure 2.24: For PIV measurements, A scale model of the wing was placed in 12x12 cross section wind tunnel. A prism was placed downstream of the model. A high speed camera was placed above the prism to capture a cross section of the downstream flow at Stations 1, 2, 3, 4, and 5.

2.3.2 University of Washington Aero Lab Wind Tunnel

In cooperation with NextGen Aeronautics, wind tunnel testing was conducted at the Kirsten Wind Tunnel at the University of Washington's Kirsten Wind Tunnel in Seattle, WA. The Kirsten Wind Tunnel has a cross sectional area of 91.5 ft². The test area is 8 ft. tall, 12 ft. wide, and 10 ft. long[28]. The wind tunnel is a closed loop, double return design 2.26. With two massive propellers, measuring more than 11 ft. in diameter 2.27 , the wind tunnel is capable of speeds up to 200 mph. Of interest to this research is the comparison of three different configurations: the first

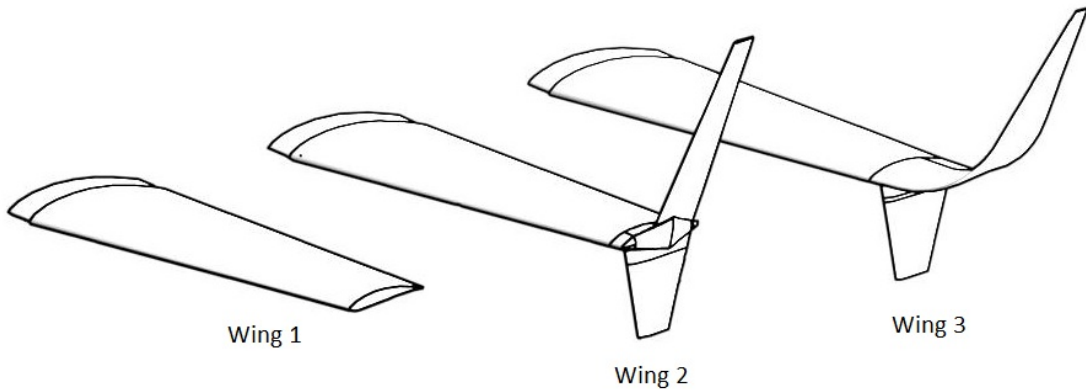


Figure 2.25: Three wings were modeled for PIV measurements. Wing 1 has no winglets, wing 2 has straight winglets, wing 3 has a straight lower winglet and a blended upper winglet.

configuration is the model with the wing only, the second configuration is the model with straight Whitcomb winglets, and the third configuration is the model with the blended winglets. For each configuration an alpha sweep was performed at approximately 100 knots. Measurements for lift and drag as well as others were recorded. The main balance is a six-component (three forces, three moments) external balance located beneath the test section floor. The balance simultaneously measures all forces and moments with respect to the wind axes at the virtual balance moment center located at the center of the test section. These forces and moments are converted to voltages by electromagnetic potentiometers. The output voltages are amplified and converted to digital numbers in engineering units. Additional details are available from the Kirsten Wind Tunnel Technical Guide.

Due to the proprietary nature of the design, only limited results from the UAV design and tests are included herein. The vehicle is currently being constructed at a 3/8 scale and full scale for flight testing. The flight tests will include evaluation of the different winglet designs. Fig. 2.28 shows the winglet models used in wind tunnel testing the Kirsten wind tunnel at the University of Washington Aero Lab in Seattle,

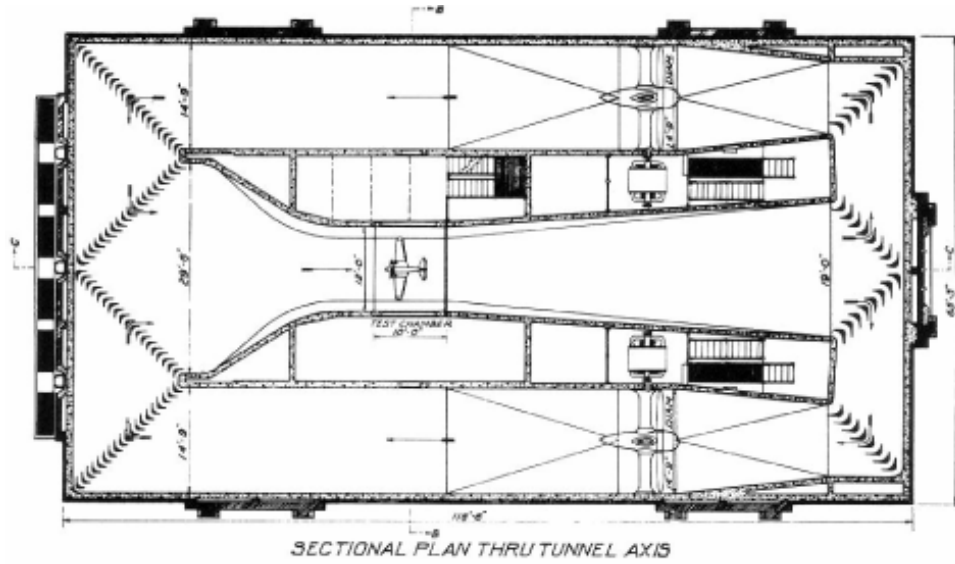


Figure 2.26: Diagram of the Kirsten wind tunnel at the University of Washington in Seattle. The wind tunnel is a closed-loop double return design.[28]

WA. The winglet on the left is the optimized blended winglet, the winglet on the right is a Whitcomb winglet design.



Figure 2.27: The Kistrten Wind Tunnel features 2 massive propellers measuring 11 ft. 4 in. in diameter, with seven blades.[28]

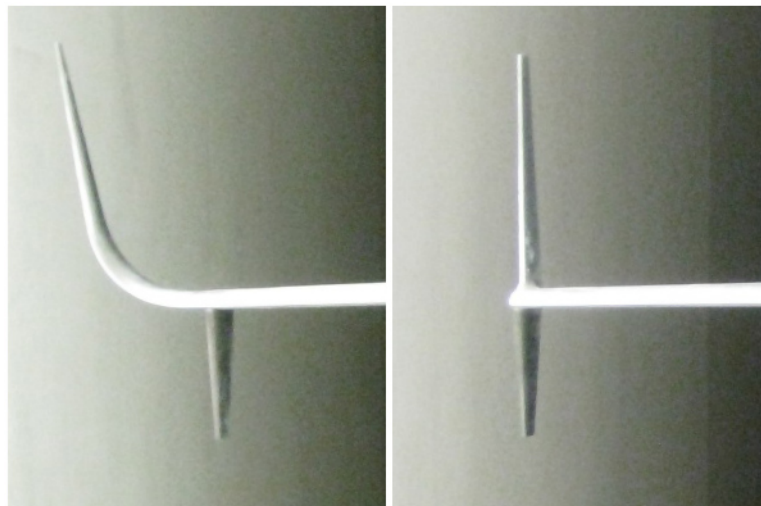


Figure 2.28: Winglet models were milled from solid aluminum for wind tunnel testing at the University of Washington Aero Lab. The image on the left is the optimized blended winglet, and the Whitcomb winglet is on the right.

CHAPTER 3

Results

Results for the design and optimization using Pecos for winglet design are described in this section. Also included are results from wind tunnel testing which are compared to VLM predictions. Finally the data from the PIV vortex dynamics study will be discussed, comparing different winglet designs, and their impact on the shed vortex.

3.1 VLM

The main wing for the test model that would be evaluated had an Eppler 396 airfoil. The test conditions were set to an airspeed of 65 knots at an altitude of 10,000 ft. The design requirements for the winglets called for a total height of 1 meter. The code for generating the winglet was adjusted so the length parameter could be used as the input for setting the total height of the winglet. This code is reflected in the PECOS_genwinglet.m file for MATLAB. A switch was defined to change the length parameter according to winglet requirements, whether the winglet design required a fixed length, height, or straight section beyond the blend radius. Table 3.1 contains the winglet parameters used for each configuration during parametric batch processing for design optimization.

Fig. 3.1 shows the results computed by Tornado for configuration BFC03 as listed in 3.1, with the radius varying from 0.1 to 0.9 meters and the angle of attack varying from -10° to 20° . The first plot displays C_L/C_D , and the plot on the right shows the root bending moment. C_L/C_D was computed using the the C_L as computed by Tornado, however, C_D was the sum of C_D as computed by Tornado plus the zero lift

drag coefficient. The zero lift drag coefficient is an estimate of the surface drag based on the surface area of the wings. If the zero lift drag coefficient was not added, C_D would be zero at α_0 , this would cause a premature peak for C_L/C_D at α_0 , and would be of no value for predicting performance. Fig. 3.1 shows that C_L/C_D increases for larger radii. The root bending moment is constant for the change in radius and is influenced mainly by the angle of attack. Fig. 3.2 shows the results for configuration BFC03 with the cant angle varying from 50° to 90° . The plots show that for C_L/C_D the best results are achieved for the lower cant angles. However, since the length is defined to maintain a constant height of 1 meter, the lower the cant angle, the longer the winglet will need to be to reach the necessary height. Therefore the optimum cant angle will be a compromise between total length (weight) and higher C_L/C_D . Fig. 3.3 shows the results for configuration BFC03 with the sweep angle varying from 0° to 40° . The values are almost invariant in relation to the sweep angle. Fig. 3.4 shows the results for configuration BFC03 with the cant angle varying from 60° to 90° and the blend radius varying from 0.1 to 0.9 meters. The angle of attack for this plot is set to 0° . $C_L/C_{D_{max}}$ lies at the maximum radius and the minimum cant angle. The minimum root bending moment however lies at the cant angle above 70° . The optimum solution, will be a compromise. In order to prevent creating a winglet that is too large and heavy and to accommodate a straight section at the end of the winglet, the blend radius was set to 0.457 meters, or equal to the wingtip chord length and the cant angle was set to 77° . This cant angle is a compromise for optimum L/D and root bending moment as well as maintaining a shorter overall length. The sweep was set to 27° , so the winglet did not extend too far beyond the trailing edge of the wing. This sweep also aligns the sweep of the leading edge of the wing to the leading edge of the winglet. Fig. 3.5 shows the results for configuration BFC04. Plotting C_L/C_D versus the twist angle and sweep angle, there is a maximum for C_L/C_D is located at a twist angle of -6° and a sweep angle of 27° . The minimum value for the root bending

moment is at the maximum sweep angle. The range for C_L/C_D is approximately 3 with an increase of 12%. The range for the root bending moment is 200 with an increase of 7%. For the final optimized design a tip twist angle is set to -6° and the sweep angle is set to 27° .

Configuration	Height (m)	Root Chord	Tip Chord	Radius	Cant	Sweep	Twist
BFC03	1.00	0.457	0.15	0.457	90°	27°	0°
BFC04	1.00	0.457	0.15	0.457	77°	27°	0°
Optimized	1.00	0.457	0.15	0.457	77°	27°	-6°

Table 3.1: Winglet Parameters for Test Model

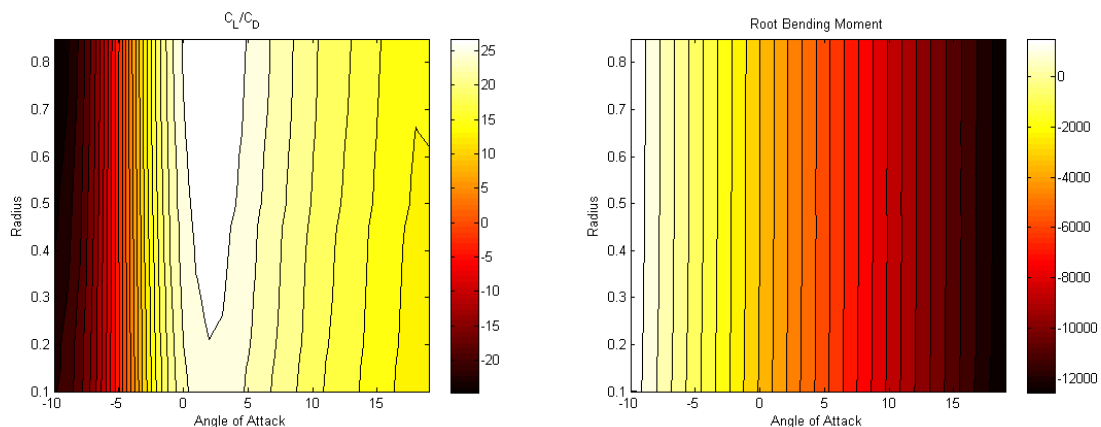


Figure 3.1: MATLAB plot for configuration BFC03 with blend radius varying from 0.1 to 0.9 meters. Angle of attack varies from -10° to 20° . Left plot indicates C_L/C_D , right plot shows the root bending moment.

3.2 UAV Performance Evaluation

The performance improvements can be measured in terms of range and endurance. Using eqn. (3.1) estimates for the range can be compared. Using eqn. (3.2) estimates for the endurance can be compared. Table 3.2 lists the values for the predicted

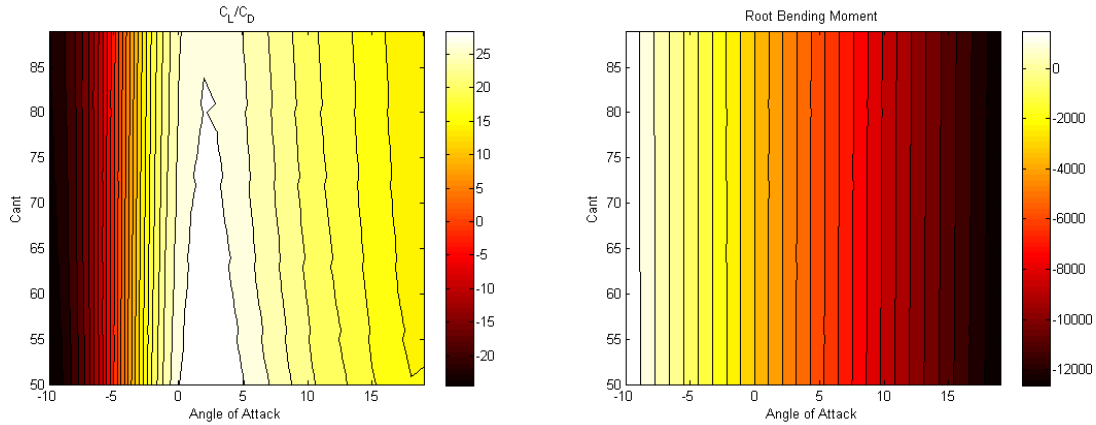


Figure 3.2: MATLAB plot for configuration BFC03 with cant angle varying from 50° to 90° . Angle of attack varying from -10° to 20° . Left plot indicates C_L/C_D , right plot shows the root bending moment.

performance improvements for this particular case. Using the optimized blended winglets, the maximum value for C_L/C_D is increased by 28%. This results in a 71% increase in endurance and the range is increased by 28%. The root bending moment at the stall angle of 15° is increased by 17%. The blended winglet also performs better than the Whitcomb winglet. The predicted performance improvements for the blended winglet are 15.61% and 33.96% better than the range and endurance respectively for the Whitcomb winglet. The root bending moment for the blended winglet is only 5% more than the Whitcomb winglet. Since the design parameters for the notional UAV require a winglet that is 1 meter high the comparison of the optimized winglet to the Whitcomb winglet is more relevant than the comparison to the configuration with no winglet. The added bending moment at the root will require more structural strength, which means the overall structure will be heavier. The performance improvements for the bended winglet are greater for the overall increase in the root bending moment when compared to the Whitcomb winglet. Fig. 3.6 plots the predicted performance for the model with no winglets, a Whitcomb winglet, and the optimized blended winglet.

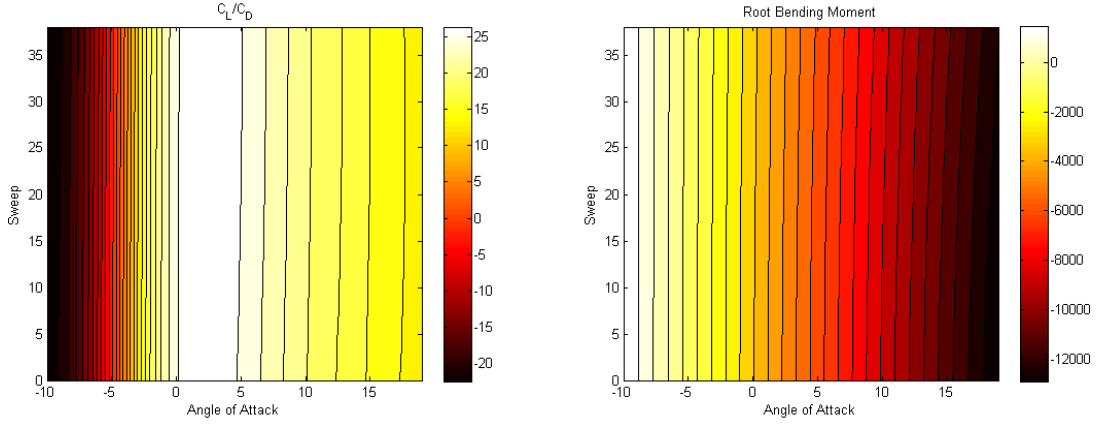


Figure 3.3: MATLAB plot for configuration BFC03 with sweep angle varying from 0° to 40°. Angle of attack varying from -10° to 20°. Left plot indicates C_L/C_D , right plot shows the root bending moment.

$$\mathbf{R} = \frac{\eta_{pr}}{c} \frac{L}{D} \ln \frac{W_0}{W_1} \quad (3.1)$$

$$\mathbf{E} = \frac{\eta_{pr}}{c} \sqrt{2\rho_\infty} S \frac{C_L^{3/2}}{C_D} (W_1^{-1/2} - W_0^{-1/2}) \quad (3.2)$$

Optimized Winglet Increase Over No Winglet			
C_L/C_{Dmax}	RBM_{stall}	Range	Endurance
28.03%	17.11%	28.03%	71.70%
Optimized Winglet Increase Over Whitcomb Winglet			
C_L/C_{Dmax}	RBM_{stall}	Range	Endurance
15.61%	5.16%	15.61%	33.96%

Table 3.2: Optimized Winglet Performance Comparison

3.2.1 Wing Configuration Study

Three wing configurations are compared in this section. Wing 1 (fig. 3.7) includes the wing only, wing 2 (fig. 3.8) includes the the wings, lower winglets and and a straight upper winglet. Wing 3 (fig. 3.9) includes the wings, lower winglets and blended upper

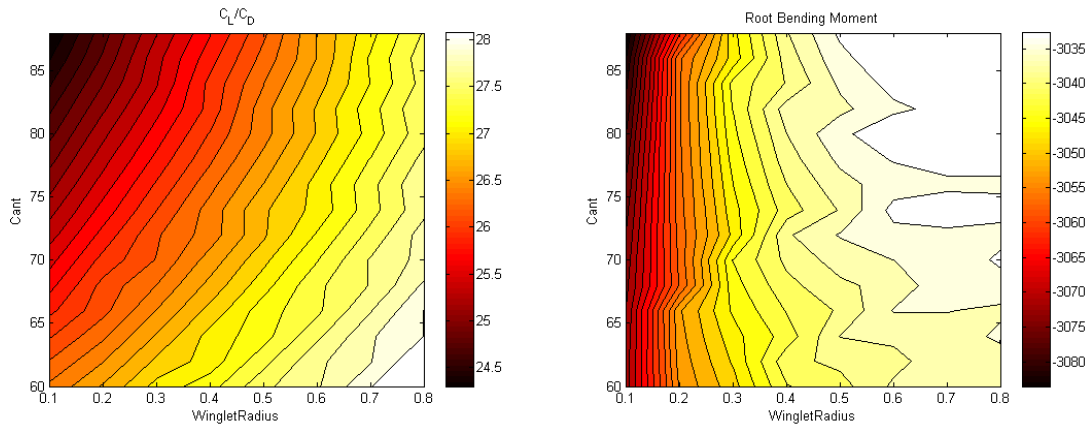


Figure 3.4: MATLAB plot for configuration BFC03 with cant angle varying from 60° to 90° and the radius varying from .1 to .9 meters. Left plot indicates C_L/C_D , right plot shows the root bending moment.

winglets. Table 3.2.1 displays the predicted lift and drag coefficients produced using the Tornado VLM. $C_L/C_D\%_1$ is the percentage increase in C_L/C_{Dmax} of the winglet design over the no winglet. $C_L/C_D\%_2$ is the percentage increase in C_L/C_{Dmax} of the blended winglet design (Wing 3) over the Whitcomb winglet design (wing 2). Vortex Lattice Method (VLM) model predicts the C_L/C_{Dmax} value for wing 3 is 29.46, C_L/C_{Dmax} for wing 2 is 25.43, and C_L/C_{Dmax} for wing 1 is 23.00. The equates to an 15.9% increase for wing 3 over wing 2, and 28.1% improvement over wing 1. These same configurations were tested in the Kirsten wind tunnel at the University of Washington in Seattle, Washington.

The results from the vortex lattice method can be compared to the results from the wind tunnel tests. The values measured in wind tunnel testing indicated a C_L/C_{Dmax} of 14.9, 16.2 and 18.7 for wings 1, 2, and 3 respectively. The values for C_L/C_{Dmax} were less for the wind tunnel measurements than those for VLM calculations. This should be expected since the drag coefficients from the wind tunnel are higher. VLM predicts lower drag coefficients because it does not measure viscous effects. The measured values show that wing 3 had an actual improvement over wing 2 of 11.8%

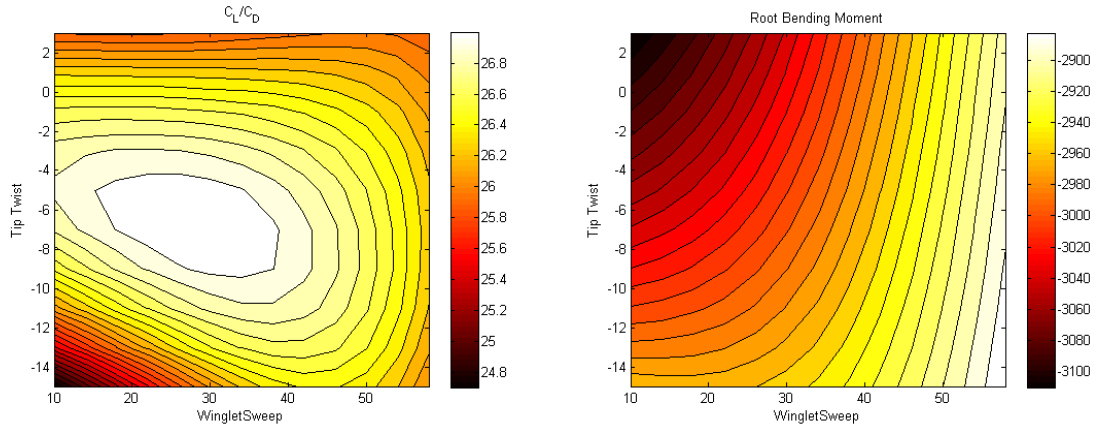


Figure 3.5: MATLAB plot for configuration BFC04 with tip twist angle varying from -15° to 5° . Sweep angle varying from 10° to 60° . Left plot indicates C_L/C_D , right plot shows the root bending moment.

and 38.7% improvement over wing 1. So, although the values differed, the trends were similar, and the performance *improvement* for the blended winglet over no winglet was actually better than predicted by the VLM model. Fig. 3.10 displays the data from the wind tunnel tests for the lift coefficient for all three wing configurations vs. alpha as well as the predicted the lift coefficient from Tornado. At the lower angles of attack, the values are nearly the same for the wind tunnel and VLM. At higher angles of attack, as the model approaches the stall angle, the lift curve for the wind tunnel data diverges, while the predicted values from the VLM continue. This is expected since, VLM does not predict stall or any viscous effects that predict flow separation. Fig. 3.11 compares the wind tunnel measured results for the lift coefficient over the drag coefficient vs. alpha. The curves for the VLM predictions are higher, but still follow the same trends among the the three wings ads the wind tunnel data. A higher value is expected for the VLM model because it does not model viscous drag effects, but can only approximate surface drag, therefore the drag from VLM will be lower, resulting in a higher value for C_L/C_D .

Table 3.2.1 lists the results for the performance parameters as calculated using

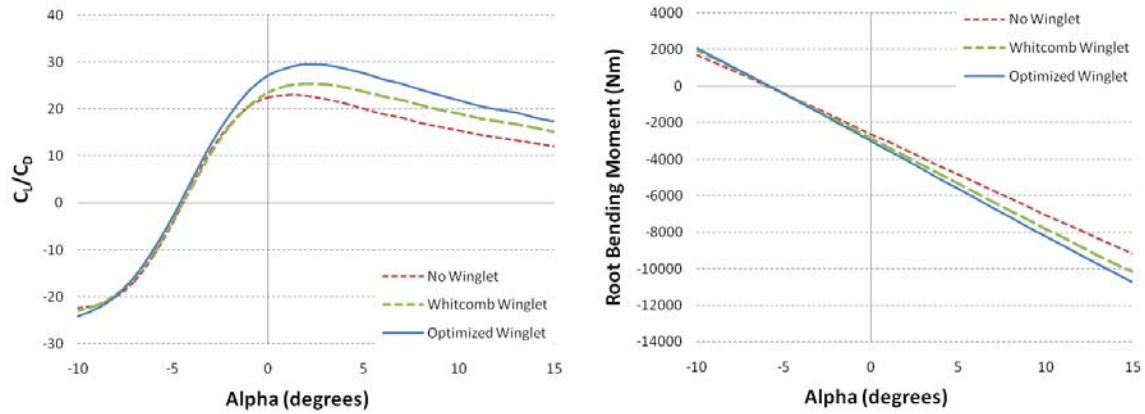


Figure 3.6: Graph of VLM results for the test model with no winglet, a Whitcomb winglet and the optimized winglet for comparison of C_L/C_D vs. Alpha and root bending moment vs. Alpha.

Tornado and as measured in the wind tunnel. $Range_1$ is the percentage increase in range of the winglet design over no winglet. $Range_2$ is the percentage increase in range of the blended winglet design (Wing 3) over the Whitcomb winglet design (Wing 2). Likewise $Endurance_1$ is the percentage increase in endurance of the winglet design over no winglet. and $Endurance_2$ is the percentage increase in endurance of the blended winglet design over the Whitcomb winglet design. The endurance is a function of $C_L^{3/2}/C_D$ and the range is a function of L/D . The range is calculated using eqn. (3.1), however for comparison, all variables were assumed constant except for L/D . The endurance is calculated using eqn. (3.2), and likewise, all variables were assumed constant except for $C_L^{3/2}/C_D$, for comparison. Estimates were first made using the predicted value for C_{D0} from Tornado, then the estimated value for C_{D0} from the wind tunnel results was substituted. The VLM model with C_{D0VLM} predicts an increase in range of 10.75% for the Whitcomb winglet design (Wing 2) and a 28.03% increase in range for the blended winglet design (Wing 3). The VLM model predicts that the Whitcomb winglet can increase endurance by 28.17% and the blended winglet can increase the endurance by 71.7%. By substituting the value

for $C_{D0_{WT}}$, the VLM predictions become very close to the values measured in the wind tunnel. Using $C_{D0_{WT}}$, the Range is increased by 14.49% using the Whitcomb winglet and 31.85% using the optimized blended winglet. The Whitcomb winglet is predicted to increase the endurance by 24.55%. Tornado predicts that the Blended winglet will increase the endurance by 22.21%. The next section of table 3.2.1 lists the results from the wind tunnel test. The Whitcomb winglet (Wing 2) provides a modest increase in range of 12.4% while the blended winglet provides a 29.1% increase in range. The wind tunnel measurements show an increase of 18.8% for endurance for the Whitcomb winglet and 38.7% increase in endurance for the blended winglet design. The predictions for the increase in range is quite good, whether using $C_{D0_{VLM}}$ or $C_{D0_{WT}}$. The predictions for endurance are higher than were calculated using wind tunnel measurements. The predictions improve when $C_{D0_{VLM}}$ is replaced by $C_{D0_{WT}}$, yet remain considerably higher.

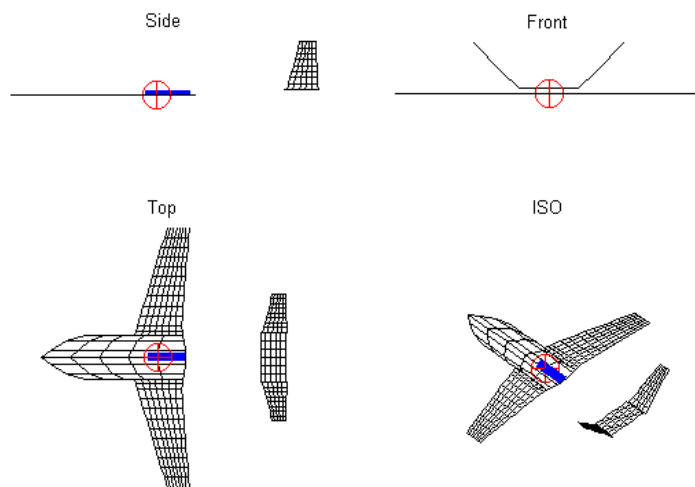


Figure 3.7: Geometry plot for wing 1 with panels. Wing 1 does not have any winglets

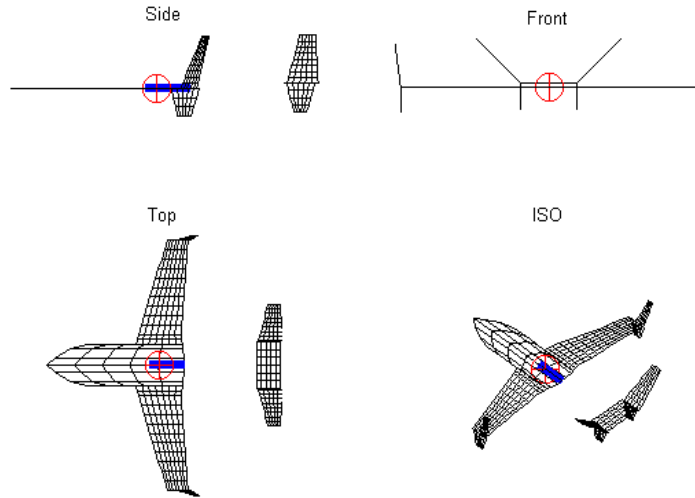


Figure 3.8: Geometry plot for wing 2 with panels. Wing 2 has the lower winglets and straight upper winglets.

3.3 Wind Tunnel Testing

Wind tunnel testing was conducted to validate the results from VLM predictions. Force balance measurements were taken at the Kirsten Wind Tunnel at the University of Washington in Seattle, WA. PIV data was collected using a small scale model in the 12 inch by 12 inch wind tunnel in the Hydrodynamics and Aerodynamics lab (HAL) at Oklahoma State University in Stillwater, OK.

3.3.1 Vortex Dynamics Study

From computational results and optimization, models were constructed for more analysis in a wind tunnel. Using the geometry created in Solidworks, A small scale model was fabricated using a rapid prototyping machine. PIV measurements were collected in a 12 inch by 12 inch wind tunnel in the HAL lab at OSU. Three wing configurations were tested. The first configuration is labeled wing 1, and consisted of the wing only, with no winglets. The second configuration is labeled wing 2, and consisted of the

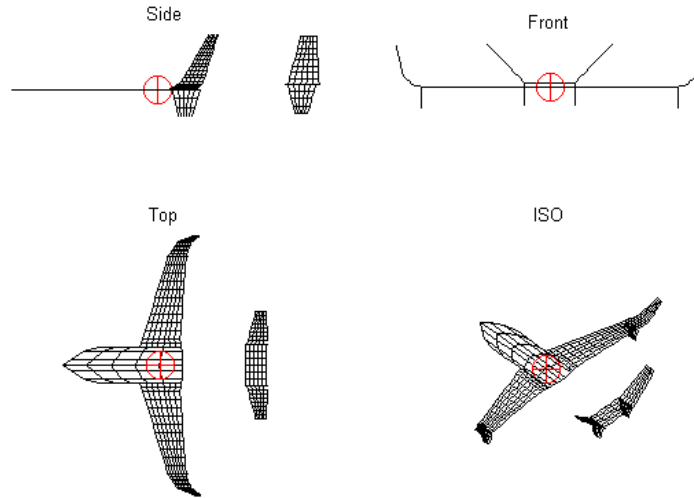


Figure 3.9: Geometry plot for wing 3 with panels. Wing 3 has the lower winglets and blended upper winglets.

wing with a straight lower winglet, and a straight upper winglet, set at an angle of 83° . The third configuration is labeled wing 3, and comprised the same lower winglet as wing 2, but with a blended upper winglet. Fig. 3.14 illustrates the position of the wing or winglet relative to the cross sectional image of the downstream flow. In each instance, the wing tip or upper winglet tip is placed near the center of the field from which data was captured.

Fig. 3.15 shows the cross sectional velocity and vorticity maps for wing 1 with an angle of attack of 0° , at stations 1, 2, and 3. The wingtip vortex shed by the wing without winglets is clearly defined, even at one chord length (station 1) downstream of the trailing edge of the wingtip. The vortex is equally visible at stations 2 and 3 (2 and 3 chord lengths downstream of the trailing edge of the wingtip) The Velocity Magnitude plots on the left side of fig. 3.15 indicate the part of the flow that is not parallel to the free stream. Velocity magnitudes that are greater indicated the flow has been deflected or redirected in a direction other parallel to the free stream. The highest velocities are near the vortex, and zero at the center of the vortex. Fig. 3.16

VLM Model Predictions With C_{D0} from VLM					
Wing#	C_{Lmax}	C_{D0VLM}	C_L/C_{Dmax}	$C_L/C_D\%_1$	$C_L/C_D\%_2$
Wing 1	2.93	0.0143	23.00	<i>N/A</i>	<i>N/A</i>
Wing 2	3.15	0.0168	25.43	10.6	<i>N/A</i>
Wing 3	3.55	0.0178	29.46	28.1	15.9
VLM Model Predictions With C_{D0} from Wind Tunnel					
Wing#	C_{Lmax}	C_{D0WT}	C_L/C_{Dmax}	$C_L/C_D\%_1$	$C_L/C_D\%_2$
Wing 1	2.93	0.0322	15.55	<i>N/A</i>	<i>N/A</i>
Wing 2	3.15	0.0343	17.80	10.75	<i>N/A</i>
Wing 3	3.55	0.0353	20.50	28.03	15.61

Table 3.3: VLM Predictions from Tornado

Wing#	C_{Lmax}	C_{D0}	C_L/C_{Dmax}	$C_L/C_D\%_1$	$C_L/C_D\%_2$
Wing1	1.53	0.0322	14.86	<i>N/A</i>	<i>N/A</i>
Wing 2	1.60	0.0343	16.24	9.03	<i>N/A</i>
Wing 3	1.70	0.0353	18.66	38.67	11.83

Table 3.4: Wind Tunnel Results

shows the plots for wing 2 (Whitcomb winglet). With these plots, the development of the shed vortex is difficult to identify. Fig. 3.17 shows the plots for the wing 3 with the blended winglet. These plots were taken at station 1 (top), station 3 (center), and station 5 (bottom). Like the plots for wing 2, the wingtip vortex structure is difficult to identify. Though the vortex is unclear for wing 2 and 3, it is clear that these configurations do not shed a strong wingtip vortex structure like the configuration of wing 1 with no winglet. In order to detect the wingtip vortex for the Whitcomb winglet and blended winglet, PIV measurements were taken at $\alpha = 10^\circ$. Fig. 3.18 shows the velocity and vorticity distributions for the three wings at station 1. The vortex is clearly defined for wing 1. The vorticity is only faintly visible for wing 2

VLM Model Predictions Using C_{D0VLM}				
Wing#	Range ₁	Range ₂	Endurance ₁	Endurance ₂
Wing 2	10.75%	N/A	28.17%	N/A
Wing 3	28.03%	15.61%	71.70%	33.96%
VLM Model Predictions Using C_{D0WT}				
Wing#	Range ₁	Range ₂	Endurance ₁	Endurance ₂
Wing 2	14.49%	N/A	24.55%	N/A
Wing 3	31.85%	15.16%	52.22%	22.21%
Wind Tunnel Results				
Wing#	Range ₁	Range ₂	Endurance ₁	Endurance ₂
Wing 2	12.4%	N/A	18.8%	N/A
Wing 3	29.1%	14.9%	38.7%	16.8%

Table 3.5: Increase in Range and Endurance

and wing 3. Fig. 3.19 plots the measured vorticity about the vortex center for each wing at station 1. As expected, wing 1 has the highest vorticity. Wing 3 is slightly higher than wing 2. Though unexpected, it reflects the values that were measured and displayed in fig. 3.18. Fig. 3.20 illustrates how the vortex develops downstream from wing 1. The vortex gains strength and structure from station 1 to station 3. Fig. 3.21 shows that the vorticity at station 3 is higher than for station 1 and 2.

Continuing Work

A variable cant winglet (fig. 3.22) has been constructed for testing in the OSU wind tunnel. Testing with a variable cant winglet will help to qualify the accuracy of the VLM predictions per change in winglet cant. Wake surveys will also be conducted in the OSU wind tunnel using a Whitcomb winglet and a blended winglet. A scale model with three wing configurations that have been included in this research is being built

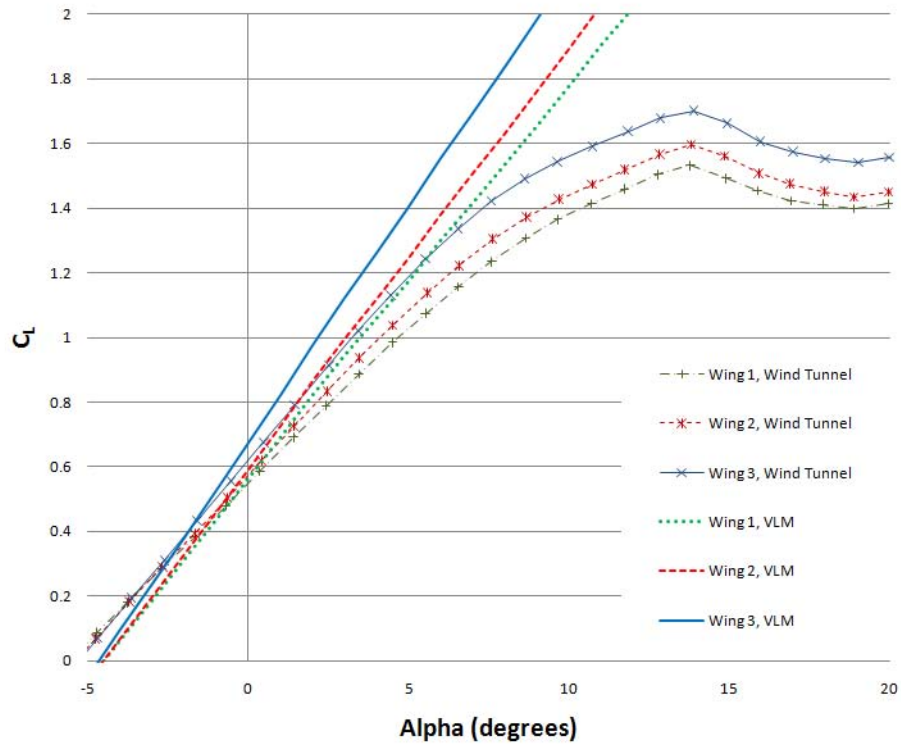


Figure 3.10: C_L vs. Alpha plots for 3 wing configurations. Results from wind tunnel testing and results from VLM model. Correlation is strong in lower angles, correlation decreases as the wind tunnel model approaches the stall angle.

for testing flight characteristics. Due to time constraints, the model has not been evaluated yet but will be available for future research efforts.

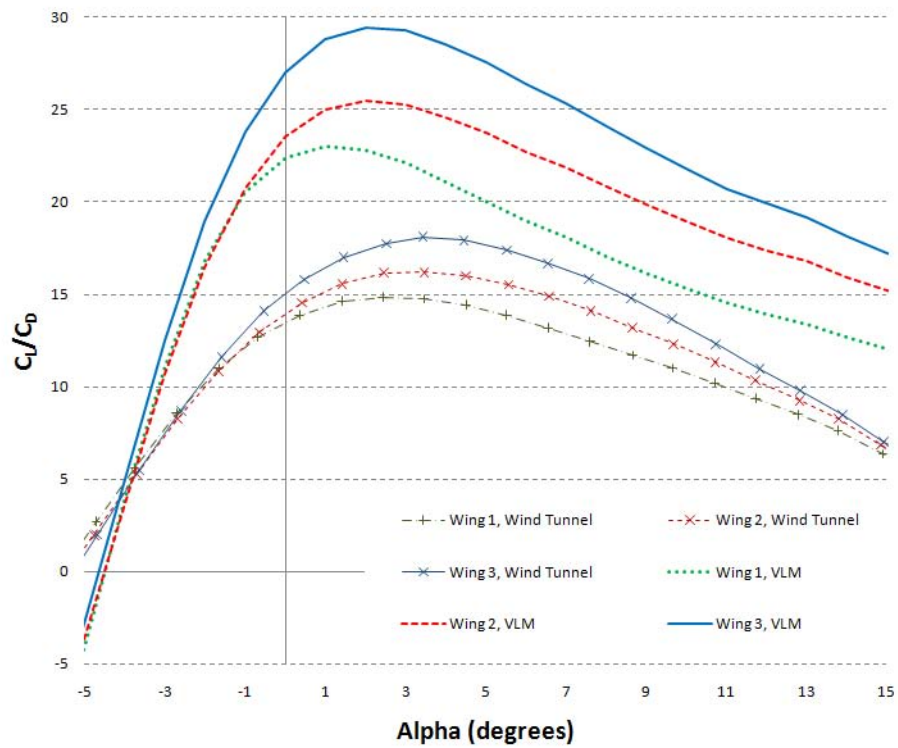


Figure 3.11: C_L/C_D vs. Alpha plots for 3 wing configurations. Results from wind tunnel testing and results from VLM model. VLM does not calculate viscous drag, so the curve for the VLM models is higher. Though the trends for three wings are similar for both the wind tunnel test and VLM model.

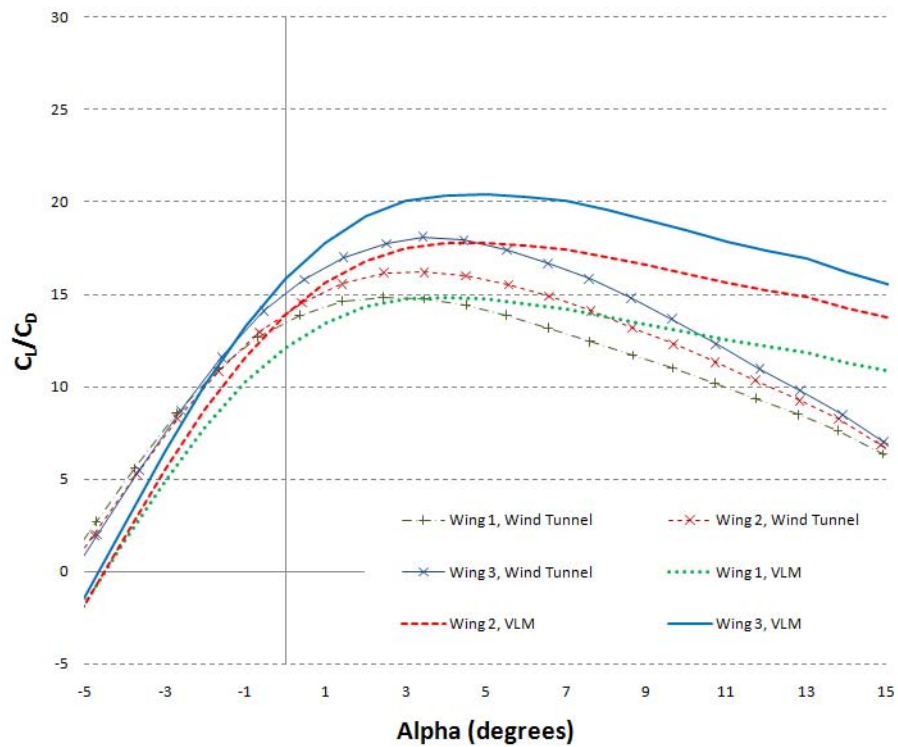


Figure 3.12: C_L/C_D vs. Alpha plots for 3 wing configurations. For the VLM plots, C_{D0VLM} was replaced by C_{D0WT} for C_D in the calculation of C_L/C_D . The curves are much closer when using C_{D0WT} .

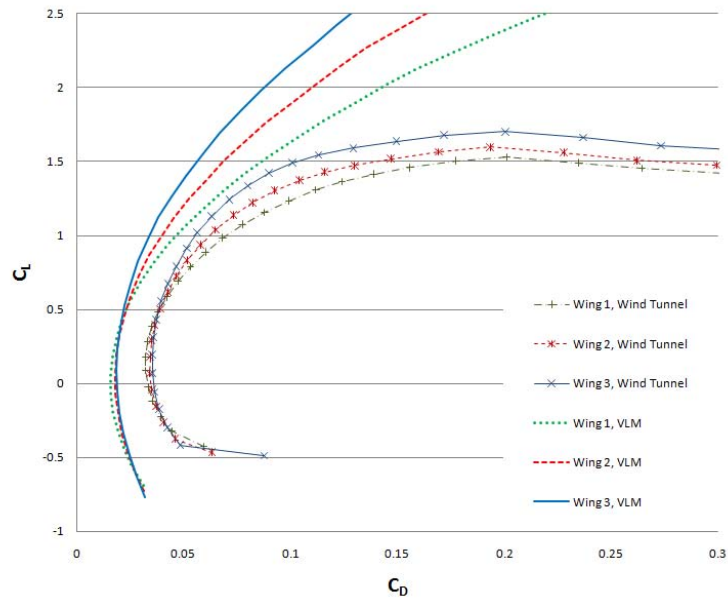


Figure 3.13: C_L vs. C_D for 3 wing configurations. Results from wind tunnel testing and results from VLM model. There is strong correlation between the graphs at lower drag values and lower lift values. The relations between the different wings are similar for both methods.

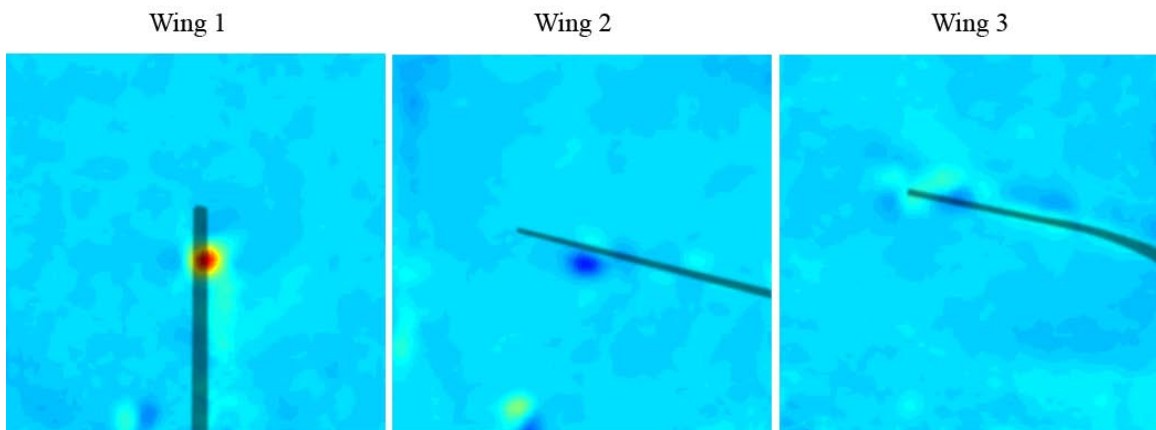


Figure 3.14: Wing or winglet position relative to MATLAB graphs showing the cross sectional vorticity for wing 1, 2, and 3. Wing tip or upper winglet tip is near the center of the image.

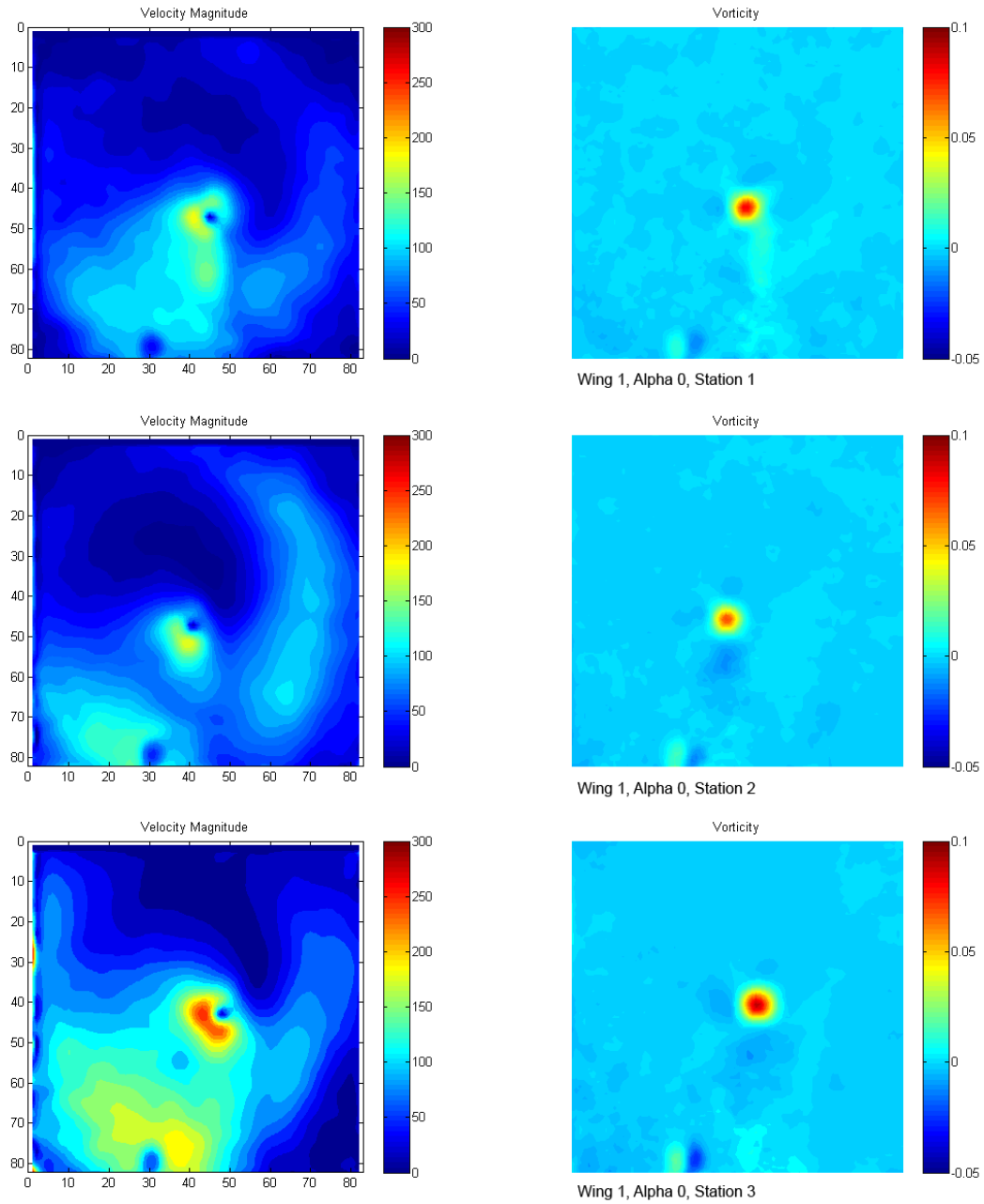


Figure 3.15: MATLAB graphs showing the cross sectional velocity and vorticity for wing 1, with an angle of attack set to 0° , at stations 1, 2, and 3.

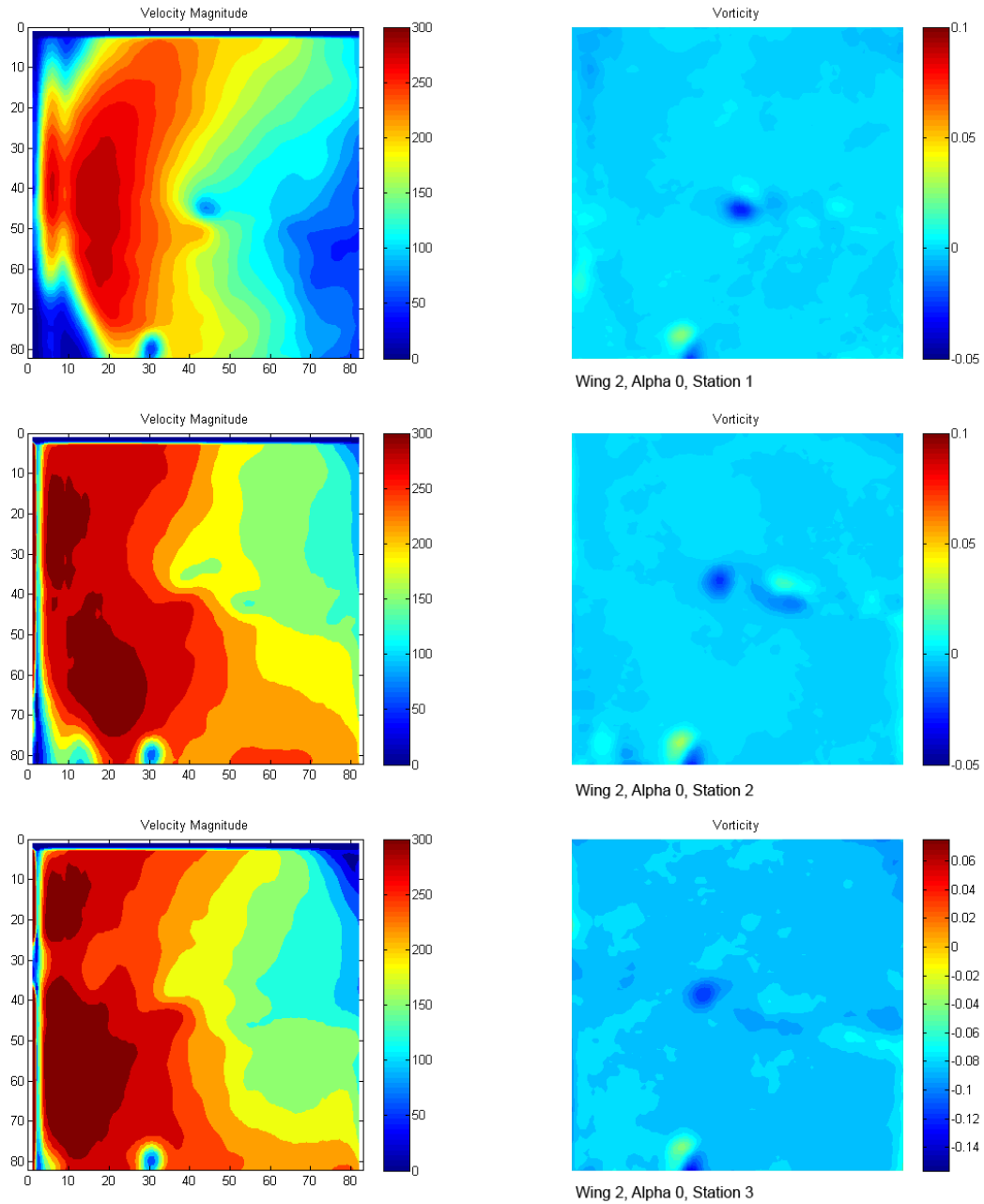


Figure 3.16: MATLAB graphs showing the cross sectional velocity and vorticity for wing 2, with an angle of attack set to 0° , at stations 1, 2, and 3.

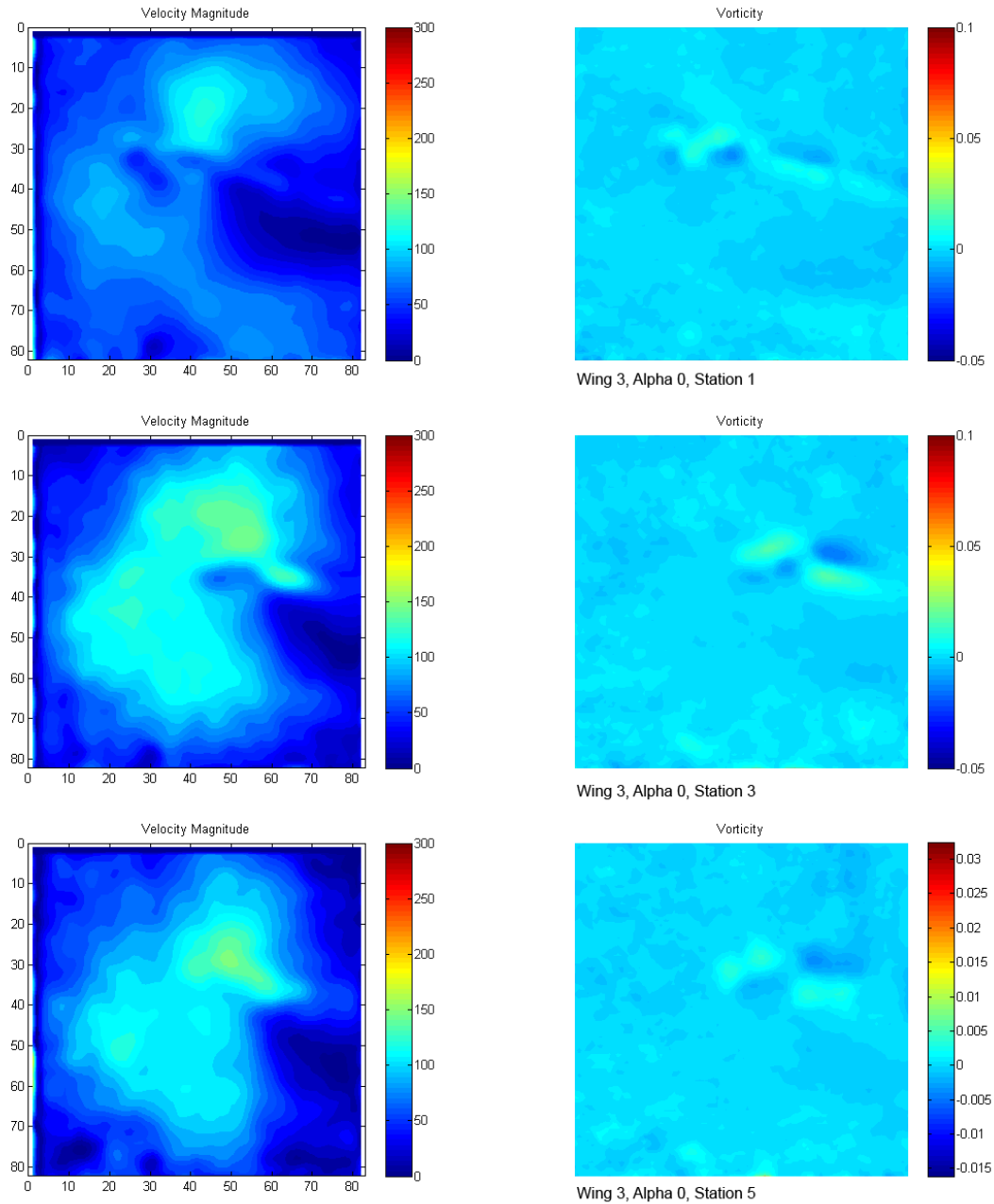


Figure 3.17: MATLAB graphs showing the cross sectional velocity and vorticity for wing 3, with an angle of attack set to 0° , at stations 1, 2, and 3.

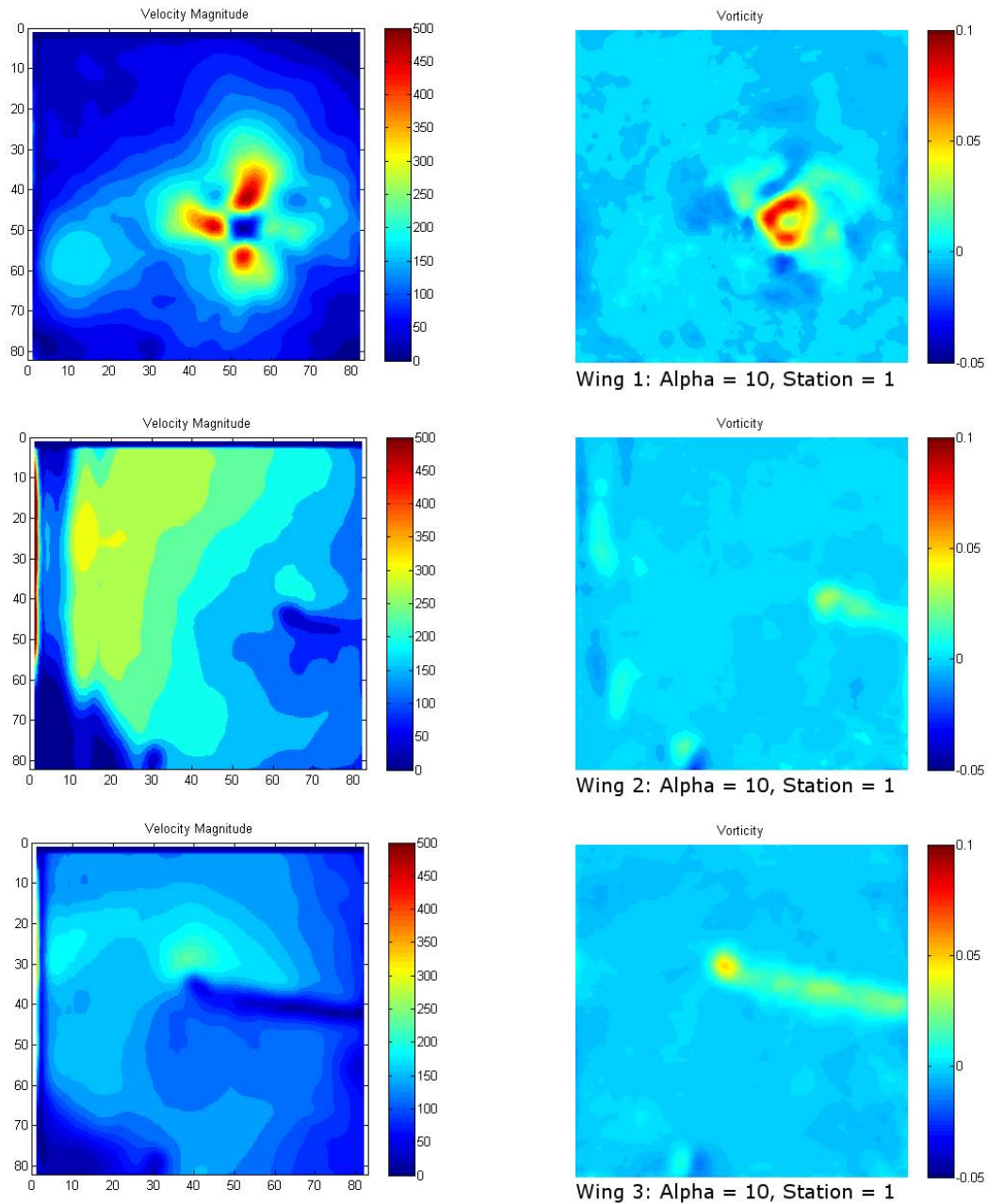


Figure 3.18: MATLAB graphs showing the cross sectional velocity and vorticity. Results for wing 1 are at the top, wing 2 are in the middle row, wing 3 results are at the bottom. Each plot is taken from station 1. Each wing is positioned at an angle of attack 10° .

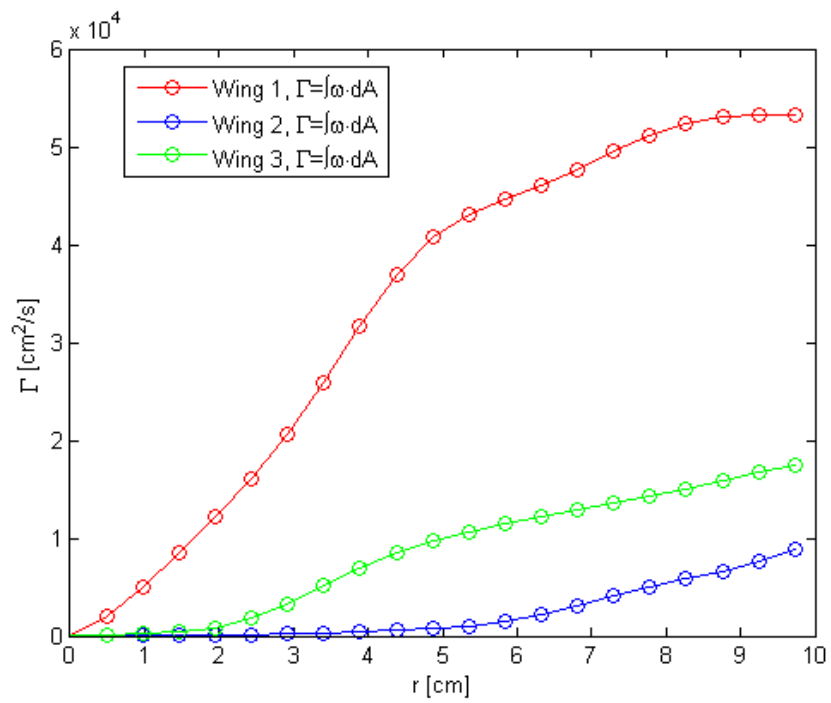


Figure 3.19: Γ values for wing 1, wing 2, and wing 3 at station 1. Alpha for each wing was set at 10° .

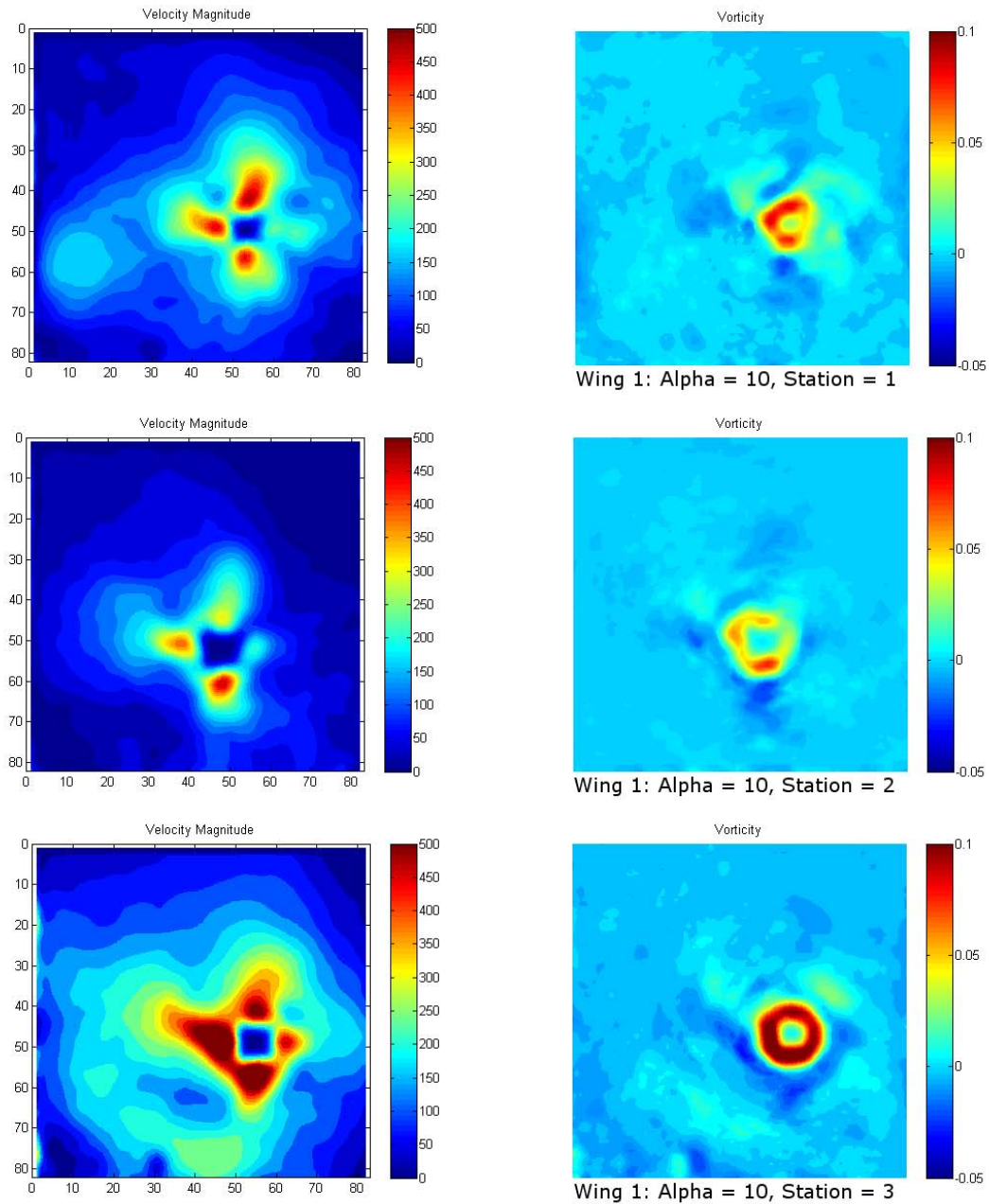


Figure 3.20: MATLAB graphs showing the cross sectional velocity and vorticity. Results are for wing 1 with an angle of attack at 10° . The plots in the top row are taken from station 1, the middle row shows results from station 2, and the bottom row is from station 3.

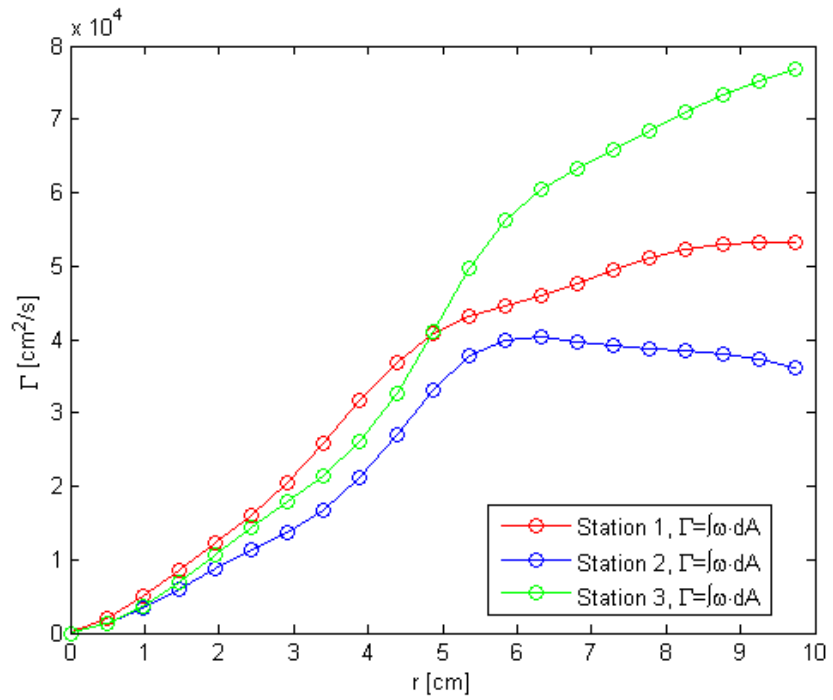


Figure 3.21: Γ values for wing 1 at station 1, 2, and 3. Alpha was set at 10° .



Figure 3.22: Wind tunnel model with a winglet that can be set to variable angles for the cant.

CHAPTER 4

Impact on UAV Design and Performance

The tools and methods developed and tested for a notional UAV were applied to existing UAV platforms. Winglets were designed and optimized for the RQ7 Shadow and Predator UAVs. The methodology that was developed using a notional UAV, was used to examine the impact of winglets on other UAVs.

4.1 Winglet Design for RQ7 Shadow

The RQ7 Shadow UAV was modeled in Tornado using the Pecos interface. The geometry was determined using published dimensions[1], where dimensions were not available measurements were interpolated from published images. The NACA 4415 airfoil was used for the main wing[24]. Winglets were generated and evaluated using the Pecos winglet generator and parametric batch processing. Table 4.1 shows the parameters used for various iterations for the winglet geometries. The flight conditions for the VLM calculations were set to the Shadow's cruise speed of 90 knots at an altitude of 10,000 feet[1]. Fig. 4.1 illustrates the constraints applied to the winglet design. The design space represents a hypothetical design challenge where performance must be improved while the span is constrained. The winglet was constrained to a fit inside a volume at the end of the wing with a length of 50% of the chord length, a height of 25% of the main wing semi-span length, and a depth not exceed 125% of the chord length (not to extend beyond the trailing edge of the wingtip by more than 25% of the chord length. For the RQ7 Shadow blended winglet configuration B1 in table 4.1, the first batch consisted of altering the blend radius and the angle of

attack. Fig. 4.2 shows the results for the Lift over Drag, C_L/C_D , and root bending moment versus the blend radius and angle of attack. The graphs indicate that a greater radius offers better performance for lift over drag as well as C_L/C_D . The root bending moment seems unaffected by the change in radius, and only a function of the angle of attack.

Fig. 4.3 shows the plots for results from configuration B2, where the tip twist angle was varied from -5° to 5° . The plots indicate that better performance is achieved when the tip is twisted to an angle of -5° (toe-out 5°). For comparison a Whitcomb winglet was also optimized. Fig. 4.4 shows how the values for lift over drag, C_L/C_D , and root bending moment change with the angle of attack and the cant angle for a Whitcomb winglet (configuration W1 in table 4.1) on the RQ7 Shadow. The cant angle was varied from 54° to 90° . 54° is the min value for the cant within the boundaries described in fig. 4.1. The plots indicate the minimum cant angle provides marginally better results for C_L/C_D . The root bending moment is constant for the cant angle. With the cant angle set at 54° , the tip twist was varied from -5° to 5° . This is configuration W2 in table 4.1. Fig. 4.5 shows the plots of the results for this configuration. There is a slight improvement in the values for C_L/C_D for a larger toe out angle. Root bending moment remains constant for tip twist angles. The values for configurations B3 and W3 from table 4.1 were then compared to the base configuration for the RQ7 Shadow.

4.2 Winglet Performance for RQ7 Shadow

Once the design has been optimized, the range can be compared using the Breguet equation (3.1)[2]. For the comparisons of the configurations, assume only the C_L/C_D changes. The range for the winglet configurations can be calculated as a percentage over the base configuration. To compare the endurance of each configuration use the endurance equation (3.2). Table 4.2 shows the percent difference in the values

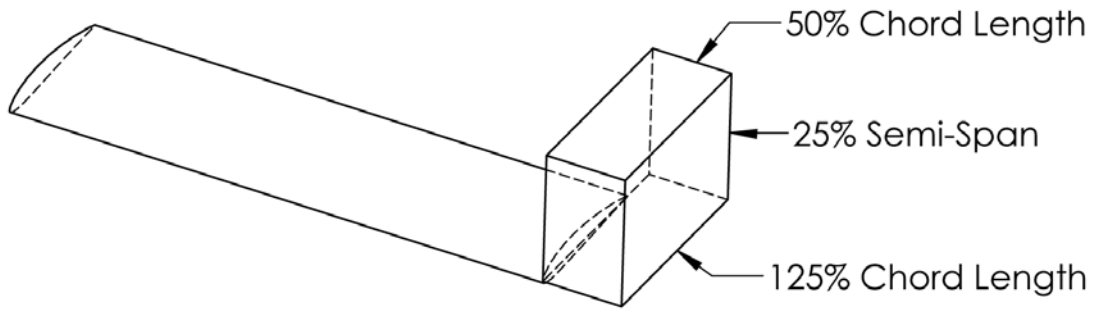


Figure 4.1: Winglets applied to RQ7 Shadow must fit within the defined constraints: winglets must not extend the overall length of the wing by more than 50% of the chord length, winglets must be no higher than 25% of the semi span of the main wing, and winglets must extend no further than 25% of the chord length beyond the wingtip trailing edge.

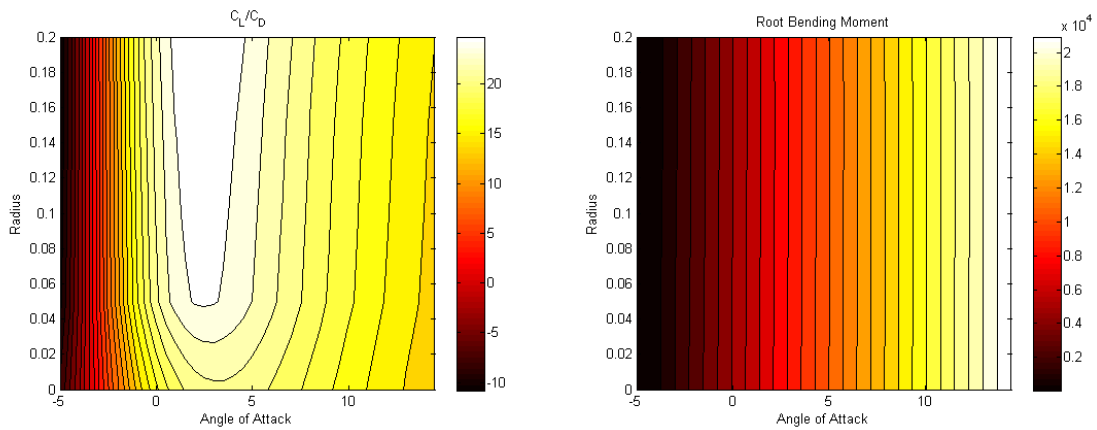


Figure 4.2: Graphs for Shadow, blended winglet (configuration B1), radius and angle of attack are varied from .0 to .25 meter and -5° to 15° respectively. The graph on the left plots C_L/C_D , and the graph on the right plots root bending moment in relation to each parameter.

Table 4.1: Winglet Parameters for RQ7 Shadow

Configuration	Length (m)	Root Chord	Tip Chord	Radius	Cant	Sweep	Twist
B1	0.45	0.55	0.09	V	90°	46°	0°
B2	0.45	0.55	0.09	0.25	90°	46°	V
B3	0.45	0.55	0.09	0.25	90°	46°	-5°
W1	0.45	0.33	0.09	0.0	V	32°	0°
W2	0.45	0.33	0.09	0.0	54°	32°	V
W3	0.45	0.33	0.09	0.0	54°	32°	-2°

that were calculated for C_L/C_D and root bending moment, and the impact on the range and endurance for each of the configurations. Calculations performed using XFOil[9] for the NACA 4415 which was used to approximate the airfoil for the RQ7 Shadow, indicate the airfoil will stall near 15% angle of attack, as illustrated in fig. 4.7. RBM_{stall} is the percent difference for the root bending moment at 15°, near the stall angle. The blended winglet improves the range by 58% compared to no winglet and 31% over the Whitcomb winglet. The blended winglet also improves the endurance by 83% over no winglet and 35% over the Whitcomb winglet. The root bending moment at the stall angle is increased by 25% for the blended winglet compared to 15% for the Whitcomb winglet. The Shadow has an endurance of 8 to 9 hours, so by adding the blended winglet the endurance could be increased to 15 hours. This is assuming the weight increase by adding the winglet is minimal. These figures should be considered optimistic at best. VLM does not calculate viscous effects, and Tornado only *estimates* skin friction drag, so the values for C_D will be low (as could be seen in the results for the values of C_{D0} when comparing the wind tunnel results to VLM predictions in the notional case.) Lower values for C_D will result in higher values for C_L/C_D and increase the predicted performance for range and endurance.

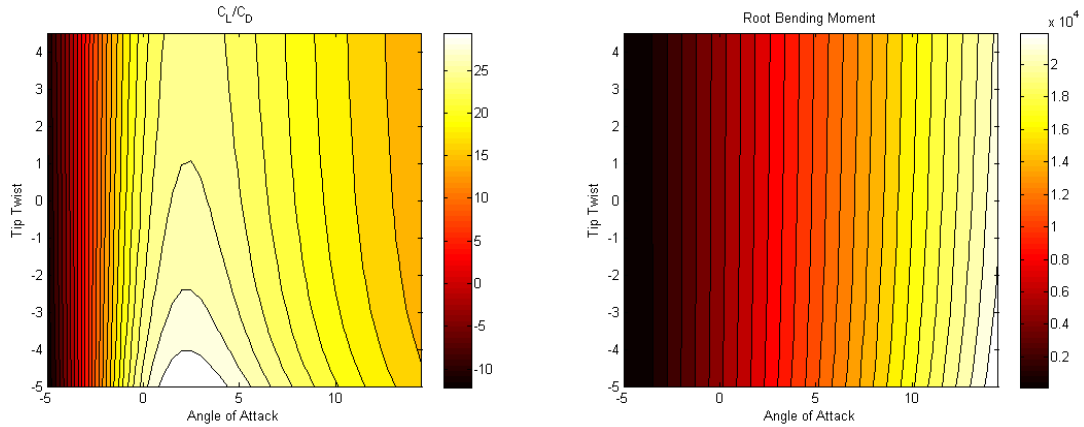


Figure 4.3: Graphs for Shadow, blended winglet (configuration B2), tip twist and angle of attack are varied from -5° to 5° and -5° to 15° respectively. The graph on the left plots C_L/C_D , and the graph on the right plots root bending moment in relation to each parameter.

4.3 Winglet Design for Predator A

The Predator drone, developed by General Atomics, is already designed for high efficiency flight with its long high aspect ratio wings. Can efficiency be improved without great effect on the root bending moment for this UAV? The Predator has a max air speed of 120 knots and altitude of 25,000 ft.[10]. Cruise conditions were set to 60% of the max air speed (72 knots) and the altitude was set to 20,000 ft. The basic wing dimensions were entered into Tornado using the Pecos interface. The Predator uses the Drela GW-19 and Drela GW-27 for the root and tip airfoils respectively[24]. Since these are proprietary, the airfoils were approximated with the Eppler 374 airfoil. Calculations were performed for an alpha sweep from -10° to 20° at the cruise conditions. For the base configuration of the Predator with no winglets, C_L/C_{Dmax} occurred at $\alpha = 5.75^\circ$, with a calculated root bending moment of approximately -10,000 Nm. This was the target angle for winglet optimizations. The goal was to minimize the increase in the root bending moment and maximize the increase in endurance. Since endurance is a function of C_L/C_D , calculations were performed at the

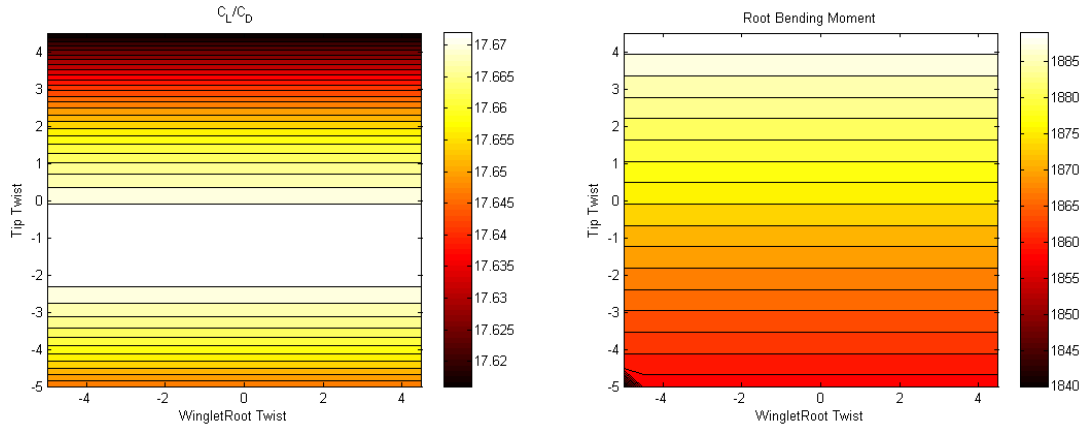


Figure 4.4: Graphs for Shadow, Whitcomb winglet (configuration W1), the cant is varied from 54° to 90° while the angle of attack was varied from -5° to 15° . The graph on the left plots C_L/C_D , and the graph on the right plots root bending moment in relation to each parameter.

cruise condition at an angle of attack of 5.75° . In order to minimize weight added by the winglet itself, the length was limited to 1/10 of the semi span. Since the semi span for the predator is 7.4 meters[10], the total winglet length was limited to 74 cm.

Starting with a basic winglet definition, listed as PW01 in table 4.3, the winglet radius and length were varied from 0.1 to 0.5 meters and 0.4 to 0.8 meters respectively. The percentage in the amount of change from the value for the base configuration at the same flight conditions was plotted for C_L/C_D and root bending moment in fig. 4.9. The results indicate that the best improvement for the C_L/C_D occur at greater values for both the winglet radius and length. These values also coincide with greater root bending moments. Since the deviation from the base configuration for the root bending moment is less than 5%, the winglet radius was set to 0.56 meters and the length set to the maximum value in the constraint, 0.74 meters. Fig. 4.10 shows the results for configuration PW04 from table 4.3. The improvement for C_L/C_D starts at 18% and extends beyond 20%. Here the root bending moment trend matches the C_L/C_D , so improving the C_L/C_D also improves the root bending

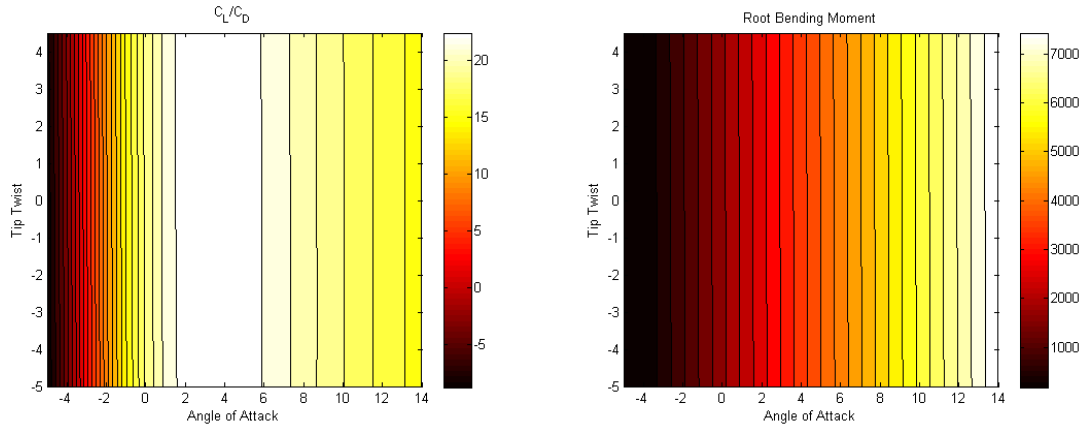


Figure 4.5: Graphs for Shadow, Whitcomb winglet (configuration W2), the tip twist is varied from -5° to 5° while the angle of attack is varied from -5° to 15° . The graph on the left plots C_L/C_D , and the graph on the right plots root bending moment in relation to each parameter.

moment. Configuration PW04 shows the final optimized configuration chosen for the Predator winglet. Fig. 4.11 shows an image of the Predator UAV alongside the VLM models of the Predator with and without the optimized winglets.

4.4 Winglet Performance for Predator A

Table 4.4 lists performance gains possible with the optimized winglet. Using eqn. (3.2) and eqn. (3.1) the endurance and range can be estimated from the predicted values for C_L/C_{Dmax} . VLM predictions estimate the optimized winglets extend the range by 20.32%, and the endurance by 20.36%. While the root bending moment is increased by less than 4%. With a maximum endurance 40 hours[10], this would extend the endurance to a full 48 hours. Because VLM is inviscid, the values for C_D will be too low, so the estimates for range and endurance can be expected to be too optimistic. Further tests will be required to validate the results for the root bending moment, though the VLM predictions for lift are very close to test results.

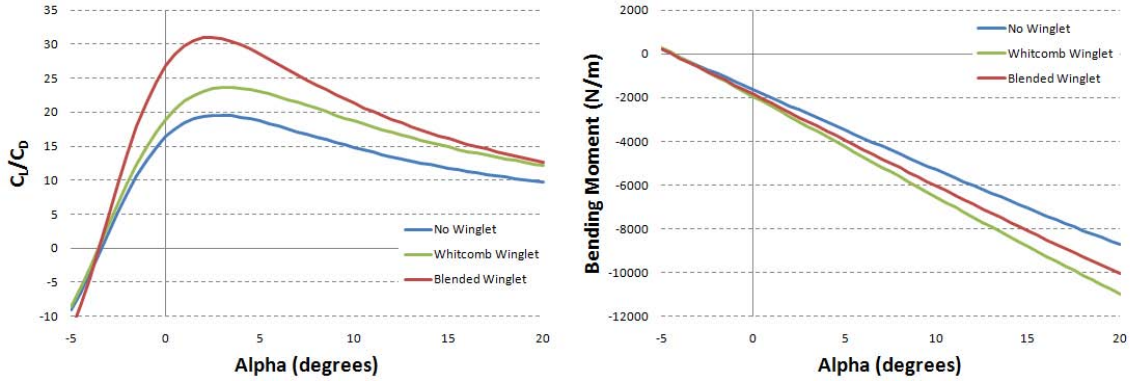


Figure 4.6: Graphs comparing the C_L/C_D and root bending moment versus alpha for 3 configurations for the RQ7 Shadow UAV.

Table 4.2: Performance Comparison for RQ7 Shadow Configurations

Blended Winglet Compared to No Winglet			
C_L/C_D	RBM_{stall}	Range	Endurance
58%	25%	58%	83%
Whitcomb Winglet Compared to No Winglet			
21%	15%	21%	35%
Blended Winglet Compared to Whitcomb Winglet			
31%	9%	31%	35%

Table 4.3: Winglet Parameters for Predator A

Configuration	Length (m)	Root Chord	Tip Chord	Radius	Cant	Sweep	Twist
PW01	0.74	0.55	0.11	0.1	90°	25°	0°
PW04	0.74	0.55	0.055	0.56	75°	40°	-5°

Table 4.4: Performance Comparison for Predator Configurations

Blended Winglet Compared to No Winglet			
C_L/C_D	RBM_{stall}	Range	Endurance
20.36%	3.55%	20.32%	20.36%

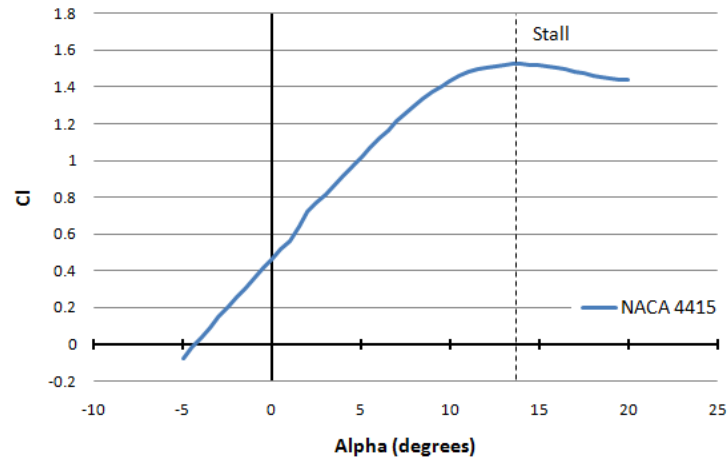


Figure 4.7: Graph of the results from XFOIL calculations performed for the NACA 4415 airfoil at airspeed of 90 knots and an altitude of 10,000 ft.

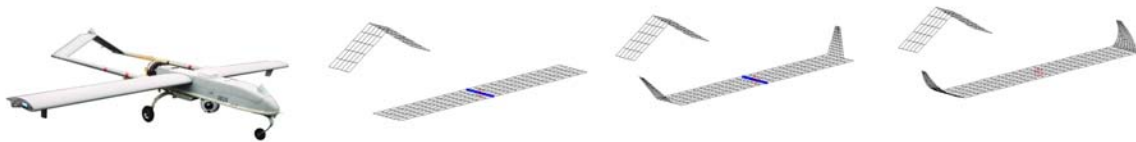


Figure 4.8: L-R: Shadow UAV, VLM model of Shadow UAV, VLM model of Shadow UAV with Whitcomb winglets, VLM model of Shadow UAV with optimized blended winglets.

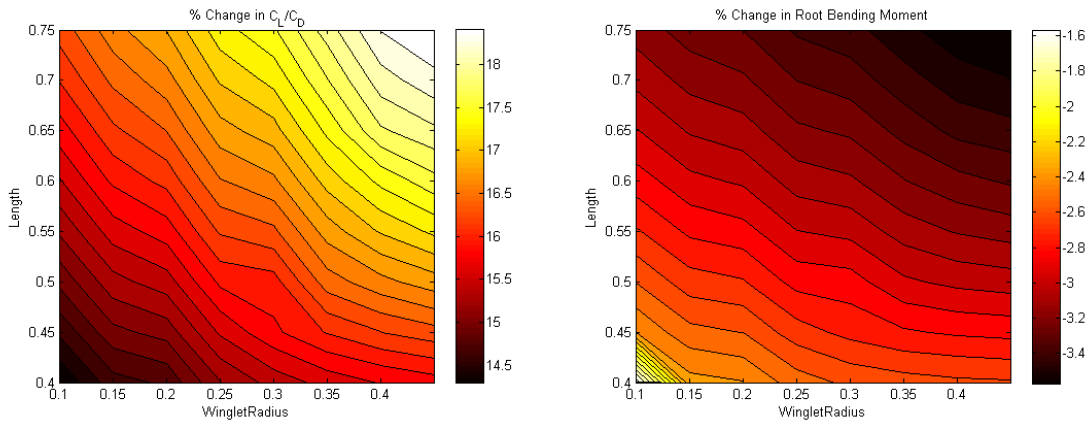


Figure 4.9: Plots showing the percent change for configuration PW01 from the base configuration at the same flight conditions. Left plot is the change in C_L/C_D and the right plot is the change in the root bending moment.

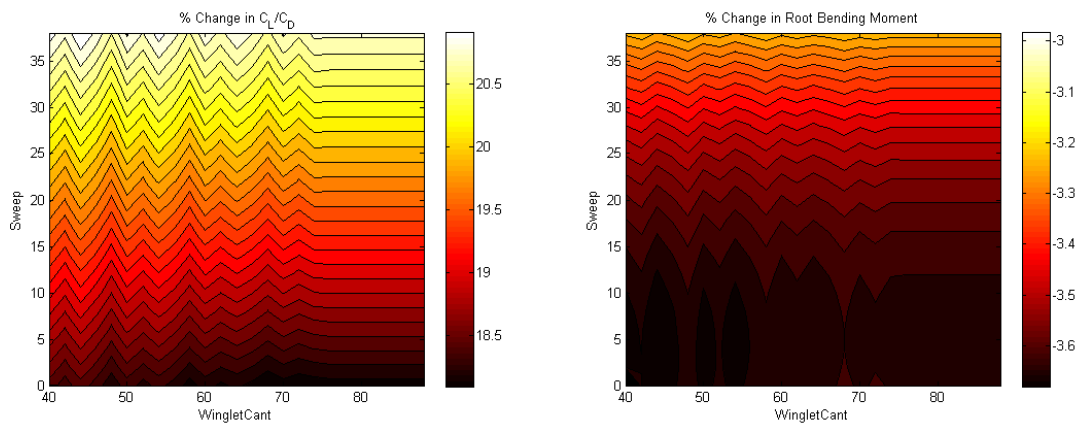


Figure 4.10: Plots showing the percent change for configuration PW04 from the base configuration at the same flight conditions. Left plot is the change in C_L/C_D and the right plot is the change in the root bending moment.

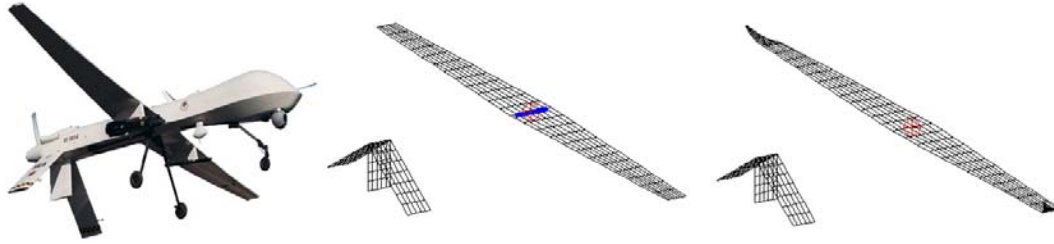


Figure 4.11: Left to Right: Predator UAV, Predator VLM model, Predator VLM model with optimized blended winglets.

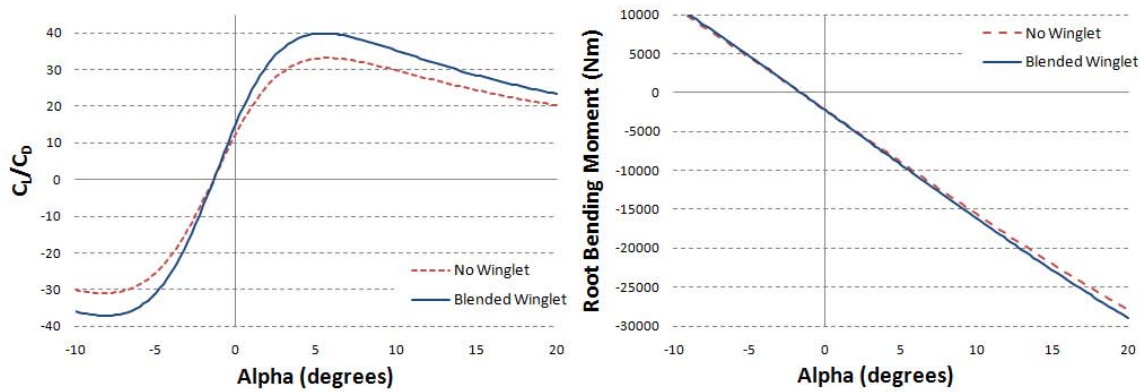


Figure 4.12: VLM results for the base Predator configuration with no winglets compared to Predator with optimized winglets. Left plot shows the predicted values for C_L/C_D vs. Alpha and the right plot shows the root bending moment vs. Alpha.

CHAPTER 5

Conclusions

The impact of using Pecos on design and optimization of winglets for UAVs can be considered for two different aspects. How does it affect the design? How does the design affect the performance? By adding the estimated value for the zero lift drag coefficient to the induced drag coefficient calculated by the VLM, the predictions from the VLM can predict trends in the aerodynamic performance of winglets using the Pecos design methodology. However, without a more accurate calculation of viscous drag forces, the Pecos design methodology should not be relied upon for performance calculations regarding range and endurance. The trends predicted by the VLM show that Pecos is a good tool for comparing variations on a design for parametric design studies.

5.1 Design

Parametric design and analysis reveals the subtle differences that minor changes in a wide array of parameters can have on the aerodynamic performance of an aircraft. Through parametric design engineers can make better decisions in preliminary aerodynamic design choices. As is the case with most factors of aircraft design, design choices are almost always a compromise to attain the desired performance characteristics in *all* aspects of the aircraft operation. Although the VLM did not produce exact results, it provided very nice predictions for performance *trends*. When approaching winglet design it is very helpful to understand what constraints to apply to the design space, otherwise, optimizations may result in infeasible designs. This tool proves that

VLM is very capable in narrowing broad field of parameters for design optimization.

5.2 Performance

Results match or exceed performance predictions from previous winglet studies. Winglets can improve the performance of UAVs, increasing range and endurance. By optimizing winglet designs, blended winglets were able to improve upon Whitcomb's winglet designs. However, the nature of VLM provides very poor results for total drag, and this in turn affects the ratio C_L/C_D . The results from wind tunnel testing compare very poorly with the results from VLM for these ratios. Only the fact that blended winglets perform better than Whitcomb winglets, and Whitcomb winglets perform better than no winglets are reflected in the VLM ratios. The VLM ratios tend to be higher than what was measured in the wind tunnel. This does not disqualify VLM altogether, the *trends* predicted for C_L/C_D matched very well. So this method is valid to a certain degree for winglet design and optimization in that it is very efficient at predicting which configuration will perform better.

5.3 Future Work

The main focus of this research has been to optimize the design and efficiency of winglets for UAVs through parametric analysis of blended winglets. Future work might expand the design space to include the C-wing, spiroid winglets, and perhaps other geometries as well. Further wind tunnel analysis will help to validate results and trends predicted using the vortex lattice method. Wake surveys will help to better understand the impact of design parameters on the shed vortex wake. Weight estimation for winglets and structures would be a natural element for helping to determine the feasibility of winglet configurations. Simple weight models such as those used by Ning and Kroo[22] might be an ideal starting point. Further research may include structural aeroelastic effects and active or passive side slip control. Controlling

flutter induced by the winglets in any part of the flight regime is critical to aircraft stability and structural integrity. It may also be beneficial, when investigating active flow control mechanisms, to investigate the feasibility of aircraft control using the same active mechanisms on the winglets to influence the motion of the aircraft.

BIBLIOGRAPHY

- [1] AAI Corporation, http://www.aaicorp.com/pdfs/shadow_200.pdf , April, 2010
- [2] Anderson, John D., “ Aircraft Performance and Design”, WCB/McGraw Hill, 1999
- [3] Anderson, John D. , “Fundamentals of Aerodynamics, 4th edition” , pp 437-443, McGraw-Hill, New York , NY 2007.
- [4] ANSYS.com www.ansys.com April, 2010
- [5] Boeing.com “bbj.jpg” http://www.boeing.com/commercial/aeromagazine/aero_17/bbj_tech_characteristics.html April, 2010
- [6] Chambers, Joseph R. “Concept to Reality:Contributions of the NASA Langly Research Center to U.S. Civil Aircraft of the 1990s”, NASA SP-2003-4529, <http://oea.larc.nasa.gov/PAIS/Concept2Reality/winglets.html> April, 2010
- [7] Chattot, Jean-Jeaques, “Low Speed Design and Analysis of Wing/Winglet Combinations Including Viscous Effects,” Journal of Aircraft, Vol. 43, No. 2, March-April, 2006.
- [8] Conley, Norm, “Winglet Toe-Out Optimization for the Gates Learjet Longhorn Wing,” J. Aircraft, Vol. 17, No. 12. December 1980.
- [9] Drela, Mark, “XFoil: Subsonic Airfoil development System,” MIT.
- [10] General Atomics, <http://www.ga-asi.com/products/aircraft/predator.php> April, 2010

- [11] George, Fred “Understanding Winglet Technology” http://www.smartcockpit.com/data/pdfs/flightops/aerodynamics/Understanding_Winglets_Technology.pdf, April, 2010.
- [12] Gundlach, John Frederick IV, “Multi-Disciplinary Design Optimization of Subsonic Fixed-Wing Unmanned Aerial Vehicles Projected Through 2025,” Doctoral Dissertation, Virginia Polytechnic Institute and State University, February, 2004.
- [13] Insitu, <http://www.insitu.com/> April 2010
- [14] Kroo, Ilan, McMasters, J., Smith, S. C., “Highly Nonplanar Lifting Systems,” September 1995.
- [15] Kroo, Ilan, “Drag Due to Lift: Concepts for Prediction and Reduction.” *Annu. Rev. Fluid Mech.* 2001. 33:587-617.
- [16] Kuhlman, John M., Liaw, Paul, “Winglets on Low Aspect Ratio Wings” *J. Aircraft*, Vol. 25, No. 10, 1988.
- [17] MATLAB release R2008b - R2010a, Copyright 1984 - 2010 The Mathworks.
- [18] de Mattos, Bento S., Macedo, Antonini P., et. al. “Considerations about Winglet Design” AIAA 2003-3502, 21st Applied Aerodynamics Conference, 23-26 June 2003, Orlando Florida
- [19] Maughmer, Mark D., “Design of Winglets for High-Performance Sailplanes” *Journal of Aircraft*, Vol. 40, No. 6, November-December 2003.
- [20] Melin, Thomas, “A Vortex Lattice MATLAB Implementation for Linear Aerodynamic Wing Applications,” Master Thesis, Royal Institute of Technology (KTH), December 2000.

- [21] NASA Dryden Flight Research Center <http://www1.nasa.gov/centers/dryden/about/Organizations/Technology/Facts/TF-2004-15-DFRC.html>
April, 2010
- [22] Ning, Andrew, and Kroo, Ilan, “Tip Extensions, Winglets, and C-wings: Conceptual Design and Optimization,” American Institute of Aeronautics and Astronautics, 2008.
- [23] Raymer, Daniel, “Enhancing Aircraft Conceptual Design Using Multidisciplinary Optimization,” Doctoral Thesis, Royal Institute of Technology (KTH), May, 2002.
- [24] Selig, Michael, “UIUC Airofil Coordinates Database - Version 2.0”. Department of Aerospace Engineering, University of Illinois at Urbana-Champaign.
- [25] Takenaka, Keizo and Hatanaka, Keita, “Multidisciplinary Design Exploration for a Winglet,” Journal of Aircraft, Vol. 45, No. 5, September-October 2008.
- [26] TetrUSS <http://tetruss.larc.nasa.gov/> April, 2010
- [27] United States Air Force, <http://www.af.mil/> April, 2010
- [28] University of Washington Aeronautical Laboratory, <http://www.aawashington.edu/uwal/>, April, 2010
- [29] Whitcomb, Richard T., “A Design Approach and Selected Wind-Tunnel Results at High Subsonic Speeds for Wing-Tip Mounted Winglets”. NASA TN D-8260, July 1976.
- [30] Wikimedia.com <http://upload.wikimedia.org/wikipedia/> April, 2010

VITA

Jacob Weierman

Candidate for the Degree of
Master of Science

Thesis: WINGLET DESIGN AND OPTIMIZATION FOR UAVS

Major Field: Mechanical and Aerospace Engineering

Biographical:

Personal Data:

Born in Pryor, OK, United States of America on August 1, 1974.

Education:

Received the B.S. degree from Oklahoma State University, Stillwater, OK, United State of America, 2003, in Applied Physics

Completed the requirements for the degree of Master of Science with a major in Mechanical and Aerospace Engineering, Oklahoma State University in June, 2010.

Experience:

Worked as a research assistant for Dr. Jamey Jacob in the Department of Mechanical and Aerospace Engineering at OSU. Worked as a research assistant for Dr. John W. Mintmire in the Department of Physics at OSU.

Name: Jacob Weierman

Date of Degree: July, 2010

Institution: Oklahoma State University

Location: Stillwater, Oklahoma

Title of Study: WINGLET DESIGN AND OPTIMIZATION FOR UAVS

Pages in Study: 92

Candidate for the Degree of Master of Science

Major Field: Mechanical and Aerospace Engineering

Winglets have been shown to improve the efficiency of large aircraft at high subsonic speeds, but winglet designs for smaller aircraft like UAVs are unproven. Winglets improve efficiency by diffusing the shed wingtip vortex, which in turn reduces the drag due to lift and improves the wings lift over drag ratio. This research investigates methods for designing and optimizing winglet geometry for UAVs that operate at Reynolds numbers near 10^6 . The design methodology is based on the vortex lattice method. Optimized designs are tested and compared with base designs for validation and include both Whitcomb and blended winglets. Designs are validated using wind tunnel tests. The resulting methodology is then applied to existing UAV platforms for specific performance improvements. For example, winglets were designed for the Shadow UAV where endurance was increased by 35% and 83% and range was increased by 21% and 31%, for the Whitcomb and blended wing designs, respectively.

ADVISOR'S APPROVAL:

Dr. Jamey Jacob